12-15-2017 10:00 AM

Assessment of Dynamic Effect of Transmission Line Conductor Longitudinal Reaction Due to Downburst Loading

Ibrahim Ibrahim, *The University of Western Ontario*

Supervisor: El Damatty, Ashraf A., *The University of Western Ontario*

A thesis submitted in partial fulfillment of the requirements for the Master of Engineering Science degree in Civil and Environmental Engineering
© Ibrahim Ibrahim 2017

Abstract

Due to the locality and non-stationary nature of downburst wind loading events, their effect on the structural response of transmission line structures is of special nature that differs from conventional atmospheric boundary layer wind loading. Acknowledging such difference, the current thesis aims to quantify the dynamic effect associated with downburst loading on transmission line systems. To achieve that, several steps had to be realized, including experimentally verifying the numerical model used for analysis using wind field that was generated using computational fluid dynamics. The verified model was extended from model scale to full scale, where the wind field used for loading was a combination of mean component generated using CFD, and turbulent component that was synthetically generated using a statistically calibrated numerical technique. Results of the analyses showed that the consideration of dynamic analysis did not affect the computed peak longitudinal reactions. Finally, the wind field used was compared to field measurements to ensure the deduced conclusions can be generalized.

Keywords

Co-Authorship Statement

This thesis has been prepared in accordance with the regulations for an Integrated Article format thesis stipulated by the School of Graduate and Postdoctoral Studies at Western University. Statements of the co-authorship of individual chapters are as follows

Chapter 2: Numerical Simulation of WindEEE Dome Downburst Using Physical Roughness Elements

Numerical simulations and analyses were conducted by I. Ibrahim under close supervision of Dr. A. A. El Damatty and Dr. H. Aboshosha with the co-operation of Dr. A. Elawady regarding utilizing the experimental data.

Drafts of Chapter 2 were written by I. Ibrahim, and modifications were done under supervision of Dr. A. A. El Damatty and Dr. H. Aboshosha. A paper co-authored by I. Ibrahim, H. Aboshosha, A. A. El Damatty and A. Elawady will be submitted to the *Journal of Wind and Structures.*

Chapter 3: The Effect of Downburst Wind Field Characteristics on the Longitudinal Forces on Transmission Towers

All the numerical models and analyses were conducted by I. Ibrahim under close supervision of Dr. A. A. El Damatty. Drafts of Chapter 3 were written by I. Ibrahim and modifications were done under supervision of Dr. A. A. El Damatty. A paper co-authored by I. Ibrahim and A. A. El Damatty will be submitted to the *Journal of Wind Engineering & Industrial Aerodynamics.*

Acknowledgments

With these few words, I would like to express my deep gratitude to those whom the past two years would have never been as productive, enjoyable and bearable for the most part. Among them, stands out my supervisor, Prof. Ashraf El Damatty, for the guidance he never failed to be generous with, the encouragement I was usually seeking during the times I struggled with my work, and being the role model he is for me and my fellow group members.

The help and valuable advice I received from Dr. Haitham Aboshosha are also acknowledged with the sincerest gratefulness. The journey has had its crests and troughs, my colleagues in the department have had a great role in helping me getting through. Some of them were really supportive and always generous with their technical knowledge. Others were a necessity for me to keep my temper and sometimes my sanity on the times the numerical models really got on my nerves. The only person I could think of who belongs to both teams is Dr. Ahmed Elshaer. I owe him a lot in return for his support, technical knowledge, and fun times we had together.

Lastly, saving the my dearest words for my dearest people, I spend my days thanking God for the family I have, doubting if anything I ever did or will ever do one day can prove me worthy of the blessing I have, with that I mean my amazing parents. To them I owe everything I have reached and everything I would ever reach. I am also grateful for the blessing of having my amazing siblings; Aya, my twin sister whom I literally shared with every day of my life, Amr, my younger, taller, cooler and funnier brother, my sister Zahraa, the light of our lives for the past eight years, Khalid, my brother-in-law, the second redhead in our family, and lastly, the first grandchild, the cutest redhead in the family, my everyday dose of joy, my nephew, Ezz.

Table of Contents

List of Tables

List of Figures

Chapter 1

1   Introduction

1.1   Background

Throughout the past century, electricity has been a major component of and contributor to how our modern world has evolved to be. Furthermore, the role of electricity in our lives has only intensified and gained more importance as new technologies are totally dependent on the undisturbed availability of energy provided by electricity. Such reliability projects great importance on the sustainability of electricity transmission line systems as a key component of a functioning electric network. As shown in Figure 1-1, transmission line systems consist of different components. These can be mainly classified in the order of load transfer from a structural perspective as follows; conductors and wires transfer the loads across spans axially to the insulators that in this case act as the supports for these non-linear components. The insulators then convey the load axially again to the nearest tower components, the cross arms, which is where the insulators are attached. The loads are then transferred through the tower members, that in turn act as a truss that can resist forces and moments developed, and finally convey these forces to the supporting foundation structure. Within the given sequence, structural engineers must ensure that every component has sufficient capacity to resist the assigned loads.
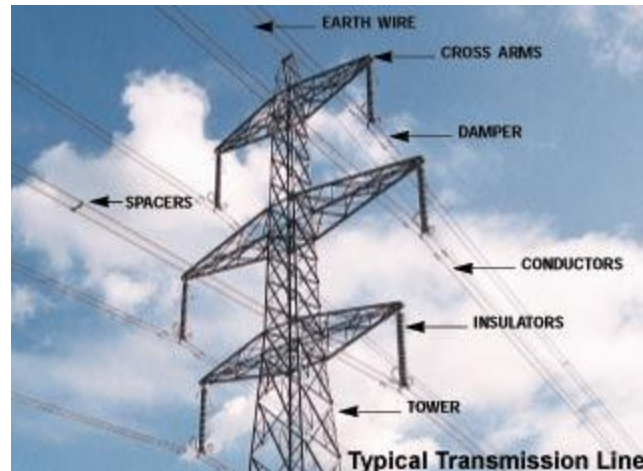
Figure 1-1 Components of transmission line system "http://electrical-power-system.blogspot.ca"

Accordingly, structural engineers must be aware of the types of loads transmission structures are susceptible to. As seen in Figure 1-2, transmission line structures usually extend through great distances in relatively open exposures, making them fully exposed to weather related loading events. Judging by how current design guide lines, such as ASCE-74 (2010), are structured, it is widely recognized that weather related loading is the governing type of loading when designing transmission line systems. Yet, some weather loading phenomena, such as tornadoes and downbursts, are still far from being completely incorporated in the design of sustainable transmission line systems. This is mainly due to two things; first, the complexity of these events, which makes them hard to implement as loading phenomena, unlike straight wind, which is arguably fully comprehended, and thus its current incorporation can be considered as a trusted representation of the loads associated with the phenomenon. The second thing, which relates more to downbursts, is the absence of sufficient database of event occurrence, which in turn complicates the efforts to quantify the precise impact these events have on transmission line systems.

Figure 1-2 A series of transmission line towers "https://www.thenews.com.pk/"

Focusing on the downburst phenomenon, it was first defined by the prominent meteorologist Ted Fujita, who defined downbursts as a descending column of air that impinges the ground, and causes a radial outburst resulting in devastating wind speeds (Fujita 1985). Such event is characterized by being a localized non-stationary event. The locality is due to the comparability of the phenomenon scale compared to the dimensions of the transmission line structures. While the descending column of air can be between 1500 to 3000 meters in diameter (Hjelmfelt 1988), the span of transmission line is in the order of hundreds of meters. This comparability in scale dictates a difference in the consideration of downburst loading on transmission line structures compared to normal wind loading where consequent spans are assumed to experience the same loading. In addition, the resulting wind field is described as being non-stationary as it demonstrates a varying mean value with time, which has its implications on the structural analysis of the

structure system, as well as combine with the locality of phenomenon to introduce new loading conditions on spans of the transmission line systems. These new loading circumstances demonstrated a devastating effect on transmission line systems, where failures reported worldwide were linked to downburst events (Kanak et al. 2007, Li 2000, McCarthy and Melsness 1996, Zhang 2006). These failures have motivated researchers to study the effect of downburst loading on transmission line systems as discussed in the next section.

1.2   Studies of Downburst Loading on Transmission Line Systems

As a result of the devastating events mentioned in the previous section, a wide spectrum of researchers have been studying the effect of downburst loading on transmission line systems and efforts to mitigate such hazards to ensure transmission line structures can sustainably withstand such loads. Researchers differed in terms of the considered structure system under downburst loading; researchers like Aboshosha et al. (2016), Lin et al. (2012), Shehata et al. (2005), Shehata and El Damatty (2007) and Darwish and El Damatty (2011)considered the tower-line system with both the towers and the conductors included in the analyses to study their combined behavior under down burst loading. Other researchers like Mara et al. (2010), Mara and Hong (2013) and Savory et al. (2001) only considered the supporting structures, focusing on the responses of the towers due to the downburst wind field. This was counter-acted by other researches who considered the downburst wind field to be more important in the case of conductor systems due to the locality of the loading phenomenon, and its comparable scale to the spans of the conductor systems. This has been demonstrated through the work of researchers like Aboshosha and

El Damatty (2015), (2014a), (2014b), Darwish et al. (2010) and Elawady and El Damatty (2016). These researchers studied the behavior of conductor systems to downburst loading under different loading configurations ignoring the effect the towers might impose on the analysis due to their relative rigidity compared to the conducting lines. The outcome of such research mainly focused on the effect the locality of the downburst had on the computed responses of the conductor systems. One of which, Elawady and El Damatty (2016), mainly studied the effect downbursts have on the computing of longitudinal reactions of a conductor system. The study carried on from where researchers like Darwish and El Damatty (2011) and Shehata and El Damatty (2007) have concluded. These previous studies examined different loading cases associated with different spatial configurations of downburst positioning relevant to the studied structure. One of the load cases examined is the oblique load case. As shown in Figure 1-3, this is the case where the line joining the downburst center is at an angle from the line perpendicular to the tower of interest. This is configuration is expected to cause differential loading across consecutive spans. This can be of specific importance for transmission structure elements like tower cross-arms. The differential loading causes the development of a longitudinal reaction that would be transferred from the conductors to the tower structure. While current design guidelines do not take such case into consideration, certain cases with high velocities of downburst events can be devastating to cross-arms as shown in Figure 1-4. Accordingly, the study performed by Elawady and El Damatty (2016) considered the oblique load case and its effect on the magnitude of the computed longitudinal reaction using the quasi-static numerical technique developed by Aboshosha and El Damatty (2014b). The study considered different configurations of downburst parameters and spatial positioning to

derive generic conclusions on the values longitudinal reactions. The outcome of this research was compiled into a comprehensive set of charts that can be easily used by practitioners to compute design values of longitudinal reactions based on the conductor's geometry and physical properties. However, such a robust technique relied on the conclusions stated by previous researchers that downburst loading can sufficiently be analyzed using quasi-static analysis (Darwish et al. 2010).
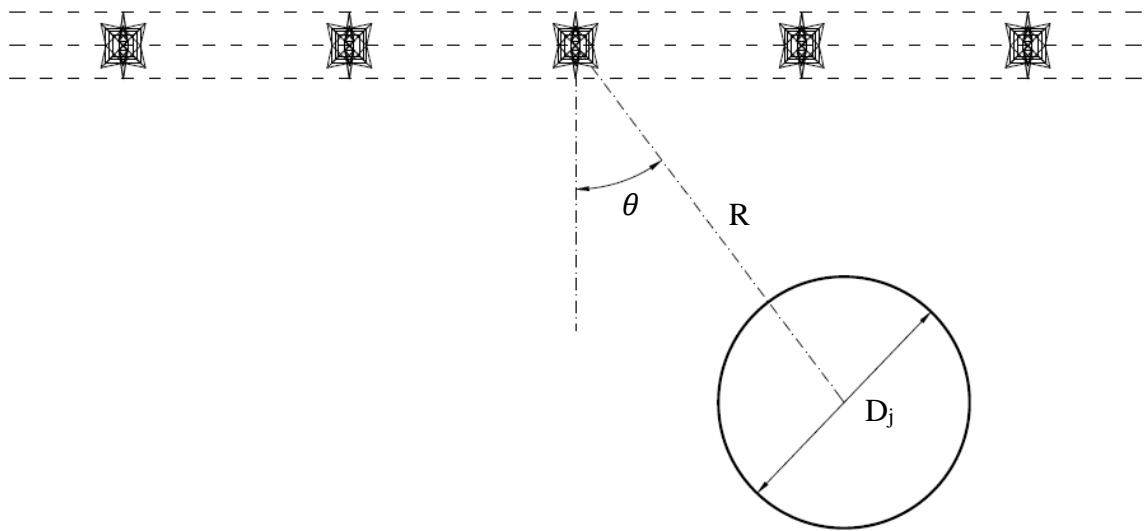
Figure 1-3 Oblique load case illustration

Yet, the fact the differential loading is the cause of the developed longitudinal reaction, can add more weight to the dynamic analysis, which considers the spatial correlations between distant nodes, a key parameter that is overlooked by quasi-static analysis. The next section will discuss the previous efforts that led to the conclusion of the quasi-static analysis being sufficient for such types of systems, and how this might be invalid for the case in hand.

Figure 1-4 Broken cross-arm due to downburst event "Aboshosha et al. (2016a)"

1.3 Structural Analysis of Transmission Lines

Previous researchers who structurally analyzed the transmission line systems mostly used the quasi-static analysis approach (Darwish and El Damatty 2011, Elawady and El Damatty 2016, Shehata et al. 2005 and Shehata and El Damatty 2007). Yet, other researchers considered the dynamic effect the downburst loading might have on the responses of the structure systems, specially conductor spans (Aboshosha and El Damatty 2015b, Darwish et al. 2010 and Lin et al. 2012). For the researchers evaluating the dynamic effects numerically, a major challenge was the choice of a representative aerodynamic damping expression that addresses both the physical properties of the conductors, as well as the transient nature of the downburst event. Accordingly, the expression given by Davenport (1962) and shown in equation (1-1) has been considered to represent the effect of the physical properties of the conductors on the value of aerodynamic damping, yet was deemed unsuitable for the use in the analysis of downburst loading analysis as it does not address the non-stationarity of the loading event.

$$\zeta_{ai} = \frac{\rho C_D DV}{4\pi m f_i} \tag{1-1}$$

Where $\boldsymbol{\zeta_{ai}}$ is the aerodynamic damping value per mode i, $\boldsymbol{\rho}$ is the air density, $\boldsymbol{C_D}$ is the drag

coefficient, $\boldsymbol{D}$ is the conductor diameter, $\boldsymbol{V}$ is the wind velocity, $\boldsymbol{m}$ is the conductor mass, and

$\boldsymbol{f_i}$ is the mode's frequency.

To address the transient nature of the loading, researchers like Darwish et al. (2010)

modified the above expression, by replacing the constant wind velocity term by another

term that varies with time. Such a modification can require special computational

measures, since the changing values of damping might not be accommodated by

mainstream structural analysis programs, which triggers the need of developing in-house

coding such as the models developed by Darwish et al. (2010) and Aboshosha et al.

(2016b). Nevertheless, these approaches lacked the creditability the original approach

(Davenport 1962) had through experimental validation of the proposed expression.

Accordingly, any further analysis done should make use of reliable experimental testing at

reasonable scales to make sure the derived conclusions can be used with confidence. Upon

deciding on a valid numerical approach to dynamically analyze the structure system, the

use of a validated wind field with nature-like turbulence is a major component that cannot

be spared. The next section will discuss the different options presented by previous

researchers to obtain downburst wind field with turbulent component suitable for dynamic

analysis.

1.4 Downburst Wind Field

As mentioned in the first section of this chapter, downburst events are localized events, which means that the event usually occurs at micro-scales, with an affected area only several kilometers wide. Such localization has so far made it difficult for researchers to capture downburst wind field data from field measurements. Instead, anemometer velocity time histories provide a limited perspective on the downburst wind filed properties, with no consideration of the spatial and temporal relations between distant points. Although this is expected to change soon due to the advances in data capturing technologies and the new Lidar systems capable of clearing out such ambiguities, the data available in the modern literature still lacks a full comprehension of spatiotemporal relations between points at different positions. Therefore, previous studies that were interested in the dynamic analysis of transmission line structure systems relied on computational fluid dynamics (CFD) to resolve the flow using either kinematic (impinging jet) scheme, or thermodynamic (cooling source) scheme to resemble the flow characteristics of downburst events. As such, the wind field provided by Kim and Hangan (2007) utilized the impinging jet scheme to produce the desired flow field. Yet, the flow field provided could only resolve for mean components of the flow due to the choice numerical scheme used in CFD analysis. Researchers like Darwish et al. (2010) extracted the turbulence component of the field measurements reported by Holmes et al. (2008), and super imposed it on the mean wind field resulting from the CFD simulation. Others like Aboshosha et al. (2016b) synthetically generated the turbulent component using the technique described by Chen and Letchford (2004) and Chay et al. (2006). However, both techniques used to create a turbulent component to be superimposed on the mean component lacked the characterizing spatial

relations between points at which the turbulent component is generated. The overlooking of characteristics like correlations and length scales can be deterministic in the case of studying dynamic effect of downburst loading on transmission line systems due to the comparability in the scales of the event and the structure system. Accordingly, a more robust technique is to be used if the same superposition technique is used to create a wind field including the turbulent component of the flow.

1.5   Objectives of the Study

The current study investigates the validity of the assumptions presumed by Elawady and El Damatty (2016) which will be discussed elaborately in chapter 3 of this thesis. Accordingly, the objectives of the current study are as follows:

1. Assess the dynamic effect downburst loading might have on the computed longitudinal reactions of conductor systems.

2. Quantify the effect of considering the correlations between spatially distinct points on the values of longitudinal reactions.

3. Judge the applicability of the conducted analysis in regard to the used wind field compared to field measured data.

1.6   Organization of Thesis

This thesis is organized following the "Integrated Article" format. The current chapter introduces the studied topic, along with the key points targeted by the research as objectives of the study. The following chapters address the objectives mentioned as follows:

Chapter 2: Numerical Simulation of WindEEE Dome Downburst Using Physical Roughness Elements

This chapter aims to provide a detailed wind field of the downburst simulation conducted in the WindEEE dome. Being the first of its kind, the WindEEE dome is able to produce downbursts using the impinging jet model at wind tunnel testing scale. The study presented in this chapter aims to replicate the experiment using Large Eddy Simulation (LES) CFD model to capture the characterizing features of the wind field. The results captured from the simulation were compared with the experiment for both the mean and the turbulent components of the flow. The flow features were also examined at different positions in the domain, and it was found that the geometry of the local components of the dome impose an undesirable effect on the flow.

Chapter 3: The Effect of Downburst Wind Field Characteristics on the Longitudinal Forces on Transmission Towers

In this chapter, the effect of downburst wind field characteristics, namely the turbulent component and the characteristics of the mean component, are examined. Starting with the turbulent component, the chapter first proposes a numerical model that is capable of dynamically analyzing conductor systems under downburst loading. Utilizing the detailed wind field availed by the study presented in chapter 2, the assumptions and hypothesis are validated using an aero-elastic experiment that was conducted in the WindEEE dome. The study was then extended to the full scale, studying the dynamic effect of downburst loading on longitudinal reactions at tower structures. To do so, a synthetic turbulent component was first generated and calibrated, then superimposed on previously available CFD mean flow field. After deciding on the significance of the dynamic effect on the computed reaction values, the following sections of the chapter compare the used wind field with data available in the literature to relate the features of downburst time histories generated by

CFD to available field measurements. Lastly, CFD wind fields were modified to match the field measurements, and the effect of the applied modifications on the computed reactions was reported.

Finally, the last chapter of this thesis presents the conclusions obtained from the performed research, as well as recommendations for future work based on the results of this study.

1.7 References

Aboshosha, H., El Damatty, A., (2015a). Engineering method for estimating the reactions of transmission line conductors under downburst winds. Eng. Struct. 99, 272–284. doi:10.1016/j.engstruct.2015.04.010

Aboshosha, H., El Damatty, A.A., (2015b). Dynamic response of transmission line conductors under downburst and synoptic winds. Wind Struct. An Int. J. 21, 241–272. doi:10.12989/was.2015.21.2.241

Aboshosha, H., El Damatty, A.A., (2014a). Span Reduction Factor of Transmission Line Conductors Under Downburst Winds Span Reduction Factor of Transmission Line. J. Wind Eng. 11, 13–22. doi:10.3850/978-981-07-8012-8

Aboshosha, H., El Damatty, A.A., (2014b). Effective technique to analyze transmission line conductors under high intensity winds. Wind Struct. An Int. J. 18, 235–252. doi:10.12989/was.2014.18.3.235

Aboshosha, H., Elawady, A., El Ansary, A., El Damatty, A.A., (2016a). Review on dynamic and quasi-static buffeting response of transmission lines under synoptic and non-synoptic winds. Eng. Struct. 112, 23–46. doi:10.1016/j.engstruct.2016.01.003

Aboshosha, H., Ibrahim, A., El Damatty, A.A., Hamada, A., (2016b). Dynamic Behaviour of Transmission Lines Structures under Synoptic Wind Loads, in: 2016 CIGRE-IEC Colloquium.

ASCE-74, (2010). American Society of Civil Engineers (ASCE). Guidelines for electrical transmission line structural loading. ASCE Manuals and Reports on Engineering Practice, No. 74, New York (NY), USA; 2010.

Chay, M.T., Albermani, F., Wilson, R., (2006). Numerical and analytical simulation of downburst wind loads. Eng. Struct. 28, 240–254. doi:10.1016/j.engstruct.2005.07.007

Chen, L., Letchford, C.W., (2004). A deterministic-stochastic hybrid model of downbursts and its impact on a cantilevered structure. Eng. Struct. 26, 619–629. doi:10.1016/j.engstruct.2003.12.009

Darwish, M.M., El Damatty, A.A., (2011). Behavior of self supported transmission line towers under stationary downburst loading. Wind Struct. An Int. J. 14, 481–498. doi:10.12989/was.2011.14.5.481

Darwish, M.M., El Damatty, A.A., Hangan, H., (2010). Dynamic characteristics of transmission line conductors and behaviour under turbulent downburst loading. Wind Struct. An Int. J. 13, 327–346. doi:10.12989/was.2010.13.4.327

Davenport, A.G., (1962). Buffeting of a suspension bridge by storm winds. J. ASCE Struct. Div. 88, 233–264.

Elawady, A., El Damatty, A.A., (2016). Longitudinal force on transmission towers due to non-symmetric downburst conductor loads. Eng. Struct. 127, 206–226. doi:10.1016/j.engstruct.2016.08.030

Fujita, T.T., (1985). The downburst: microburst and macroburst. Satellite and Mesometeorology Research Project (SMRP). Res. Pap. 210, Dep. Geophys. Sci. Univ. Chicago.

Hjelmfelt, M.R., (1988). Structure and life cycle of microburst outflows observed in Colorado. J. Appl. Meteorol. 900–927.

Holmes, J.D., Hangan, H.M., Schroeder, J.L., Letchford, C.W., Orwig, K.D., (2008). A forensic study of the Lubbock-Reese downdraft of 2002. Wind Struct. An Int. J. 11, 137–152. doi:10.12989/was.2008.11.2.137

Kanak, J., Benko, M., Simon, A., Sokol, A., (2007). Case study of the 9 May 2003 windstorm in southwestern Slovakia. Atmos. Res. 83, 162–175. doi:10.1016/j.atmosres.2005.09.012

Kim, J., Hangan, H., (2007). Numerical simulations of impinging jets with application to downbursts. J. Wind Eng. Ind. Aerodyn. 95, 279–298. doi:10.1016/j.jweia.2006.07.002

Li, C.Q., (2000). A stochastic model of severe thunderstorms for transmission line design. Probabilistic Eng. Mech. 15, 359–364.

Lin, W.E., Savory, E., Mcintyre, R.P., Vandelaar, C.S., King, J.P.C., (2012). The response of an overhead electrical power transmission line to two types of wind forcing. J. Wind Eng. Ind. Aerodyn. 100, 58–69. doi:10.1016/j.jweia.2011.10.005

Mara, T.G., Galsworthy, J.K., Savory, E., (2010). Assessment of vertical wind loads on lattice framework with application to thunderstorm winds. Wind Struct. An Int. J. 13, 413–431.

Mara, T.G., Hong, H.P., (2013). Effect of wind direction on the response and capacity surface of a transmission tower. Eng. Struct. 57, 493–501. doi:10.1016/j.engstruct.2013.10.004

McCarthy, P., Melsness, M., (1996). Severe weather elements associated with September 5, 1996 hydro tower failures near Grosse.

Savory, E., Parke, G.A.R., Zeinoddini, M., Toy, N., Disney, P., (2001). Modelling of tornado and microburst-induced wind loading and failure of a lattice transmission tower. Eng. Struct. 23, 365–375. doi:10.1016/S0141-0296(00)00045-6

Shehata, A.Y., El Damatty, A.A., (2007). Behaviour of guyed transmission line structures under downburst wind loading. Wind Struct. 10, 249–268.

Shehata, A.Y., El Damatty, A.A., Savory, E., (2005). Finite element modeling of transmission line under downburst wind loading. Finite Elem. Anal. Des. 42, 71–89. doi:10.1016/j.finel.2005.05.005

Zhang, Y., (2006). Status quo of wind hazard prevention for transmission lines and countermeasures. East China Electr Power 34, 28–31.

Chapter 2

2 Numerical Simulation of WindEEE Dome Downburst Using Physical Roughness Elements

2.1 Introduction

Over the past decades, experimental wind tunnel testing focused on the simulation of Atmospheric Boundary Layer (ABL) and its effect on various structures. Recently, this has extended to include the simulation of High Intensity Wind events associated with thunderstorms and represented by downbursts and tornadoes. Li (2000) reported that strong thunderstorms including downbursts and tornadoes are responsible for 90% of the weather-related failures of transmission line structures in Australia. Dempsey and White (1996) also reported that 80% of weather-related failures of transmission lines are attributed to high intensity wind, which incorporates tornadoes and downbursts. A downburst is known as an intense downdraft that impinges towards the ground and convicts radially causing high damaging wind speeds near the ground as described by Fujita (1985a). This can be viewed as the opposite of the tornado, where a warm updraft of swirling air forms that sucks the air near the ground and feeds into the cloud base.

Despite the fact that downbursts have a relatively lower wind speed than tornadoes, they impose greater damage to structures because of their high occurrence rate. Detection of downbursts is very challenging compared with synoptic winds. That is because downbursts have relatively short duration (i.e. 20-30 min) and have relatively small size (up to 5000 m) as reported by Hjelmfelt (1988). This encouraged many researchers to study downbursts experimentally and computationally in addition to the full-scale measurements.

Earlier research was directed to full-scale measurements trying to provide field data for the newly explored wind event. Metrological projects like the Northern Illinois Meteorological Research on Downbursts (NIMROD) and the Joint Airport Weather Studies (JAWS) were reported by Fujita (1985a), while the Federal Aviation Administration Lincoln Laboratory Operational Weather Studies (FLOWS) project has been reported by Wolfson et al. (1985). More recent field measurements have been reported by Orwig and Schroeder (2007) who presented the results obtained from a linear array of mobile towers for two captured events. They also presented their analyses for the results that were compared to synoptic wind data analysis. Choi (2004) has also reported measurements taken using one tower for more than 50 thunderstorm events. The author furtherly investigated the different variables affecting the velocity profiles of the measured events. In addition, a relatively large project, that took place between 2009 and 2012, has been reported by Solari et al. (2015a) as an extensive in-situ wind monitoring network. The Wind and Ports project relies on 22 ultrasonic anemometers to capture high-resolution thunderstorm records that are then processed to extract statistical properties of thunderstorm events. Gunter and Schroeder (2015) have also presented measurements collected using two mobile Doppler radars to provide enhanced understanding of the vertical profiles through analyzing three events.

Adjacently, researchers have managed to replicate the phenomenon of downburst experimentally at laboratory scales. This was mainly done through the impinging jet model as suggested by Hjelmfelt (1988) to resemble much of the flow characteristics of microbursts. This was further studied by researchers like Wood et al. (2001), Chay and Letchford (2002), Mason et al. (2005), Sengupta and Sarkar (2008), McConville et al. (2009), Das et al. (2011) and Li and Ou (2012). All the previously mentioned attempts

were executed in relatively small laboratory scales. While these efforts are credited for providing much of our current understanding of downbursts, their small scales did not allow for a detailed understanding of the flow field including the turbulent structure.

This has motivated the researchers at University of Western Ontario to build the Wind Engineering, Energy and Environment (WindEEE) dome, the world's first testing facility capable of simulating three-dimensional axisymmetric flows including downbursts (Jubayer et al. 2016).

Furthermore, a wider spectrum of researchers have simulated the downburst numerically utilizing CFD through different schemes for physical models. Choosing between cloud models, cooling source models and impinging jet models, researchers usually balanced the accuracy of the results provided, with the computational power needed. For example, researchers with interest in wind engineering usually preferred the sub-cloud model over the full cloud model due to its computational efficiency, as well as its ability to resolve near the surface flows (Mason et al. 2009). Examples for the cloud scheme of downburst simulation could be found through the work of researchers like Lin et al. (2007), Mason et al. (2009), Mason et al. (2010), Otsuka (2006) and Vermeire et al. (2011). As for the impinging jet scheme, illustrated in Figure 2- 1, researchers like Chay and Letchford (2002), Sengupta and Sarkar (2008) and Wood et al. (2001) have used the simplest application of the scheme, looking at the wind field at the steady state (i.e. after the downdraft hit the ground) and achieved comparable results. Other researchers like Kim and Hangan (2007), Mason et al. (2005), Xu and Hangan (2008), and Aboshosha et al. (2015) investigated the transient nature of the downburst wind field before and after the downdraft hit the ground.
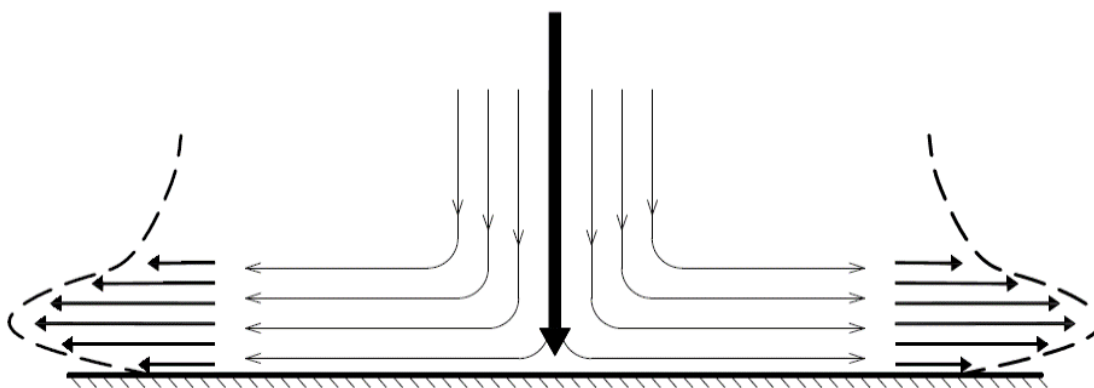
Figure 2- 1 Schematic view of the impinging jet model

Researchers in the numerical stream have used several viscous models, from RANS and its several derived models (k-ε, RSM and k-Ω), to the shear adaptive simulation (SAS), shear stress transport (SST), and finally the large eddy simulation (LES) model. Out of the researchers who studied the turbulent component of the flow, those who utilized the LES model including Hadžiabdić (2006), Chay et al. (2006), Sengupta et al. (2008) and Aboshosha et al. (2015) showed the adequacy of using the LES model in resolving downburst flows. Yet, for resolving the turbulent component, Tamura and Kareem (2013) state that the scales of turbulence resolved are bounded at a maximum that is attributed to the domain size, and a minimum attributed to the grid resolution. This implies that for turbulence to be resolved, the grid resolution, through the flow path, shall be kept constant and at least smaller than or equal the minimum turbulence scale required to be resolved, similar to what Elshaer et al. (2016) have applied. The aforementioned feature, although deterministic for the resolved turbulence scales, was not taken into consideration by previous studies. The general approach was to densify the grid near the ground where flow features are of most importance, and coarsen it elsewhere for computational efficiency. This leads to the scales being dictated by larger grid sizes, which impacts the range of

captured turbulence frequencies. A more detailed collection of these efforts associated with downburst flow studies can be found through the comprehensive review done by Aboshosha et al. (2016a).

The current study belongs to the numerical simulation group but focuses on simulating the downbursts experimentally simulated at the WindEEE dome. This study aims at characterizing the detailed turbulent wind field generated at WindEEE and understanding the role of the experimental elements affecting the flow. The study utilizes the basic wind field collected from a previous downburst experiment reported by Elawady et al. (2016) and Elawady et al. (2017) to validate the CFD model. The manuscript is presented in five sections. In section 1 (this section), an introduction and a literature review is presented. Section 2 illustrates the previous experiment conducted at WindEEE. Section 3 discusses the detailed CFD simulations of the WindEEE dome and Section 4 presents the results from the simulations. Finally, section 5 includes the conclusions and recommendations.

2.2   Experimental Simulation

The experiment presented in this section was a preliminary stage of the aeroelastic transmission line model testing conducted by Elawady et al. (2017). The procedures described hereafter were aiming at characterizing downburst wind field at the WindEEE dome, before testing the aeroelastic model. The WindEEE dome, schematically shown in Figure 2- 2, utilizes 106 individually controlled fans to simulate a variety of straight flows, as well as axisymmetric flows like tornadoes and downbursts. Similar to conventional wind tunnel methods, the turbulent component can be imposed using upstream flow modifiers and about 1600 roughness blocks. The blocks are grouped into a number of sectors and each sector can be individually controlled to reach a height between 0 and 12 inches to
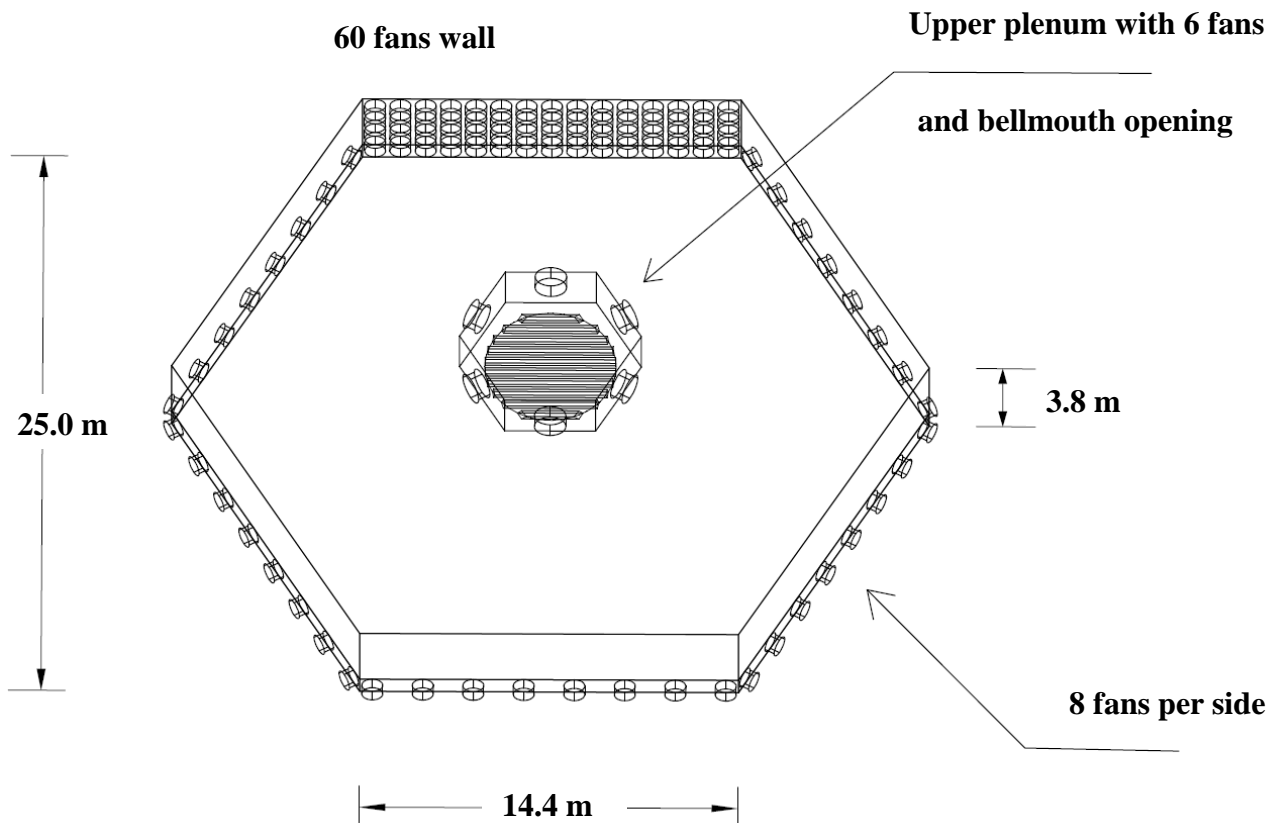
Figure 2- 2 Schematic view of the WindEEE dome as per (Jubayer et al. 2016)

simulate target terrain exposure for a wide range of length scales. Simulation of the downburst is performed by pressurizing the air in an upper room (called the upper plenum) using a number of 6 fans, and then opening the vents between the upper room and the space underneath to form the downdraft. The vents connecting the room to the space underneath operate in a circular nozzle (called the bell mouth) as shown in Figure 2- 2. The bell mouth allows for simulating downbursts with variable jet diameters (here it was set to 3.2 m) and it has a height of 3.8 m from the ground. Although this leads to relatively small diameter-to-height ratio of 1.2, such a small ratio was proven adequate for producing reliable downburst wind field (Aboshosha et al. 2015 and Elawady et al. 2017). After impingement, the flow convects radially until it reaches the lower peripheral, which act as outlets by opening the louvers without the fans being operated. The downdraft speed depends on the power input to pressurizing air in the upper plenum and it was estimated at 4-9 m/s.
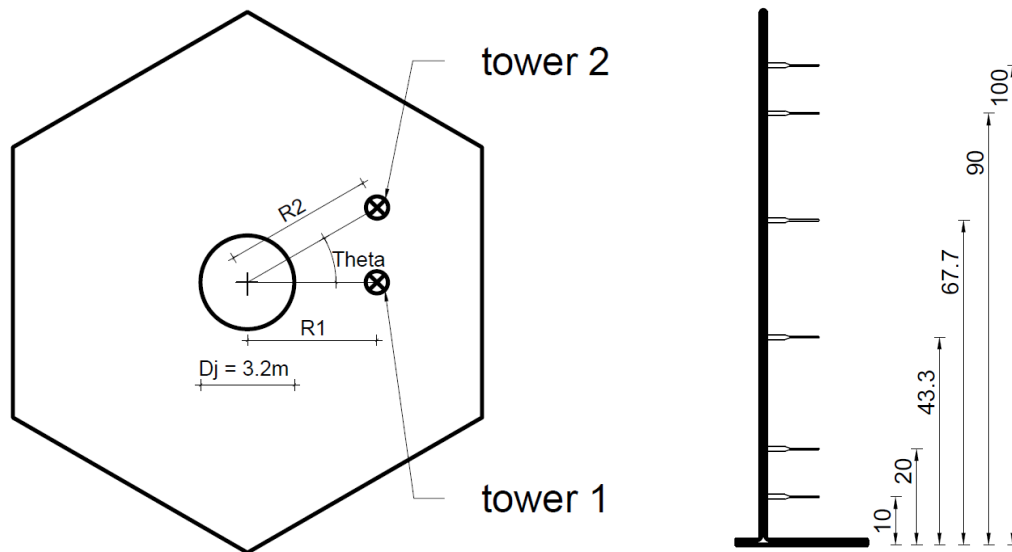
Figure 2- 3 Probe tower locations and probe heights in meters

A basic wind field was collected experimentally using 12 high-resolution cobra probes distributed evenly on 2 towers as shown in Figure 2- 3 and operating at a sampling frequency of 156 Hz. These probes were oriented towards the chamber's centre to align the downburst radial velocity component with the longitudinal component of the probes. Since the flow field was characterized by only 2 towers, multiple downburst tests were conducted while altering the tower locations. The location of the first tower is referred to as **R1** and the second tower location is referred to as **R2** as shown in Figure 2- 3. The first tower was consistently placed at the location of the maximum radial speed which was found to be at **R1**=1.0 **D$_j$**. The second tower was placed at a variable distance **R2** ranging between 0.7 **D$_j$** and 3.0 **D$_j$** and at an angle theta ranging between -60 to +60 degrees. The measurements were retaken to assess the repetitiveness of the profiles corresponding to certain fan power and it was found satisfactory.
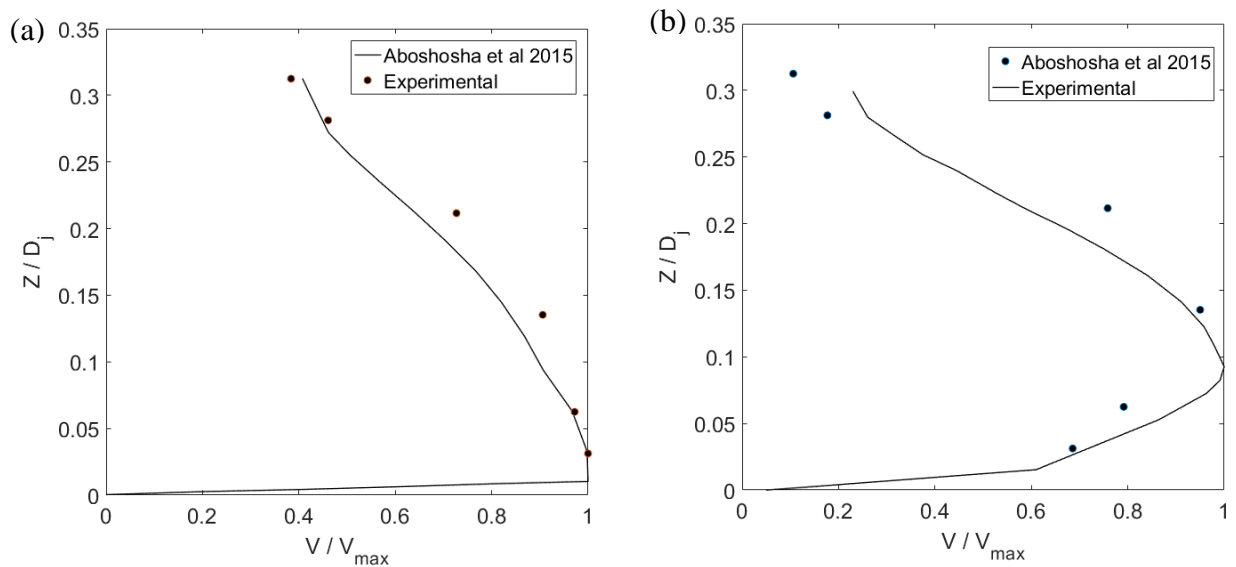
Figure 2- 4 Radial velocity profiles comparison for (a) open and (b) suburban terrain

Open and suburban terrain exposures were simulated by setting the roughness blocks at 6 and 9 inches respectively. The profiles of the mean radial velocities resulting from the chosen block heights were compared with those simulated by Aboshosha et al. (2015) for open and suburban exposures and have shown a good agreement as indicated in Figure 2-4.
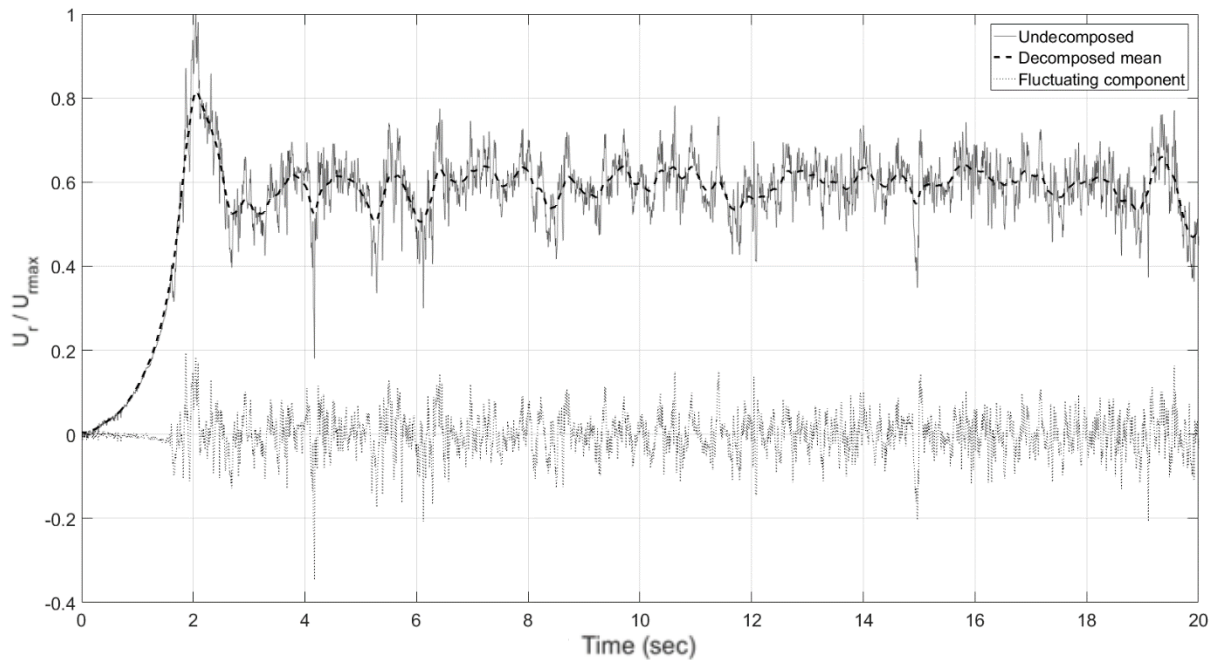
Figure 2- 5 Decomposed time history

Highlighting the comparison discussed above, the mean component was extracted from the time histories using a decomposition technique similar to that reported by Holmes et al. (2008). The decomposition technique relies on the shedding frequency, where the cut-off frequency, separating the mean and the fluctuating component, is taken as a multiple of the shedding frequency. This technique will be discussed in more details in the following section. Figure 2- 5 shows the decomposed time history acquired using the mentioned technique.

2.3   Numerical Model Setup

Computational Fluid Dynamic (CFD) simulations replicating the downbursts simulated at the WindEEE dome are discussed in this section. First, details about the governing equations and CFD solver are provided. This is followed by a description of the employed model, boundary conditions and details of the simulation are presented.

2.3.1   LES Governing Equations

CFD models were conducted using Large Eddy Simulation (LES) due to its efficacy to properly simulate the turbulent component and thus the transient details of the flow field. Naiver-Stoke Equations presented by equations (2-1~2-5) are resolved at each time step using ANSYS FLUENT solver (ANSYS Inc. 2016)) employing the dynamic sub-grid model introduced by Germano et al. (1991) and then modified by Lilly (1992). In this model, the model constant C_s (in equation 2-5) is computed dynamically based on the resolved flow field and has proven to properly simulate the turbulence energy dissipation. Pressure and velocity coupling was conducted using Pressure-Implicit with Splitting of Operators (PISO) scheme. This scheme has proven to outperform for cells with relatively high skewness. This usually proves worthy, although the computing time per iteration might increase compared to the other coupling schemes. As for the spatial discretization, the Least Squares Cell Based, Second Order and Bounded Central Differencing schemes are used for gradient, pressure and momentum discretization respectively. Finally, for the temporal discretization, second-order implicit time integration was chosen. These choices were based on the recommendations and descriptions of all available schemes in the program's documentation (ANSYS Inc. 2016).

$$\frac{\partial \bar{u}_\iota}{\partial t} + \bar{u}_j \frac{\partial \bar{u}_\iota}{\partial x_\iota} = -\frac{1}{\rho}\frac{\partial \bar{P}}{\partial x_\iota} + \frac{\partial}{\partial x_j}\left(-\tau_{ij} + 2\nu \overline{S_{ij}}\right) \tag{2-1}$$

$$\tau_{ij} = \overline{u_\iota u_j} - \overline{u_\iota}\,\overline{u_j} \tag{2-5}$$

$$\overline{S_{ij}} = \frac{1}{2}\left(\frac{\partial \bar{u}_\iota}{\partial x_j} + \frac{\partial \bar{u}_j}{\partial x_\iota}\right) \tag{2-3}$$

$$\tau_{ij} - \frac{1}{3}\delta_{ij}\tau_{kk} = -2\nu_e \overline{S_{ij}} \tag{2-4}$$

$$\nu_e = (C_s \Delta)^2 |\overline{D}| \tag{2-5}$$

Where u, t, ρ, P, τ, ν and S stand for velocity, time, density, pressure, subgrid-scale turbulent stresses, molecular viscosity coefficient and the strain rate tensor. The i, j and k annotations represent the along, across and out-of-plane directions. ν_e is the eddy viscosity, $|\overline{D}|$ is the grid scale tensor, Δ is the cell size and C_s is the Smagronisky constant.

2.3.2   Model Details

The computational domain was carefully constructed to include most of the elements utilized in the experimental setup as shown in Figure 2- 6. This includes detailed modeling of the inflow condition (i.e. the bell mouth with the opening flaps, roughness blocks and the outflow condition). As shown in Figure 2- 6, the bell mouth was fully modelled with its flaps (vents). The plenum on the other hand was spared, where a constant velocity with synthesized turbulence inlet boundary condition with the jet diameter shall suffice to resemble its physical role. Turbulence intensity of the downdraft was unknown during the test since there was no cobra probe placed in the test near the bell mouth. To account for this in the simulation, three downdraft turbulent intensities of 0%, 7% and 15 % were

considered and the simulation was repeated for each. It was found that the results for the

7% turbulence intensity led to the best match with the experiment as will be discussed later

in the following section.
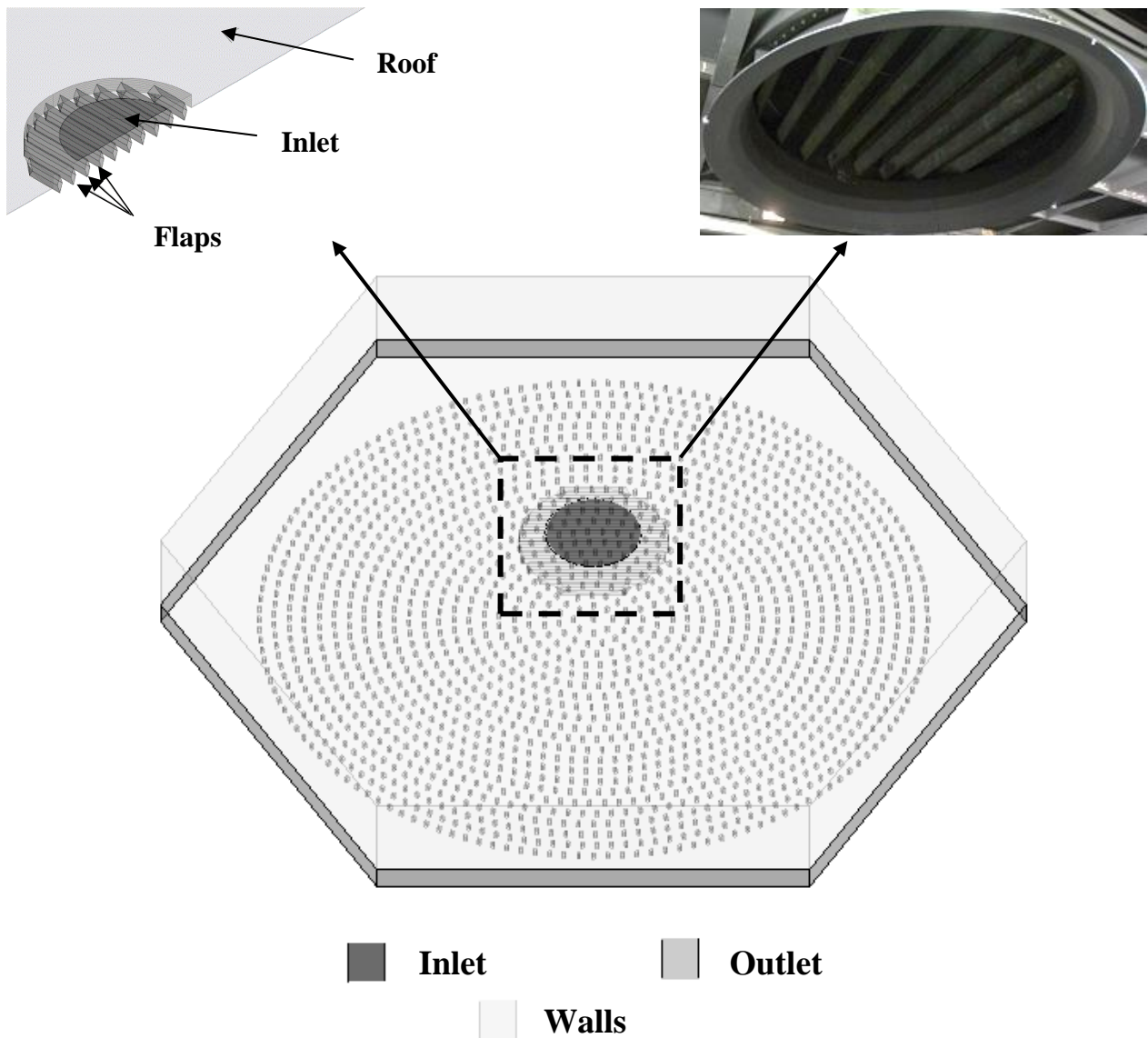
Figure 2- 6 Boundary conditions assignment for different boundaries with details of inlet

The roughness blocks were simulated exactly as they were considered during the test. A

number of 1600 blocks was used with a block dimension of 4 x 4 inches (~10 cm x 10 cm)

by either 6 or 9" (15 cm 22.5 cm) for open and suburban exposures. As for the outlet, the geometric projection of the peripheral was modelled as a continuous surface throughout the perimeter, where the louvers of the fans were not modelled due to their insignificance on the flow features.
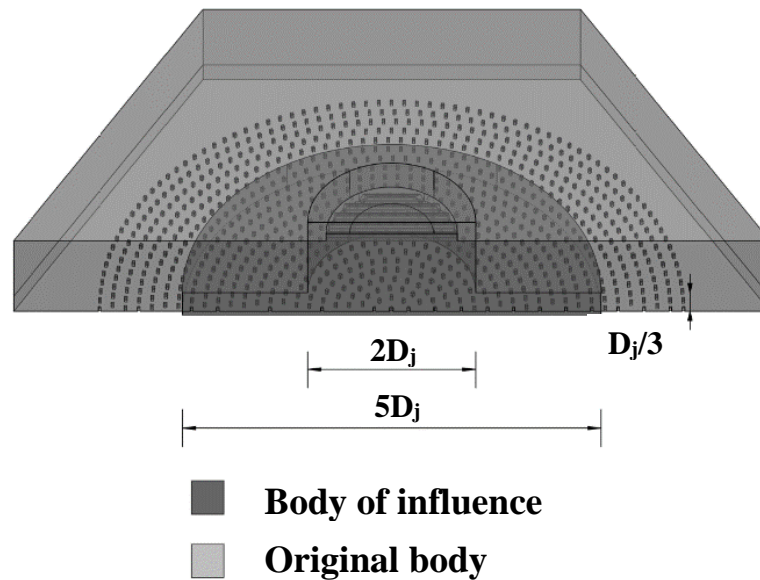
Figure 2- 7 Influence Zone

After constructing the model, ANSYS Mesher software was utilized to produce a volumetric grid to resolve the flow. The mesh density distribution was chosen such that the volume where the main flow develops shall have consistent grid size. Figure 2- 7 shows the volumetric section where the influence zone was chosen. As demonstrated, the zone was chosen to bound the core of the flow at a diameter of twice the jet diameter descending from the inlet. Stretching beyond the jet diameter was decided to make sure the development of vortices due to Kelvin-Helmholtz instability is fully captured within the fine grid range. In addition, the lower segment of the domain, where the convective flow is expected to occur, was also included in the fine grid zone. This zone was truncated at a radial distance of 2.5 times the jet diameter for computational efficiency.
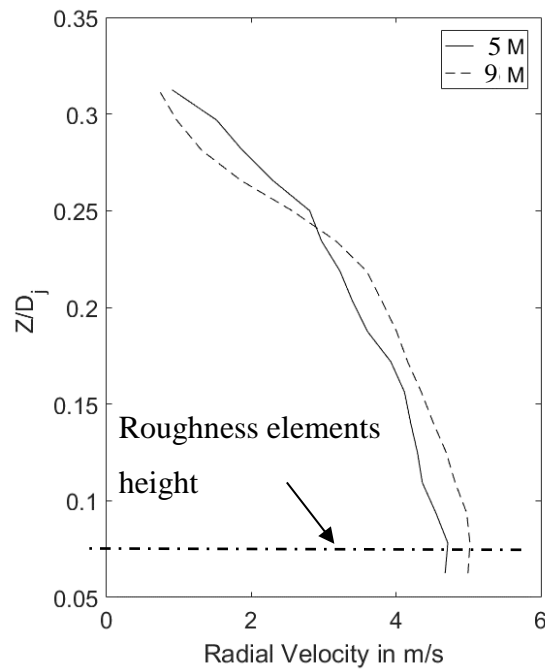
Figure 2- 8 Grid dependency plot

Choosing polyhedral cells due to their efficiency in resolving rotational flows (ANSYS Inc. 2016), a total cell count of ~ 5 million for a cell size of D_j/64, and ~9 million for a cell size of D_j/80 were obtained. A limited grid independence test was carried out for the two grids based on the profiles of the maximum mean velocities. The resulting profile from both grids is shown in Figure 2- 8, which demonstrates that both grids leads to compatible profiles. It should be noted that the region beneath the dashed line in the figure has been excluded from the plot, as it resembles the height that would be affected by the roughness elements. The maximum difference between the two profiles was found less than 5%, which indicates the grid independency of the results. It is worth to note that the coarser grid (i.e. 5 million cells) was utilized in presenting the results. Figure 2- 9 shows a comparison between the CFD velocity contours and the experimental smoke visualization, showing the relevance between the developed main vortex in both simulations.

Main vortex
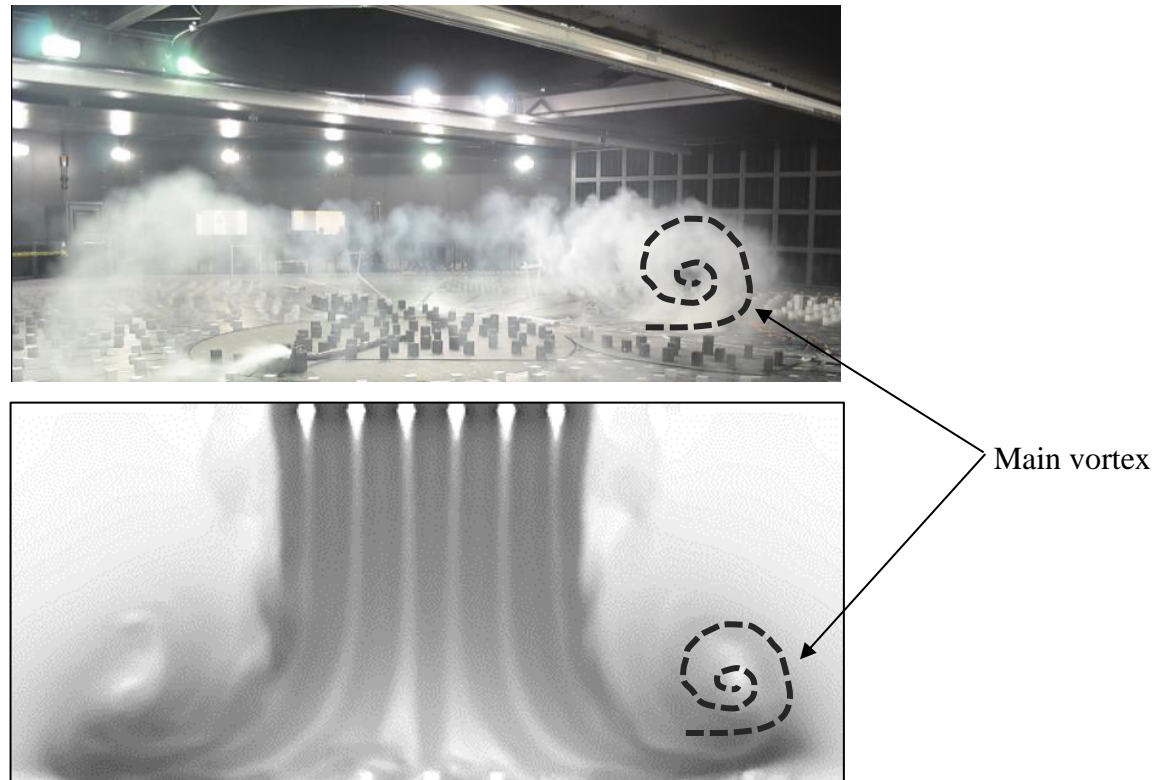
Figure 2- 9 Experimental smoke visualization vs CFD velocity contour

2.4   Results and Discussion

The CFD model described in the earlier section was utilized to obtain the wind field for the

downburst simulation and the resulting wind field is discussed in this section. First, an

overview of the transient nature of the wind field is presented, which is then followed by

describing the utilized technique to decompose the wind field into a non-stationary

"running" mean component and a turbulent component. Afterwards, a comparison between

mean and turbulent components of the wind field obtained from the CFD simulations with

those obtained from the experiment is provided.

2.4.1   Development of Wind Field

Snapshots of the velocity contours of different time instants showing how the wind field

gradually develops through the domain can be seen in Figure 2- 10. The snapshots are

calibrated in τ, which is the time normalized by the peak radial velocity instant. At the beginning of the simulation, when the flow is released from the inlet boundary, the presence of the flaps with their considerable cross-section generally impacts the flow. This can be deduced throughout the whole time range, where the flaps cause streaming of the flow within the region of pre-impingement. The streaming limits the contribution of the inner region of the descending downdraft to the interaction between the downdraft and the ambient air. Such interaction can be seen in the first three time instances (i.e. $\tau = 0.2$, 0.4 and 0.6) where the Kelvin-Helmholtz instability is formed as a result of the shear between the descending and the still air. After that, time instances beyond the impingement ($\tau > 0.8$), illustrate the radial convection mechanism, where the transported vortices are obstructed by the roughness elements. The influence of the modelled elements can be generally described as turbulence generators for the convecting flow. Yet, some important features can be noticed from the figure. Firstly, the roughness elements right below the centre of the jet can be clearly seen to entrap flow structures ($\tau > 0.6$). The fact that the dimensions of the modelled elements result in significant canopy zones can also be noted from the displayed figure. Adding to the streaming caused by the flaps, this is believed to result in preventing the inner core of the jet from contributing to the radial out flow after impingement. This means that the main driving force of the outflow is generated by the outermost part of the jet. Secondly, the main convecting vortex generally maintains its structure throughout the monitored period, surpassing the main areas of interest located at a jet diameter distance from the jet centre. The secondary vortex formed after impingement due to separation, that was reported by Kim and Hangan (2007) and Aboshosha et al. (2015) and can be seen to form the snapshot at $\tau = 1$. However, the following instances

show that the newly formed structure fails to keep up with the flow and diminishes as it encounters more roughness blocks. This can be again attributed to the size of the roughness elements, as well as the spacing between them which is comparable to that of the formed vortices, leading to destroying the structure of the secondary vortex. Accordingly, only the main vortex is able to maintain its structure and carry the driving energy for the radial convection. Thirdly, closely observing the development of the flow, secondary vortices formed due to quasi-static Kelvin-Helmholtz instability reported by Kim and Hangan (2007) can be noticed. These are the structures that follow the main vortex from the inlet, later as the flow progresses. Finally, while the impact of the flaps is clearly observable in Figure 2- 9, the roughness blocks also have a noticeable effect that can hardly be seen from the elevation view. Figure 2- 11 representing a planar view at an elevation right above the blocks height clearly demonstrates the effect they have on the flow. The unevenly distributed shades are revealing the shedding, channeling and irregularity the blocks impose on the flow. Noting that the block height is in the order of 5 and 7 percent of the jet diameter for the open and suburban exposures respectively, the canopy zone over shades the zone where peak radial velocities are expected.

$\tau = 0.2$ $\tau = 1.4$

$\tau = 0.4$ $\tau = 1.6$

$\tau = 0.6$ $\tau = 1.8$

$\tau = 0.8$ $\tau = 2.0$

$\tau = 1$ $\tau = 2.2$

$\tau = 1.2$ $\tau = 2.4$
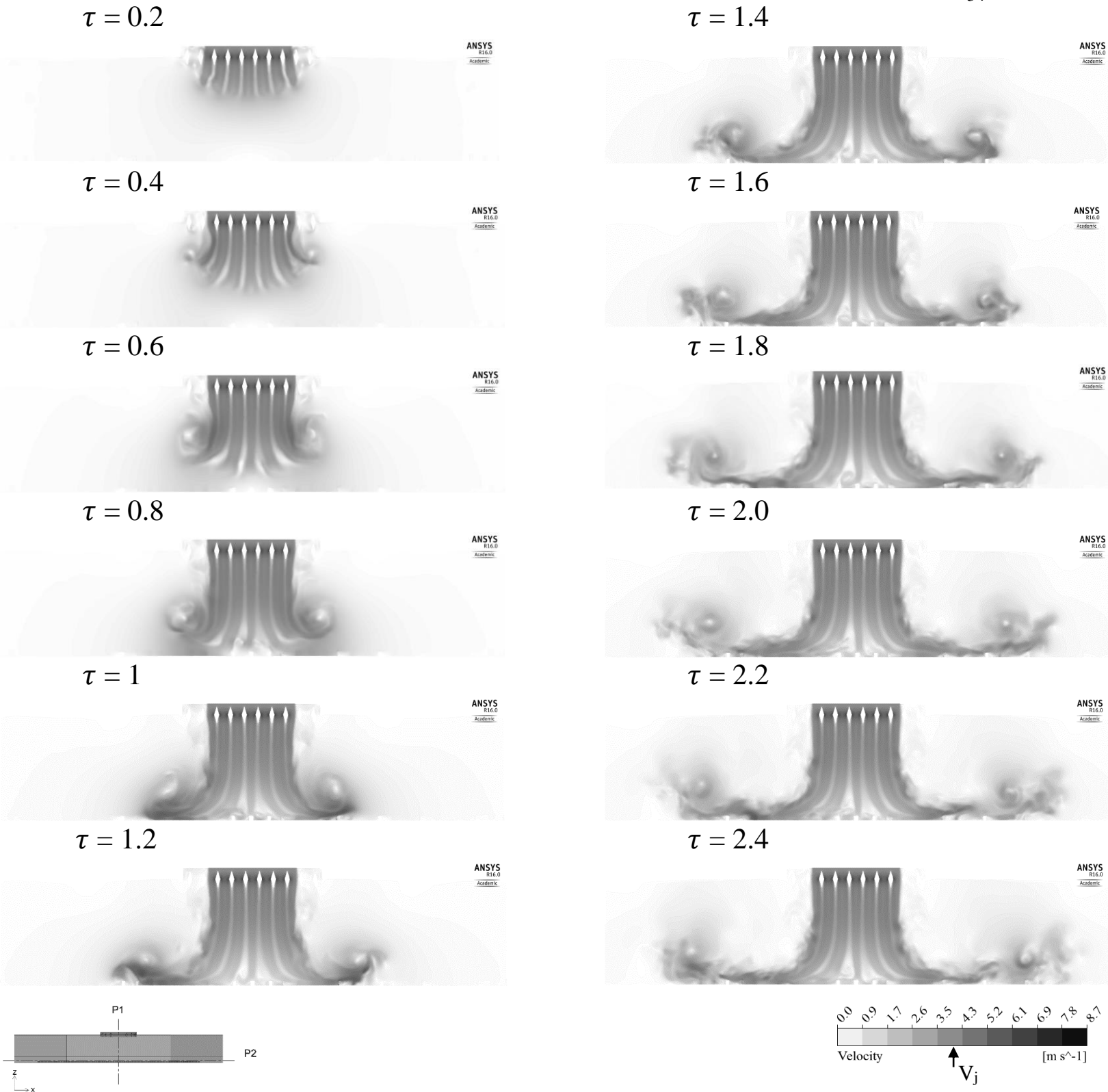
Figure 2- 10 Development of wind field represented by velocity contours for different $\tau = t / T_{max}$ at P1

Moreover, the plot shown in Figure 2- 12 illustrates the envelope of radial velocities distribution throughout the entire simulation. The data plotted show that peak radial velocities happen at a radial distance R of 1.0 D_j, a jet diameter measured from the jet centre. Although the location of the peak wind speed happens at a closer distance to the downdraft center compared with other simulations by Mason et al. (2009) and Aboshosha et al. (2015a) (R_{max}=1.0 D_j compared with 1.3 D_j), the obtained location well matches the location of peak wind speed seen in the experiment.

After a close observations, it was found that the streaming effect imposed by the flaps is the main reason that the peak radial velocity occurs at the closer radius to the center (R_{max}=1.0 D_j). This is relatively less than the values found in the literature, where studies like Aboshosha et al. (2015b) and Kim and Hangan (2007) found R_{max} to be in the order of 1.25~1.3. It is believed that simulating a model that follows the same physical conditions as the previous simulations (i.e. no flaps and roughness elements with less significant heights), R_{max} would reach the same values reported by previous researchers.
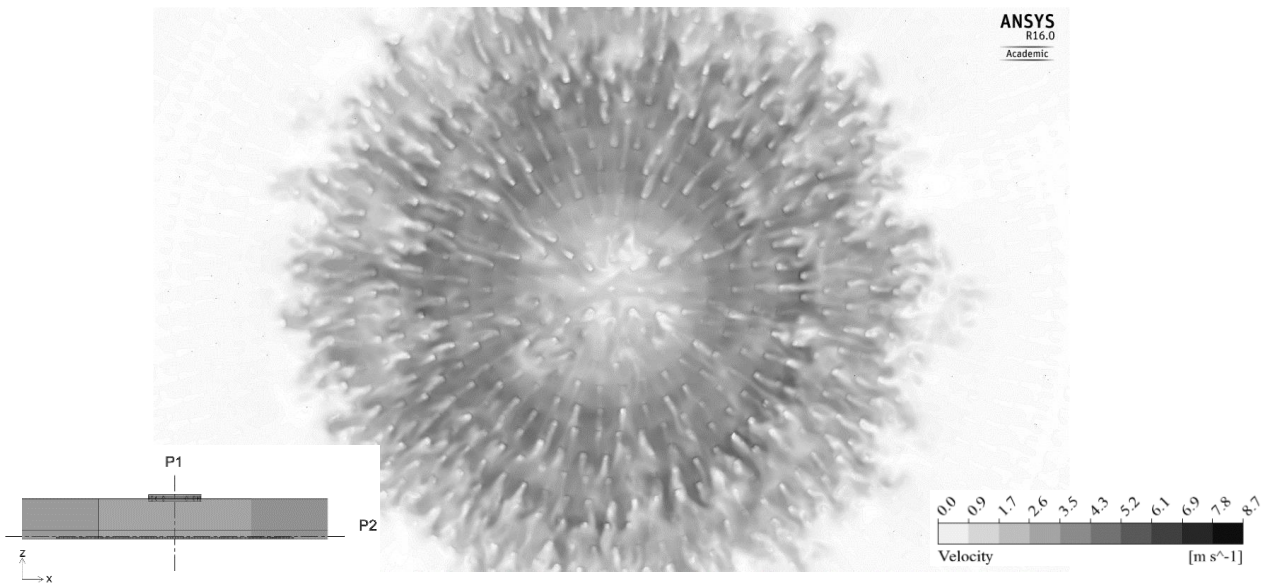
Figure 2- 11 Roughness blocks impact on the flow through velocity contour of horizontal plane at Z = 0.05 Dj at P2

Figure 2- 12 Envelope of peak radial velocities at P1
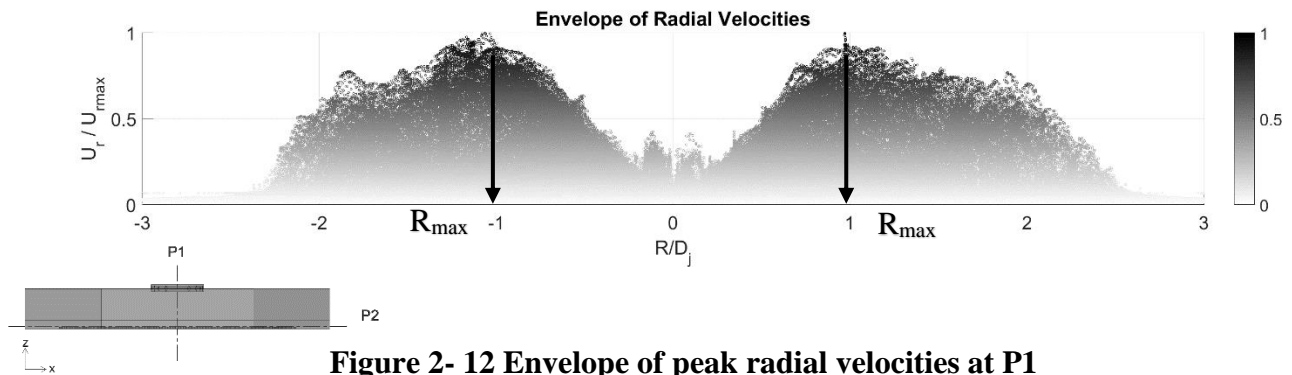
2.4.2   Wind Field Decomposition

The wind field associated with downburst events is uniquely distinguished by its non-stationarity which sets it apart from the conventional atmospheric boundary layer (ABL) flow. While ABL is characterized by a constant mean and a zero average fluctuating component, the downburst time history can only have a zero average fluctuating component when the mean is itself fluctuating. This is widely agreed upon in literature, where researchers like Holmes et al. (2008), Aboshosha et al. (2015a) and Solari et al. (2015b) used a moving average technique to discretize the mean component from the time history. The technique relies on an averaging window by which the time history is averaged within the range of this moving average, resulting in a slowly varying mean, while the residual is considered to be the zero average fluctuating component. The challenge here is to decide upon the value of this moving average window. The chosen value shall result in a mean component that resembles the main driving flow characteristics, without a significant fluctuating component. Researchers like Holmes et al. (2008) and Solari et al. (2015a) have tried different values of averaging periods, and relied on their judgement to decide on which period could result in mean and fluctuating components that satisfy the above criteria. Yet, researchers like Aboshosha et al. (2015a) relied on equation (2-6) to

calculate the averaging period T_{av} as being a factor X_{av}, taken to be 0.67 in this study, multiplied by the shedding period $T_{shedding}$. This technique with an averaging period less than the shedding vortex assures that main vortex is included in the running mean. This method was utilized in the current study to decompose running mean which was subtracted from the overall wind field to obtain the turbulent component. Figure 2- 13 illustrates the effect the factor X_{av} has on the mean value of the fluctuating component, which is expected to have a near zero value for a representative fluctuating component. As shown, different studies in the literature chose values generally smaller than unity. Although the current study seems to yield a higher mean of the residuals, the chosen value of 0.67 still resulted comparable results, where the mean of the fluctuating residuals is considerably small. Furthermore, the chosen value is shown to maintain the mean characteristics as indicated by Holmes et al. (2008) and Solari et al. (2015a), where the mean profile follows the general characteristics of the flow as shown in Figure 2- 14. The calculated averaging period is then applied to the velocity time history using a bi-directional moving average
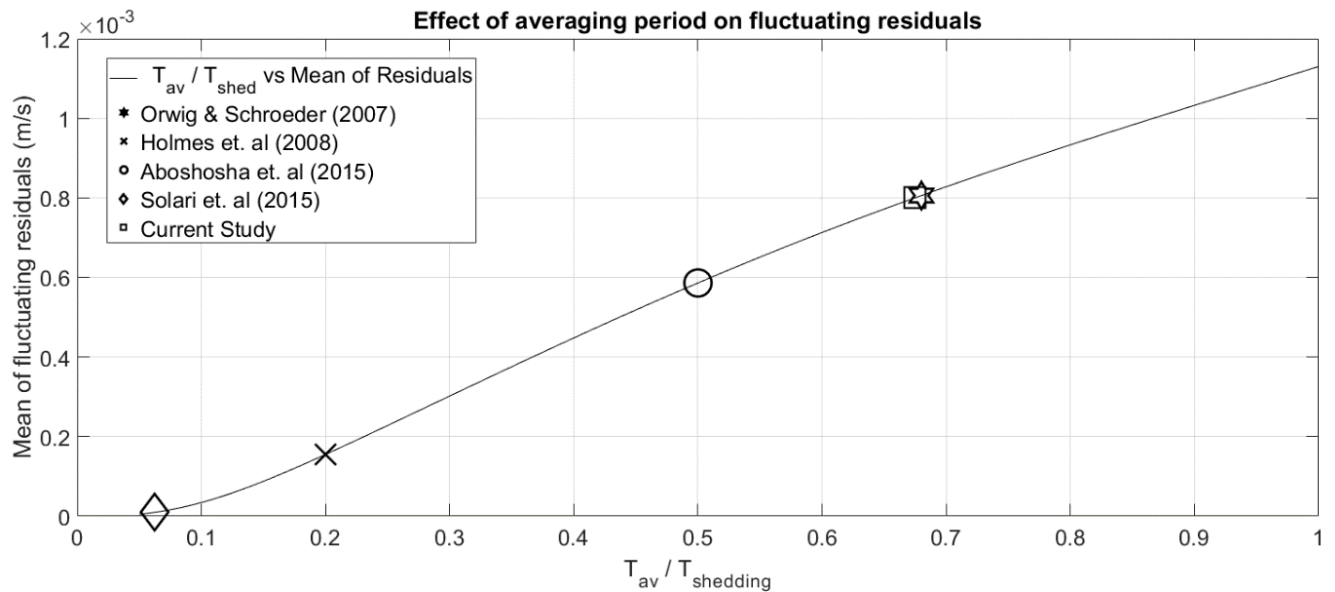
Figure 2- 13 Effect of averaging period on mean of fluctuating residuals

filter to eliminate the lag that would shift the decomposed mean in case of uni-directional averaging. The same technique was applied on the experimental results reported in the previous section.

$$T_{av} = X_{av} * T_{shedding} \qquad (2\text{-}6)$$

Applying the resulting moving average on the time history at a sample probe point, the resulting time histories are shown in Figure 2- 14. As shown in the figure, the total time history plotted contains fluctuation that was separated to a slowly varying mean, and a zero mean fluctuation. The velocity time history data was collected using a 3 dimensional grid of vertex averaging probes. Adding to the fact that polyhedral cells increase the accuracy due to better approximation of gradients between neighbouring cells, averaging in between vertices adds more confidence to the results monitored by probes.
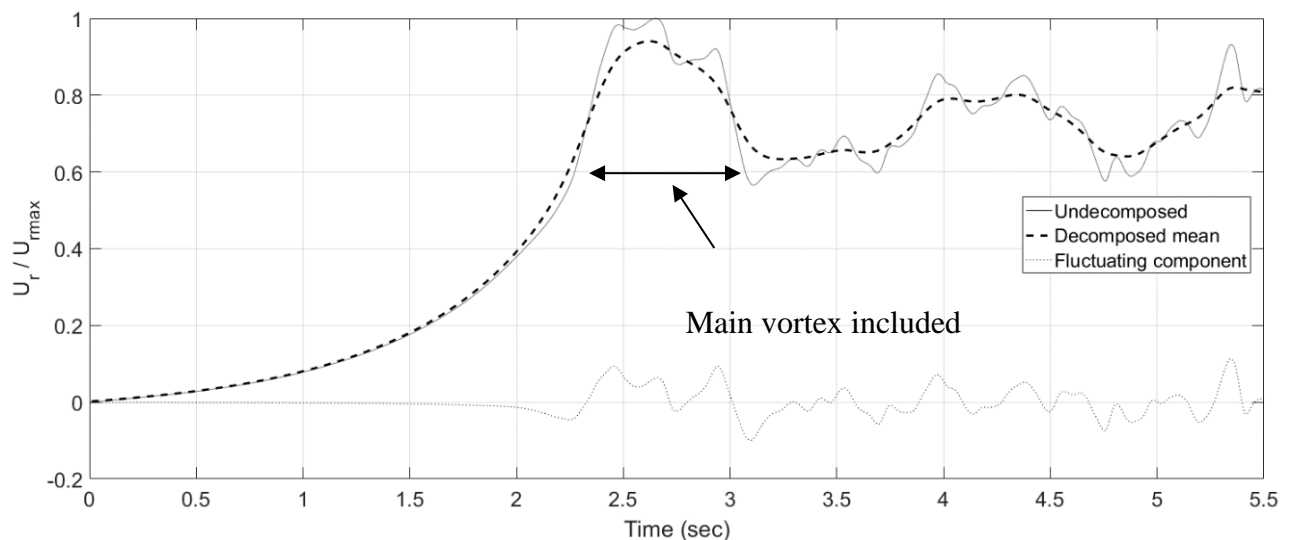
Figure 2- 14 Decomposed time history at R/Dj = 1 and Z/Dj = 0.078

2.4.3   Mean Component of Wind Field

A comparison between the CFD and the experimental mean components of the flow is shown in Figure 2- 15. The plot shows the decomposed mean profiles at a time instant corresponding to the occurrence of the peak mean radial velocity. Comparison between the CFD and the experimental data show satisfying agreement within the monitored range. Yet, due to the impact of the roughness elements on the flow, shown in Figure 2- 11 and discussed above, no probe points were taken below the height of the roughness blocks for both the open and the suburban exposures. It was expected that, below the roughness height, either shedding or channeling effects would yield misleading results. Therefore, although being one of the key parameters for wind engineering, the height at which the peak velocity occurs was not detected due to it being within the canopy zone of the roughness blocks.
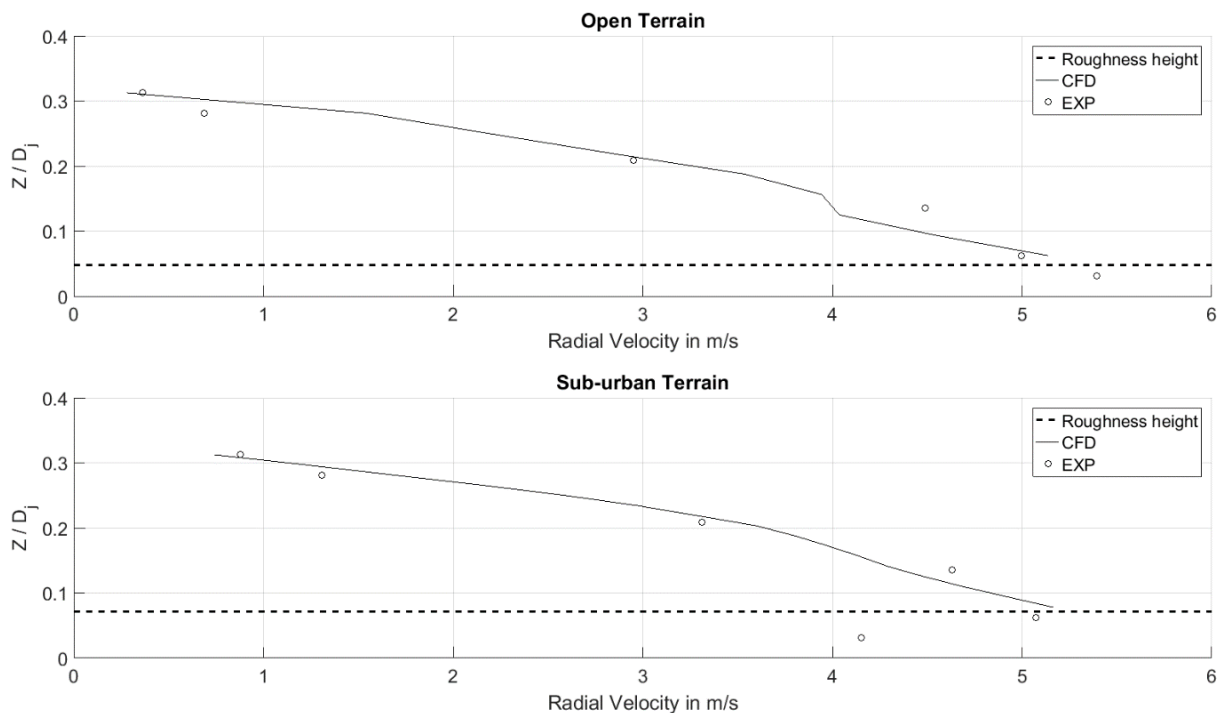
Figure 2- 15 Mean radial velocity validation

2.4.4 Turbulent Component of Wind Field

2.4.4.1 Turbulence Spectra

Power spectral density of the turbulence resulting from the decomposition technique discussed earlier was generated and plotted in Figure 2- 16 at the location of the maximum mean (i.e. R_{max}=1.0 D_j) for the open and suburban terrains. Power spectral density function of the turbulent speeds obtained from the experiment are also shown in the figure for comparison purpose. As seen from the figure, both PSDFs are in a good agreement.
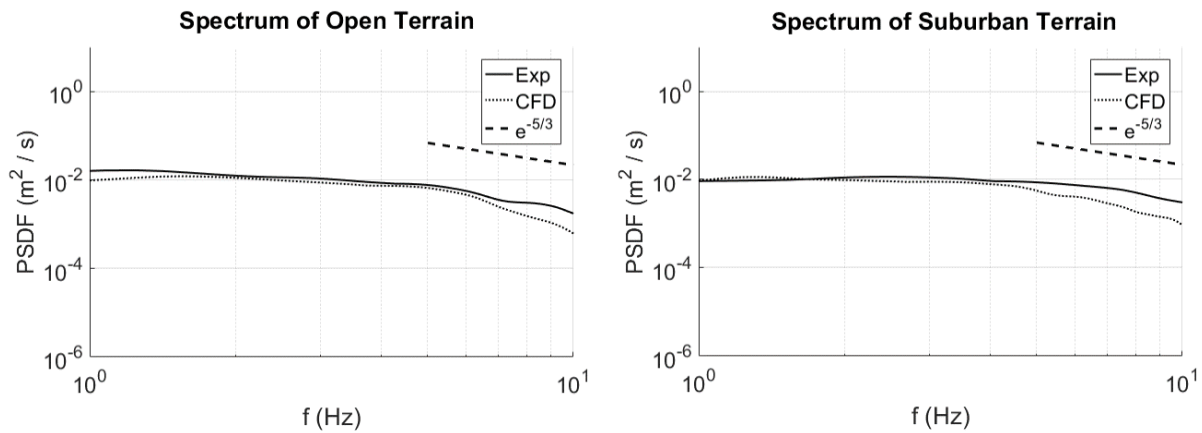
Figure 2- 16 Power spectral density function validation

Match between CFD PSDF and experimental PSDF is up to a certain frequency, which is the maximum frequency of the resolvable eddies by the employed computational mesh. This maximum frequency was found equal to 7Hz. It is worth to mention that PSDF for downburst speeds converged to the -5/3 power after a frequency of 5 (<7) Hz for both experiential and numerical simulations. It is also important to note that the CFD predicted turbulent component is missing the contribution form high frequencies.
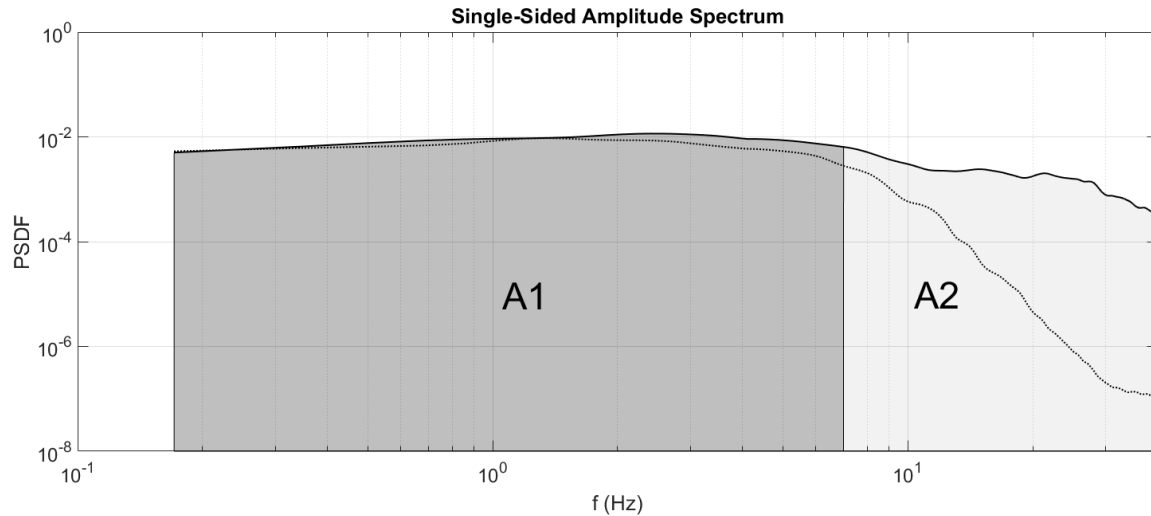
Figure 2- 17 Effect of LES grid size on captured frequencies (-) EXP (….) CFD

Figure 2- 17 shows the area under the curve where the LES simulation could capture frequencies (*A1*), compared to the area where the simulation could no longer detect frequencies (*A2*). Although the current simulation used a relatively fine grid size, the ratio between A1 to the total area (*A1+A2*) is about 40%. This is also evident from the plots illustrated in Figure 2- 18, showing the turbulence intensity profiles for different turbulence intensities specified at the inlet boundary conditions. It appears that the 7% profile gives the best match, where the ratio between the experimental and the numerical turbulence intensities is roughly 1.7~1.9. The plot also shows the corrected turbulence intensity profile of the 7% inflow turbulence after correcting it with the factor of 1.8. Accordingly, the simulation with 7% turbulence intensity at the inlet will be used from this point forward.
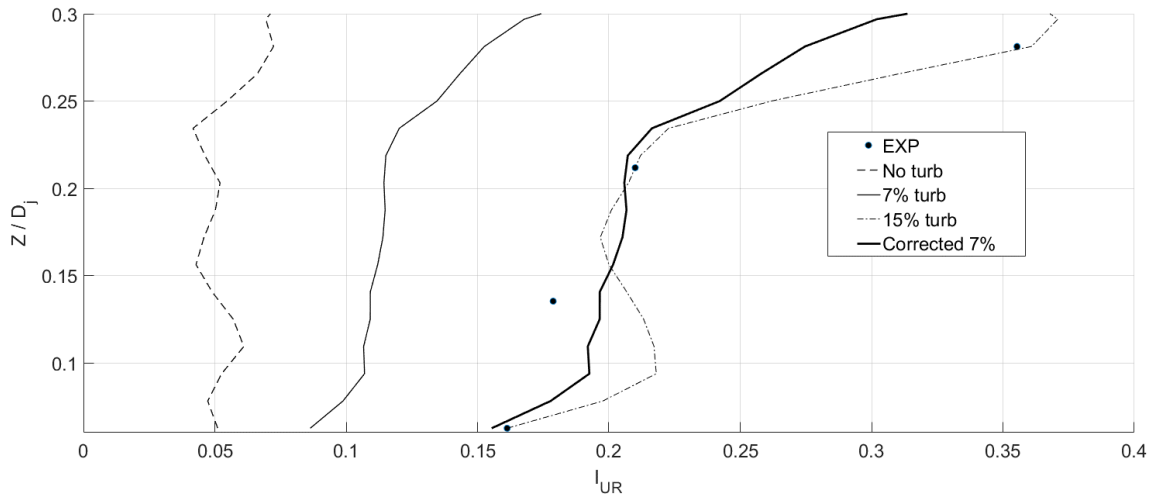
Figure 2- 18 Turbulence intensity profile for different inlet turbulence ratios

2.4.4.2   Turbulence Intensity

Turbulence intensity (I_{ur}) represents an important parameter that indicates the relation between the mean and the peak values of turbulent flows. Following equation (2-7), the turbulence intensity is generally defined as the ratio between the statistical root mean square and the mean value of time history. Yet, the fact that the mean component of downburst wind field is not a constant value, requires some adjustment to account for the non-stationarity of downbursts. Accordingly, the statistical properties are calculated within a certain range rather than the complete time history. Following Holmes et al. (2008) and Aboshosha et al. (2015a), the turbulence intensities were calculated at time instants where the maximum mean velocities occurred. With the time instant known, the clipped range at which statistical properties were computed spreads one half of the averaging period before and after the specified instance. As shown in equation (2-8), the value of the total undecomposed velocity ($u(t)$) and the mean velocity corresponding to the considered time step ($\overline{u}(t)$) are used in calculating the standard deviation (σ_{range}) of the considered range.

$$I_{ur} = \frac{\sigma_{range}}{U_{mean\,range}} \qquad (2\text{-}7)$$

$$\sigma_{range} = \sqrt{\frac{\sum(|u(t) - \bar{u}(t)|)^2}{n - 1}} \qquad (2\text{-}8)$$

With that, the time frame is clear to be a representation of the most important range, that of the maximum mean instant. As for the spatial frame, the turbulence intensities were computed for vertical profiles of different radial distances. Aiming to know the variation of I_{ur} along both the vertical and the radial directions, Figure 2- 20 and Figure 2- 19 show the envelope distribution of I_{ur} along the vertical height at different radial locations for the Open and the Suburban exposures respectively. The values displayed have been corrected by multiplying the turbulence intensities by the ratio between the experimental and the numerical values discussed in the previous section. It can be noted that the turbulence intensity generally decreases with height for the considered range, which agrees with the results reported by Aboshosha et al. (2015a). Moreover, to be able to assess the values plotted, the envelope mean velocities were also plotted for the same considered spatial range. This would provide comparable results to be able to judge the significance of the reported turbulence intensity values. As shown, the turbulence intensities corresponding to the location of maximum mean velocities are between 16 and 23 % for the open and suburban exposures respectively. This is relatively high compared to previous values reported in the literature, which are available for open terrains. This is believed to be a direct result of the roughness elements used, which yield higher turbulence than anticipated.
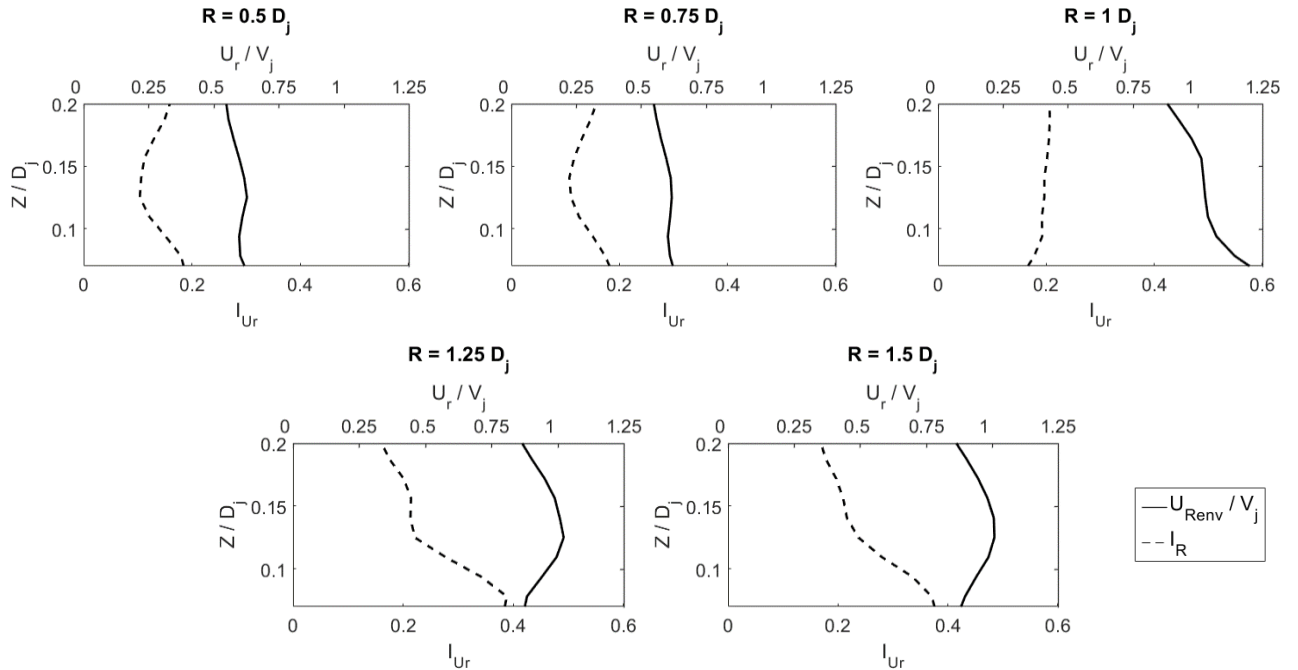
Figure 2- 20 Turbulence intensity vs mean velocity envelope distribution along height for different radial distances for Open Terrain
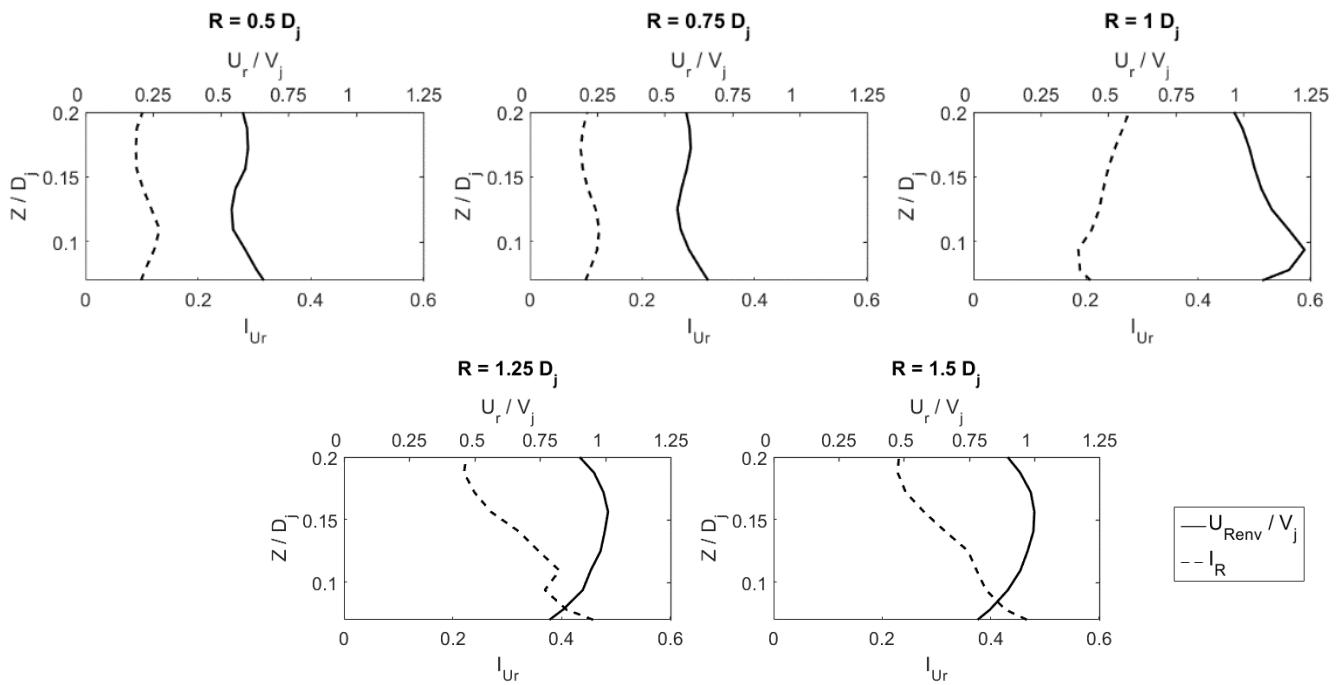
Figure 2- 19 Turbulence intensity vs mean velocity envelope distribution along height for different radial distances for Suburban Terrain

2.5   Conclusions

The current study mainly presented a replication of the downburst simulation done in wind tunnel testing scale in the WindEEE dome for two exposures, open and suburban. The simulation was repeated using a LES with an enhanced grid resolution to capture the flow characteristics through the space and time frames. Afterwards, the analyses results were compared with the experimental results to both validate the CFD results, as well as interpret some of the flow features shown in the experimental results. The following points summarize the findings of results comparison:

1- The comparison of mean wind speeds showed good agreement between the experiment and the CFD simulation.

2- Both results showed maximum radial speeds occurring at radial distance equal to the jet diameter, noticeably less than values in the literature. This is suggested to be attributed to the inlet flaps cross-section, as well as the roughness elements used.

3- Examining the wind field development showed the flaps had a streaming effect on the flow. It was shown that the effect was manifested through the streaming imposed on the descending downdraft. The roughness blocks were also shown to canopy the region within their height, as well as entrap the inner portion of the downdraft column.

4- Comparisons of the turbulence characteristics showed a good agreement within the range where the CFD model could resolve frequencies. In addition, after accounting for the unresolvable scales, the corrected turbulence intensity profiles were presented against the envelope mean radial velocity profiles. Results showed

turbulence ranged between 16 to 23% at the peak velocity positions for open and suburban exposures.

Most importantly, the current study provides a validated CFD model, that replicated a wind tunnel scale experiment, and yielded acceptable results. This can be used to model simulations of higher complexity, in full scale, to explore finer details of the downburst wind field. The validated wind field can also be used to validate structural experimental results as will be shown in the following chapter.

2.6   References

Aboshosha, H., Bitsuamlak, G., El Damatty, A.A., (2015a). Turbulence characterization of downbursts using LES. J. Wind Eng. Ind. Aerodyn. 136, 44–61. doi:10.1016/j.jweia.2014.10.020

Aboshosha, H., Elawady, A., El Ansary, A., El Damatty, A.A., (2016). Review on dynamic and quasi-static buffeting response of transmission lines under synoptic and non-synoptic winds. Eng. Struct. 112, 23–46. doi:10.1016/j.engstruct.2016.01.003

Aboshosha, H., Elshaer, A., Bitsuamlak, G.T., El Damatty, A.A., (2015b). Consistent inflow turbulence generator for LES evaluation of wind-induced responses for tall buildings. J. Wind Eng. Ind. Aerodyn. 142, 198–216. doi:10.1016/j.jweia.2015.04.004

ANSYS Inc., (2016). ANSYS® FLUENT, Release 17.0,Theory Guide.

Chay, M.T., Albermani, F., Wilson, R., (2006). Numerical and analytical simulation of downburst wind loads. Eng. Struct. 28, 240–254. doi:10.1016/j.engstruct.2005.07.007

Chay, M.T., Letchford, C.W., (2002). Pressure distributions on a cube in a simulated thunderstorm downburst. Part B: Moving downburst observations. J. Wind Eng. Ind. Aerodyn. 90, 733–753. doi:10.1016/S0167-6105(02)00163-0

Choi, E.C.C., (2004). Field measurement and experimental study of wind speed profile during thunderstorms. J. Wind Eng. Ind. Aerodyn. 92, 275–290. doi:10.1016/j.jweia.2003.12.001

Das, K.K., Ghosh, A.K., Sinhamahapatra, K.P., (2011). Physical simulation of dry microburst using impinging jet model with swirl. Int. J. Eng. Sci. Technol. 3, 20–29.

Dempsey, D., White, H.B., (1996). Winds wreak havoc on lines. T&D World Mag. 32–42.

Elawady, A., Aboshosha, H., Damatty, A. El, Bitsuamlak, G., Hangan, H., Elatar, A., (2017). Aero-elastic testing of multi-spanned transmission line subjected to downbursts. J. Wind Eng. Ind. Aerodyn. 169, 194–216. doi:10.1016/j.jweia.2017.07.010

Elawady, A., Aboshosha, H., El Damatty, A.A., Bitsuamlak, G., (2016). Wind tunnel testing of a multiple span aeroelastic transmission line, in: Resilient Infrastructure, CSCE 2016. London, Ontario, Canada.

Elshaer, A., Aboshosha, H., Bitsuamlak, G., El Damatty, A.A., Dagnew, A., (2016). LES evaluation of wind-induced responses for an isolated and a surrounded tall building. Eng. Struct. 115, 179–195. doi:10.1016/j.engstruct.2016.02.026

Fujita, T.T., (1985). The downburst: microburst and macroburst. Satellite and Mesometeorology Research Project (SMRP). Res. Pap. 210, Dep. Geophys. Sci. Univ. Chicago.

Germano, M., Piomelli, U., Moin, P., Cabot, W.H., (1991). A dynamic subgrid-scale eddy viscosity model. Phys. Fluids A 3, 1760. doi:10.1063/1.857955

Gunter, W.S., Schroeder, J.L., (2015). High-resolution full-scale measurements of thunderstorm outflow winds. J. Wind Eng. Ind. Aerodyn. 138, 13–26. doi:10.1016/j.jweia.2014.12.005

Hadžiabdić, M., (2006). LES, RANS and Combined Simulation of Impinging Flows and Heat Transfer. Simulation.

Hjelmfelt, M.R., (1988). Structure and life cycle of microburst outflows observed in Colorado. J. Appl. Meteorol. 900–927.

Holmes, J.D., Hangan, H.M., Schroeder, J.L., Letchford, C.W., Orwig, K.D., (2008). A forensic study of the Lubbock-Reese downdraft of 2002. Wind Struct. An Int. J. 11, 137–152. doi:10.12989/was.2008.11.2.137

Jubayer, C., Elatar, A., Hangan, H., (2016). Pressure distributions on a low-rise building in a laboratory simulated downburst, in: 8th International Colloquium on Bluff Body Aerodynamics and Applications. Northeastern University, Boston, Massachusetts, USA.

Kim, J., Hangan, H., (2007). Numerical simulations of impinging jets with application to downbursts. J. Wind Eng. Ind. Aerodyn. 95, 279–298. doi:10.1016/j.jweia.2006.07.002

Li, C.Q., (2000). A stochastic model of severe thunderstorms for transmission line design. Probabilistic Eng. Mech. 15, 359–364.

Li, H., Ou, J., (2012). Experimental simulation of downburst-generated wind loading on building structure, in: The Seventh International Colloquium on Bluff Body Aerodynamics and Applications (BBAA7). Shanghai, China, pp. 1266–1275.

Lilly, D.K., (1992). A proposed modification of the Germano subgrid-scale closure method. Phys. Fluids A 4, 633. doi:10.1063/1.858280

Lin, W.E., Orf, L., Savory, E., Novacco, C., (2007). Proposed large-scale modelling of the transient features of a downburst outflow. Wind Struct. An Int. J. 315–345.

Mason, M.S., Fletcher, D.F., Wood, G.S., (2010). Numerical simulation of idealised three-dimensional downburst wind fields. Eng. Struct. 32, 3558–3570. doi:10.1016/j.engstruct.2010.07.024

Mason, M.S., Letchford, C.W., James, D.L., (2005). Pulsed wall jet simulation of a stationary thunderstorm downburst, Part A: Physical structure and flow field characterization. J. Wind Eng. Ind. Aerodyn. 93, 557–580. doi:10.1016/j.jweia.2005.05.006

Mason, M.S., Wood, G.S., Fletcher, D.F., (2009). Numerical simulation of downburst winds. J. Wind Eng. Ind. Aerodyn. 97, 523–539. doi:10.1016/j.jweia.2009.07.010

McConville, A.C., Sterling, M., Baker, C.J., (2009). The physical simulation of thunderstorm downbursts using an impinging jet. Wind Struct. An Int. J. 12, 133–139. doi:10.12989/was.2009.12.2.133

Orwig, K.D., Schroeder, J.L., (2007). Near-surface wind characteristics of extreme thunderstorm outflows. J. Wind Eng. Ind. Aerodyn. 95, 565–584. doi:10.1016/j.jweia.2006.12.002

Otsuka, K., (2006). Effects of topography on the surface wind of an isolated wet microburst, in: The Fourth International Symposium on Computational Wind Engineering. Yokohama, Japan, pp. 463–466.

Sengupta, A., Haan, F.L., Sarkar, P.P., Balaramudu, V., (2008). Transient loads on buildings in microburst and tornado winds. J. Wind Eng. Ind. Aerodyn. 96, 2173–2187. doi:10.1016/j.jweia.2008.02.050

Sengupta, A., Sarkar, P.P., (2008). Experimental measurement and numerical simulation of an impinging jet with application to thunderstorm microburst winds. J. Wind Eng. Ind. Aerodyn. 96, 345–365. doi:10.1016/j.jweia.2007.09.001

Solari, G., Burlando, M., Gaetano, P. De, Repetto, M.P., (2015a). Characteristics of thunderstorms relevant to the wind loading of structures. Wind Struct. 20, 763–791. doi:10.12989/was.2015.20.6.763

Solari, G., De Gaetano, P., Repetto, M.P., (2015b). Thunderstorm response spectrum: Fundamentals and case study. J. Wind Eng. Ind. Aerodyn. 143, 62–77. doi:10.1016/j.jweia.2015.04.009

Tamura, Y., Kareem, A., (2013). Advanced structural wind engineering, Advanced Structural Wind Engineering. doi:10.1007/978-4-431-54337-4

Vermeire, B.C., Orf, L.G., Savory, E., (2011). Improved modelling of downburst outflows for wind engineering applications using a cooling source approach. J. Wind Eng. Ind. Aerodyn. 99, 801–814. doi:10.1016/j.jweia.2011.03.003

Wolfson, M.M., DiStefano, J.T., Fujita, T.T., (1985). Low altitude wind shear in the Memphis, TN area based on Mesonet and LLWAS data. Indianapolis, US.

Wood, G.S., Kwok, K.C.S., Motteram, N.A., Fletcher, D.F., (2001). Physical and numerical modelling of thunderstorm downbursts. J. Wind Eng. Ind. Aerodyn. 89, 535–552. doi:10.1016/S0167-6105(00)00090-8

Xu, Z., Hangan, H., (2008). Scale, boundary and inlet condition effects on impinging jets. J. Wind Eng. Ind. Aerodyn. 96, 2383–2402. doi:10.1016/j.jweia.2008.04.002

Chapter 3

3 The Effect of Downburst Wind Field Characteristics on the Longitudinal Forces on Transmission Towers

3.1 Introduction

3.1.1 Background

Electricity is a vital component of our contemporary way of living. The reliability of such a crucial element to socio-economical growth is heavily dependent on the sustainability and resiliency of transmission line system components facing various weather-related loading conditions. Aside from the conventional loading attributed to synoptic wind, loading cases associated with thunderstorms (i.e. tornadoes and downbursts), have recently been acknowledged for their devastating impact on transmission line systems. Downbursts that were first defined by Fujita (1985a) as "*a strong downdraft that induces an outburst of damaging wind near the ground*" are believed to be the cause of several reported transmission line failures. Kanak et al. (2007) reported the failure of 19 towers in Slovakia due to a downburst event. Another event that occurred in Manitoba, Canada, has been reported by McCarthy and Melsness (1996) and resulted in the failure of 19 transmission towers. Similarly, Hydro One Ontario Company has also revealed that its failing tower in the year 2006 was due to a downburst event. All these incidents, and more that occurred in Australia as reported by Li (2000), and in China as reported by Zhang (2006), have directed researchers to study the effect of downburst loading on transmission line systems.

Consequently, researchers studying the effect of downbursts on transmission line systems have followed different paths in choosing the wind field used to examine the behaviour of different transmission line components corresponding to downburst loading cases. Many

of those researchers used wind field that was developed using computational fluid dynamics (CFD). Shehata et al. (2005) scaled up the wind field resulting from the CFD simulation conducted by Kim and Hangan (2007) to study the behavior of both the conductors and the supporting towers due to the applied downburst wind field. The finite element analysis showed that downburst loading would yield higher peak values of internal forces than that resulting from normal wind. The study also concluded that the consideration of six spans should suffice when studying a localized downburst event. Building on that study, another study was conducted by Shehata and El Damatty (2007) to study the spatial configurations of downburst that would lead to the highest forces in the studied elements of a guyed tower. The results of the study emphasize on the importance of considering the spatial locality of the event, which proved to be essential when studying transmission line structures extending for great horizontal distances. To generate the wind field, the same procedures were adopted by Darwish and El Damatty (2011) and Mara and Hong (2013) who also concluded on both studies that downburst loading can lead to more severe loading conditions compared to normal wind loading cases.

It is worth mentioning that all the aforementioned studies could only use the quasi-static analysis approach due to the availed CFD wind field, which was produced using the RANS turbulence scheme, producing only mean component type of flow. This was generally justified by the fact that the studied structural components, whether it is the conductors or the tower structures, have distinctive natural periods, which are relatively distant from that of the loading phenomenon. Yet, further studies have considered the dynamic effect associated with downburst loading to investigate its impact on the structural elements. To do so, researchers had to produce the fluctuating component using different techniques,

and then super-impose it on the mean component. In the case of Darwish et al. (2010), researchers extracted the turbulent component from field measurements that were reported by Holmes et al. (2008), and then added it to the extracted time histories produced by RANS CFD simulations. The study concluded that the inclusion of turbulent component into the dynamic analysis showed minor differences compared to the quasi-static analysis, which was attributed to the high aerodynamic damping exhibited by the conductors, attenuating the dynamic response. Another approach was used by Wang et al. (2009) who studied the dynamic response on tall transmission towers, where the turbulent component was synthetically produced using harmony superposition method combined with FFT algorithm, and the same conclusion was reached, that the dynamic effect could be neglected due to the difference in frequencies between the tower and the studied event.

Adjacently, the study performed by Savory et al. (2001) utilized the empirical model developed by Holmes and Oliver (2000) to produce downburst wind field, and evaluate the loading on lattice towers by performing dynamic analysis on the tower structures. The analysis concluded that the tower structures were found be safe, suggesting failure occurrence is dependant on the inclusion of conductor loading in the analysis. Dynamic performance was also evaluated by Lin et al. (2012), who used the slot jet model discussed by Lin and Savory (2006) to test an aero-elastic model of a transmission line system in a boundary layer wind tunnel, simulating downburst wind field. Results from the downburst wind field test cases were compared to those of the synoptic wind, and results showed less significance of dynamic effect, and a generally quasi-static behaviour.

In summary, most of the researchers who studied downburst effect on transmission line systems have used wind fields produced by CFD simulations. Of those, researchers who

were interested in the dynamic effect or studying the wind field including the turbulent component, had to either extract turbulent data from field measurements, or synthetically produce turbulent time histories, and super-impose them on the mean component of the flow.

Furthermore, researchers studying downbursts on transmission line systems can also be categorized based on the components examined in their studies. While researchers like Aboshosha et al. (2016b), Lin et al. (2012), Shehata et al. (2005), Shehata and El Damatty (2007) and Darwish and El Damatty (2011) considered the combined tower-line system, other researchers like Mara et al. (2010), Mara and Hong (2013) and Savory et al. (2001) have considered the effect of downburst loading on the supporting tower structures with no regard to the conductors. On the other hand, researchers like Aboshosha and El Damatty (2015b), (2014a), (2014b), Darwish et al. (2010) and Elawady and El Damatty (2016) have focused on the conductors, studying their impact either on the loading process, or their indispensable aerodynamic damping that helps stabilize the system against dynamic excitation in case of dynamic analysis. The current study is an extension of the work performed by Elawady and El Damatty (2016), examining the limitations associated with the performed analysis, the validity of the assumptions used, and finally the applicability of the work done in regards to the used wind field. The next section elaborates on the definition of the considered problem, the targeted focus points, and finally, an outline of the following sections and how they are structured.

3.1.2   Problem Definition

The latter of the mentioned studies, Elawady and El Damatty (2016), complimented a series of previous studies that studied the effect of downburst loading on transmission line

systems. The studies performed by Darwish and El Damatty (2011) and Shehata and El Damatty (2007) looked into the effect of the spatial localization of downburst loading on transmission line systems. One of the cases considered was the oblique load case, a case where the downburst center is neither perpendicular to the tower of interest, nor on the transmission line projection, but rather somewhere in between. This forms an inclination angle θ between the line perpendicular to the tower of interest, and the line joining the downburst center with the tower as shown in Figure 3- 1.
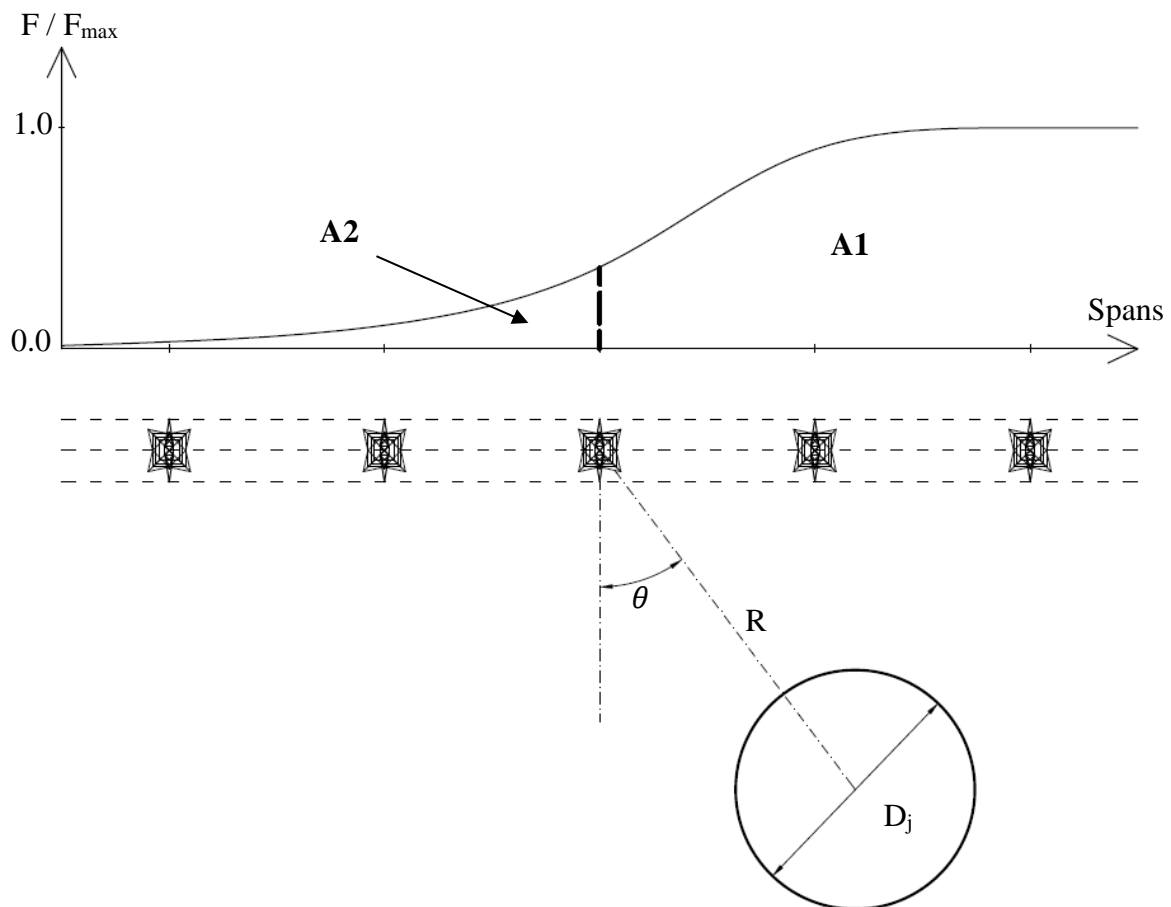
Figure 3- 1 Oblique load case illustration

Accordingly, the positioning of the downburst center at an angle from the line perpendicular to the tower of interest results in differential loading on the consecutive conductor spans attached to the tower of interest. This is represented in the figure as the difference between *A1* and *A2* being the forces acting on the consecutive conductor spans separated by the tower of interest. The loading exhibited due to this case is similar in configuration to that of the broken wire loading case considered by ASCE-74 (2010). The differential loading on consecutive spans results in a longitudinal force due to the difference in tension at the spans closest to the tower of interest. This is of particular importance to components like the cross-arms that experience devastating force moments, due to forces that were quantified to peak reaching 60% more than the transverse forces as reported by Aboshosha and El Damatty (2013). Yet, the variability introduced by the location parameters, radial distance *R*, inclination angle $\boldsymbol{\theta}$ and jet diameter $\boldsymbol{D_j}$, along with the variability in the intensity of the phenomenon and the properties of the considered tower-line system, can lead to loading cases that are more severe than that of the broken wire.

As such, Elawady and El Damatty (2016) conducted an elaborate parametric study to find the configuration resulting in the highest longitudinal loading. To do so, the authors utilized the technique described by Aboshosha and El Damatty (2015b) to compute the reactions on a six-span conductor system. The loads applied on the system were those corresponding to the downburst wind field availed by Kim and Hangan (2007). However, the usage of this wind filed, which only contains the mean component of the flow, along with the analysis technique used, result in the exclusion of the dynamic effect of the flow on the

considered system. This can result in computing values of longitudinal reactions that are not on the conservative side due to the following:

1. The exclusion of the turbulent component of the flow, which in turn excludes the dynamic effect, might have resulted in an increase in the computed values if considered.

2. The assumption of full correlation when extruding a three dimensional wind field from two dimensional CFD analysis, where the inclusion of coherency flow properties might result in an increase in the differential loading, and thus higher values of longitudinal reactions.

Conducting a dynamic type of analysis using this wind field, the current study aims to quantify these effects. The results can help to either confirm that the quasi-static analysis should suffice in computing the longitudinal reactions resulting from a downburst wind field, or that the inclusion of turbulent component in dynamic analysis that considers the spatial correlation shall be considered in calculating the longitudinal force due to downburst loading. To do so, the current study will follow the steps illustrated in Figure 3-2 . This can be segmented into two main stages:

1. Perform analysis at model-scale using the CFD wind field developed in chapter 1 of this thesis, then compare the results of numerical analysis with experimental results to verify the used numerical model.

2. Perform the analysis at full-scale using the same wind field used by Elawady and El Damatty (2016) for mean component, generate synthetic turbulence, and consequently assess the conservativeness of the results in regard to the dynamic and the correlation effects, as well as the applicability of the used wind field.

Develop a CFD model replicating the WindEEE downburst simulation

(Section 2.3)

Validate the CFD results using experimental wind field data

(Section 2.4)

Apply the wind field from CFD analysis on model-scale structure

(Section 3.2.1)

Validate the used structural numerical model using experimental data for a single span conductor experiment conducted at WindEEE (Elawady et al. 2017)

(Section 3.2.2)

Extend analysis to full-scale using the validated structural numerical model

(Section 3.3)

Mean component: CFD wind field by Kim and Hangan (2007)

(Section 3.3.1)

Turbulent component: Aboshosha et al (2015) technique

(Section 3.3.1)

Use results of numerical analysis to assess dynamic effect of downburst loading on longitudinal reactions computed

(Section 3.3.3)

Compare responses from used wind field with results from more realistic wind fields to judge the applicability of the CFD wind field used

(Section 3.4)

Figure 3- 2 Flow chart of the work conducted

Accordingly, the current study is presented in five main sections. The first section is the introduction, which includes two subsections; general background of previous studies in the literature (Section 3.1.1), and a more specific description of the problem approached in the current study presented in the current subsection (Section 3.1.2).

The second section (Section 3.2) includes the analysis performed at model scale, where the numerical model and the used wind field are described in the first subsection (3.2.1), and the resulting structural responses are compared to experimental results on the second subsection (3.2.2).

The analyses are then conducted at full-scale in the third section (Section 3.3), where the first subsection provides a description of the considered structure and the numerical model (Section 3.3.1). The second subsection (Section 3.3.2) elaborates on the wind field used for full-scale analysis, being a summation of a mean component resulting from CFD analysis, and turbulent component that is synthetically generated and then statistically calibrated to match given correlations. Lastly, the third subsection (3.3.3) presents the results obtained from the analysis and discusses their significance on the drawn conclusions.

Afterwards, the next section (Section 3.4) examines the characteristics of the wind field used in the full-scale analysis, and compares it to the characteristics of wind fields reported by previous literature. Finally, the last section (Section 3.5) lists the conclusions drawn from the conducted work.

3.2   Model-Scale Analysis

In this section, a numerical model is proposed to dynamically resolve for longitudinal reactions of transmission lines on supporting towers due to downburst loading. The model and the used wind field are discussed in the first subsection (Section 3.2.1), and the results are compared with experimental results on the second subsection (Section 3.2.2).

3.2.1   Numerical Model

Dynamic analysis of conductor systems under downburst loading is usually a complicated task due to the geometric nonlinearity of the conductors, along with the time varying properties of the wind filed, that accordingly require the modification of properties such as the aerodynamic damping considered in dynamic analysis. Previous studies that conducted dynamic analyses on transmission line systems due to synoptic wind such as Dua et al. (2015), Keyhan et al. (2013) and Mcclure and Lapointe (2003) considered an equivalent viscous damping to account for the aerodynamic damping. The values used by Dua et al. (2015) and Keyhan et al. (2013) were those resulting from the Fluid Structure Interaction model computed by the latter study. The values were then implemented through different commercial software to conduct 3D finite element model. It can be argued that the constant damping values used are in line with the expression proposed by Davenport (1962) and shown in equation (3-1). The aerodynamic damping value per mode i is shown to depend on the air density ρ, the drag coefficient C_D, the conductor diameter D, the wind velocity V, conductor mass m, and finally the mode's frequency f_i. Thus, for these studies that considered synoptic wind, a constant damping value can be considered reasonable, as synoptic wind is a stationary process, which means it has a constant statistical mean. In contrast, researchers like Darwish et al. (2010) and Aboshosha and El Damatty (2015b)

used a modified version of the aerodynamic damping expression to account for the temporal variation of wind speed. The non-stationarity of the downburst wind field, illustrated by the varying mean component of the flow shown in Figure 3- 3, would result in a variation in the computed values of aerodynamic damping with respect to time.

$$\zeta_{ai} = \frac{\rho C_D D V}{4\pi m f_i} \qquad (3\text{-}1)$$
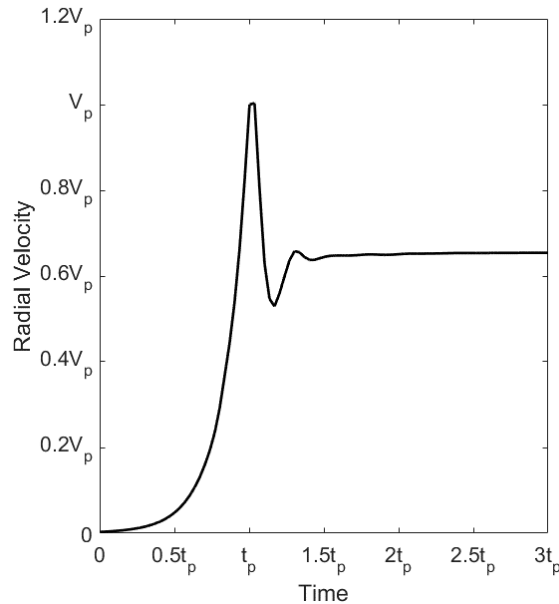
Figure 3- 3 Mean radial velocity vs Time for downburst wind field at a probe point

The current study utilizes the commercial software SAP2000, which does not accommodate such variability in damping values. Accordingly, the constant damping value that is to be chosen needs further verification to provide confidence in the output of the numerical model. To do so, an experiment that was part of the work done by Elawady et al. (2017) will be used to verify the numerical model, along with the assumption of a constant damping, and its sufficiency in representing the aerodynamic damping of a cable

system. The aforementioned study reported three layouts that tested different angles of attack and the corresponding reactions of the tower-cable system. Yet, another layout was also tested using a single span of conductors, hanging between rigid frames as shown in Figure 3- 4. The cable ends attached to the towers were instrumented with leaf springs, shown in Figure 3- 5 that measured strains, which were converted to moments, indicating the reaction values at the tower support.
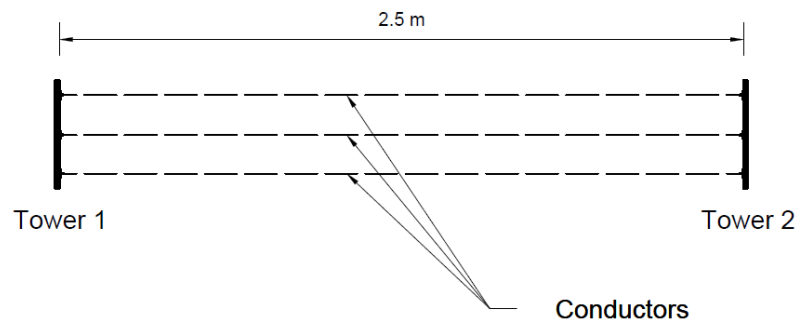
Figure 3- 4 Layout of tested conductor system
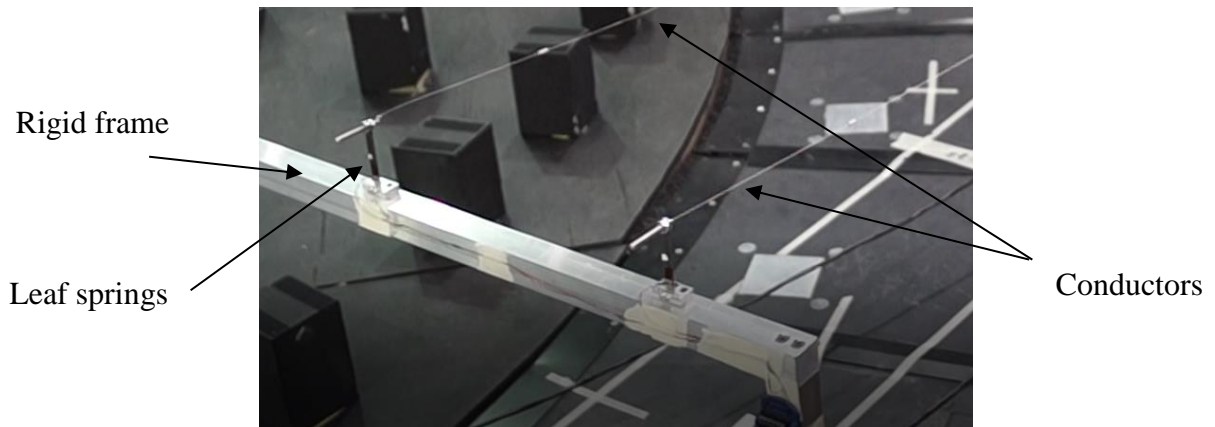
Figure 3- 5 Leaf spring instrumentation at cable ends

Consequently, a SAP2000 model was developed simulating a single span of cable elements with a span of 2.5 meters and a sag of 9.75 cm. The boundary conditions were set as hinged on both ends, and the simulated 2-noded cable element had the properties reported by Elawady et al. (2017). Modal analysis was first conducted to determine the natural frequencies for different modes of the system, and damping values were computed per mode using equation (3-1). The procedure's most challenging aspect was the choice of a single value of velocity that could represent the whole time history in calculating a fixed aerodynamic damping value.
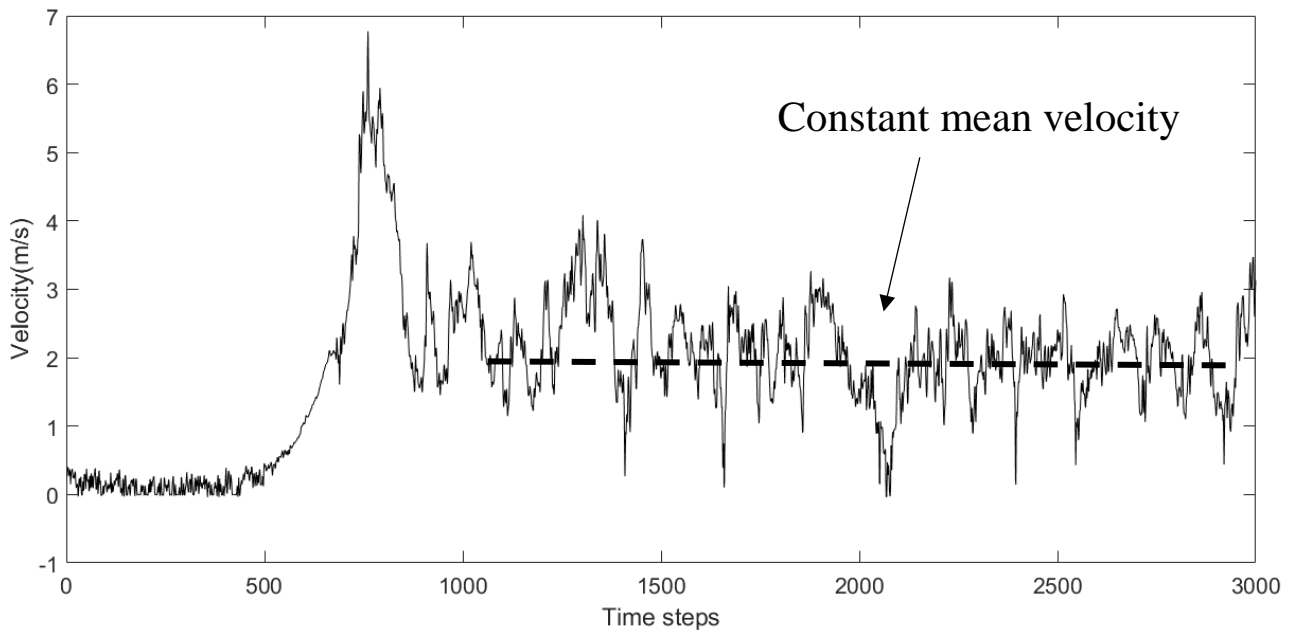
Figure 3- 6 Time history of radial velocity for a probe point

The wind field used in this analysis was that resulting from the CFD analysis conducted in the previous chapter of this thesis and reported by Ibrahim et al. (2017) with the addition of turbulence from the wind field reported by Elawady et al. (2017), using a procedure similar to that used by Darwish et al. (2010). Examining the resulting velocity time history shown in Figure 3- 6, it appears that the preceding part of the time history, where the ramp-

up occurs, is completely governed by the mean part of the flow, having a relatively low frequency. Yet, the part that follows the ramp-up appears to have a rather constant mean, with fluctuating velocity revolving around that fixed value. Hence, it is suggested that the constant value of damping is to be calculated using the constant value following the ramp-up, which will be annotated V_{pr} in the sections that follow.
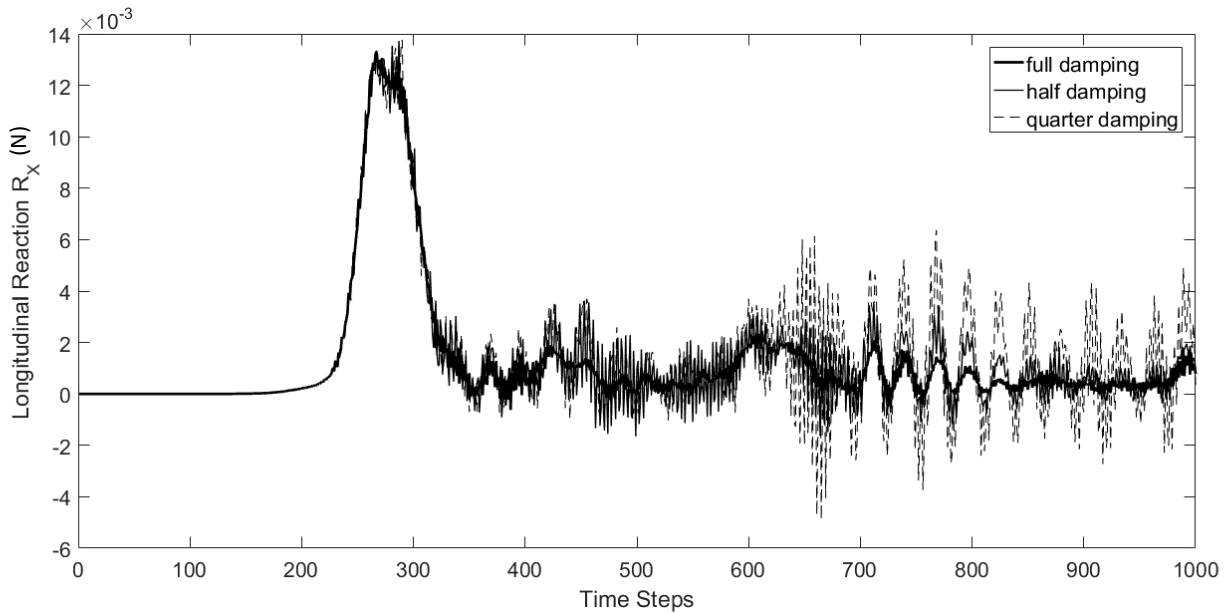
Figure 3- 7 Comparison between time histories of longitudinal reaction corresponding to different damping

With the velocity value known, damping values were computed, and proportional damping coefficients were calculated based on the frequencies provided by the modal analysis. Loads were implemented as time histories of transverse forces acting as point loads on cable nodes. The analysis was then run as a transient non-linear direct integration case, considering the p-delta effect with large displacements. To validate the hypothesis of considering a constant damping that was computed based on V_{pr}, and overlooking the effect of the ramp-up on the dynamic responses, the analysis was repeated two more times, using half the initial damping, and a quarter of it for the two replications respectively. The results shown in Figure 3- 7, which shows the time history of the computed longitudinal reaction

R_X, suggest that the assumption of concentrating on the post ramp-up region for evaluating the aerodynamic damping values is in fact a valid assumption. This is due to the agreement between the three plots for the ramp-up zone, despite the significantly varying damping values, and the differences being limited to the post ramp-up part of the time history.

3.2.2 Comparison of Numerical Results with Experimental Measurements
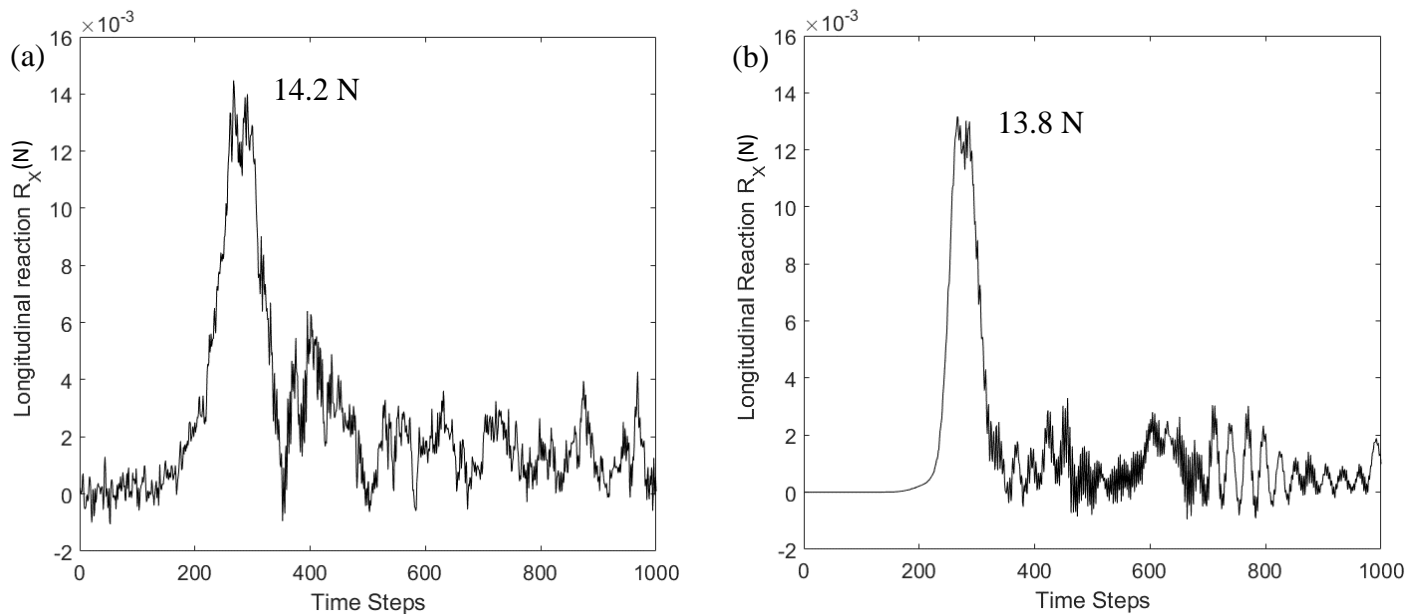
Figure 3- 8 Comparison between longitudinal reaction for
(a) experiment and (b) SAP 2000 numerical model

Afterwards, the results from the SAP2000 analysis were compared to the experimental data to verify the numerical model, as well as the validity of considering a constant damping value. As shown from Figure 3- 8(a) and Figure 3- 8(b), representing the experimental and numerical longitudinal reactions respectively, the peak reaction values were 14.2 and 13.8 N for the experimental and the numerical responses respectively, with a difference in the order of 3%. As for the post ramp-up zone, the dynamic effect also seems to be comparable. Yet, there seems to be discrepancy in the zone around time step number 400. This discrepancy is believed to have no effect on the comparison of dynamic effect due to two

reasons; first, the time zone at which it happens is not expected to experience dynamic amplification as it is in the immediate vicinity of the ramp-up zone. Second, close examination of the response at that zone show clearly that the abrupt increase in the response value is a mean governed behaviour due to the relatively low frequency causing the increase. This sudden increase is probably related to the vertical component of the wind speed, which is ignored in the considered wind field. Examining Figure 2- 10, it appears that the leading vortex would cause such effect due to the downward directed vertical component of the flow at the trailing edge of the vortex.

Moreover, the comparison of the fluctuating component of the reaction, taken as the residual of the filtered time history illustrated by Figure 3- 9(a) and Figure 3- 9(b), demonstrates a quantitative comparison between the resulting fluctuating components where differences were in the order of 4%. This residual resulted from the decomposition technique described elaborately in the previous chapter. Hence, the same numerical model with the assumptions elaborated will be used for the full-scale analyses discussed in the following sections.
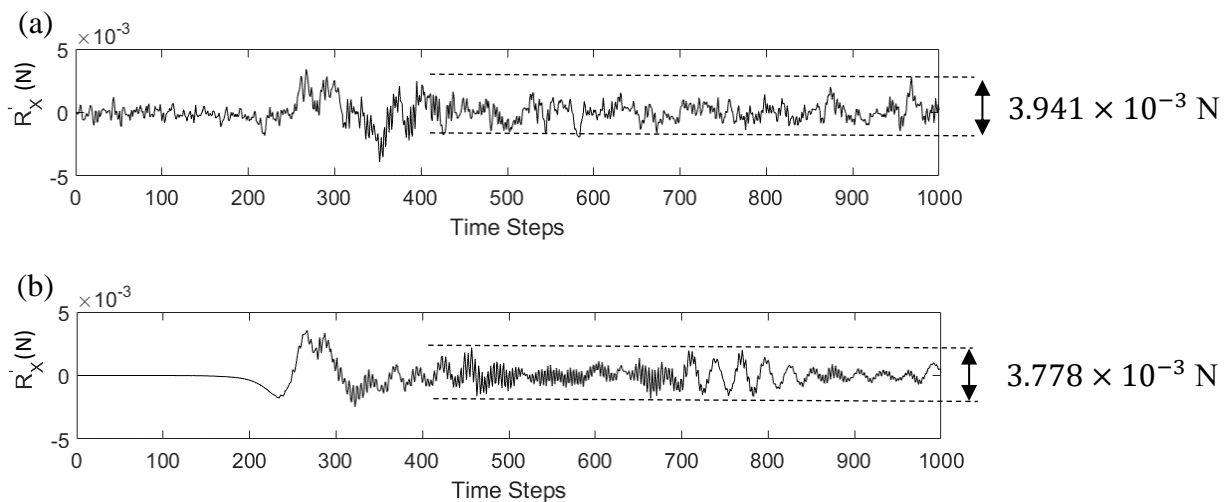
Figure 3- 9 Comparison between fluctuating component of longitudinal reaction for (a) experimental and (b) SAP 2000 analysis

3.3　　　Full-Scale Analysis

In this section, the wind field used in the analysis is clearly described in the first subsection (Section 3.3.1) being the result of superimposing a synthetically generated turbulent component on a scaled-up mean component resulting from CFD analysis. The second subsection (Section 3.3.2) elaborates on the modelled structure and the considered parameters. The last subsection (Section 3.3.3) presents the results of the numerical simulation, and their interpretation.

3.3.1　　Wind Field

Mean Component

As described in the first section of this chapter, the majority of researchers studying downbursts on transmission line systems used CFD produced wind field to determine the loading on the structure system. The current study utilizes the wind field produced by Kim and Hangan (2007). An elaborate description of the numerical model and the validation with full-scale data can be found in that study. Nevertheless, the study was conducted on a model scale, which needs to be scaled up to produce a full-scale wind field. Accordingly, the current study adopted the scaling procedure proposed by Shehata et al. (2005) which relates the length scale to the jet dimensions, and the velocity scale to the velocity of the downdraft at the jet inlet, and finally, the time scale as the ratio between the length and the velocity scales. The jet diameter used was 1000 m, and the downdraft velocity was 70 m/s.

Accordingly, the mean velocity data were first computed using the downburst data, as well as the coordinates of the conductor nodes relative to the jet center. The case considered for this study was that identified by Elawady and El Damatty (2016) as the most critical case

for longitudinal reactions corresponding to downburst loading. Referring to Figure 3- 1, this is the case where the jet center is at an inclination angle $\boldsymbol{\theta}$ equal to 30 degrees, and $\boldsymbol{R}$ equal to 1.6 times the jet diameter, as well as having the span length equal to $\frac{1}{2}$ the jet diameter.

Realizing that the study by Kim and Hangan (2007) yielded a 2D flow field, extruding the wind field circumferentially results in a perfectly correlated flow field. Moreover, examining the sample time history presented in Figure 3- 3 makes it clear that the resulting wind field lacks any turbulence, specially for the post ramp-up part of the time history. Accordingly, the remainder of this section will present the procedure adopted to generate turbulence that is to be added to the wind field, mainly considering the introduction of the missing turbulence frequencies, as well as maintaining appropriate coherency between distant locations according to their spatial position.

Turbulent Component

The turbulent component of the wind field is essential for the current analysis and has to be generated by a technique that provides two things; first, introduce the finer frequencies that are to be added to the mean component of the flow, and second, ensure the generated turbulence maintains the statistical characteristics desired. This should be applicable for both types of properties; single point properties (spectra and turbulence intensities), and cross-space properties (coherencies and length scales). Different techniques can be found in the literature for synthetically generating turbulent time histories, reader is referred to Huang et al. (2010), Kim et al. (2013), Klein et al. (2003) and Kondo et al. (1997). Yet, a recent study done by Aboshosha et al. (2015b) proposed a modification to the technique

proposed by Huang et al. (2010), as it suggested the latter study yields a non-conforming spectral content, as well as an over correlated relationship for the considered band of frequencies. In contrary, the modification proposed was found to give a series of time histories that had a better agreement with the target frequency content, as well as conforming decaying coherency that eliminates the excessive correlation found in the original technique and following the relation given by Davenport (1993) to a great extent.

The technique used to generate the turbulent component of the flow, named Consistent Discrete Random Flow Generation (**CDRFG**), has been thoroughly explained in the study done by Aboshosha et al. (2015b). The study proposed discretizing the frequency content into segments, which should produce a better conforming spectral content, as well as a matching coherency with the expression proposed by Davenport (1993). For the current study, a slight change has been adopted, where the frequencies were discretized using a logarithmic scale rather than a linear one, since the smaller frequencies, corresponding to the larger vortices, are overstepped in the case of linear scale. This could be avoided by either using a finer frequency step, which means more computational time, or using the adopted solution, discretizing the frequencies using a logarithmic scale. In addition, another difference that had to be implemented was the spatial discretization being changed from a Cartesian system to a polar system. This was essential since the wind field represents a downburst, which convects radially from a center point, unlike straight winds expected in the case of synoptic wind. Accordingly, the radial distance from the jet center R, the angular coordinate from a datum centerline θ, where the datum is the virtual line between the jet center and the line system, perpendicular to the line system, and finally the height Z

were used as the three coordinates identifying any point in space where the turbulence field is to be generated.

Yet, to ensure consistency of the coordinates system, the second coordinate, which is the angular coordinate $\boldsymbol{\theta}$ was replaced by the coordinate $\boldsymbol{R}.\boldsymbol{\theta}$, representing the circumferential coordinate, where $\boldsymbol{R}$ and $\boldsymbol{Z}$ are in meters, and $\boldsymbol{\theta}$ is in radians.

The illustration shown in Figure 3- 10 presents the steps used by the technique to generate the turbulent velocity component. As shown, the technique requires the input of values characterizing the turbulent wind field. The first value required is the mean wind velocity, which in the case of synoptic wind is a single value that is easy to determine based on the point height, where a conventional vertical power profile is enough to characterize the flow for a whole plane perpendicular to the flow. In contrary, the downburst wind field is more complex than that due to the localized nature of the flow. Accordingly, for each point, the value of $\boldsymbol{V_{pr}}$, introduced previously, is used as $\boldsymbol{u_r}$, the mean velocity value, based on the observation that the post ramp-up section of the time history is the part affected by the inclusion of dynamics and thus turbulent flow into analysis. As for the turbulence intensity $\boldsymbol{I_r}$, it was taken as 0.12, which reasonably agrees with the values reported by Aboshosha et al. (2015a), Holmes et al. (2008) and Orwig and Schroeder (2007). Yet, the fact that the values reported by the latter two studies are for heights much less than that of the conductor system to be studied might yield a wind field that leans towards conservativeness. This particular assumption, assuming the turbulence intensity to be height independent, is inline with the work done by Solari et al. (2017) and Zhang et al. (2017).

Input the following parameters:

Mean radial velocity u_r Turbulent intensity I_r Characteristic length D

Turbulent length scale per direction L_j Coherency decay constant per direction C_j

Generate a series of random frequencies $f_{m,n}$, where m is the number of segments, and n is the number of random numbers per segment

Generate p and q as follows:

$$p_i^{m,n} = sign(r_i^{m,n})\sqrt{\frac{1}{N}S_{ui}^{m}.\Delta f(m)\frac{(r_i^{m,n})^2}{1+(r_i^{m,n})^2}}$$

$$q_i^{m,n} = sign(r_i^{m,n})\sqrt{\frac{1}{N}S_{ui}^{m}.\Delta f(m)\frac{(r_i^{m,n})^2}{1+(r_i^{m,n})^2}}$$

Generate $k_j^{m,n}$, a random Gaussian number with zero mean & unit standard deviation, correct to satisfy

$$\begin{bmatrix} p_r^{m,n} & p_{r\theta}^{m,n} & p_z^{m,n} \\ q_r^{m,n} & q_{r\theta}^{m,n} & q_z^{m,n} \\ k_r^{m,n} & k_{r\theta}^{m,n} & k_z^{m,n} \end{bmatrix}\begin{Bmatrix} k_r^{m,n} \\ k_{r\theta}^{m,n} \\ k_z^{m,n} \end{Bmatrix} = \begin{Bmatrix} 0 \\ 0 \\ 1 \end{Bmatrix}$$

$$x_j^m = \frac{x_j}{L_j^m} \qquad L_j^m = \frac{U.\beta^{0.3}}{3.7.C_j.f_m} \qquad \beta = \frac{C.D}{L_u}$$

$$u_r(R,R\theta,z) = \sum_{m=1}^{M}\sum_{n=1}^{N} p_r^{m,n}cos(k_j^{m,n}.x_j^{m,n} + 2.\pi f_{n,m}t) + q_r^{m,n}cos(k_j^{m,n}.x_j^{m,n} + 2.\pi f_{n,m}t)$$
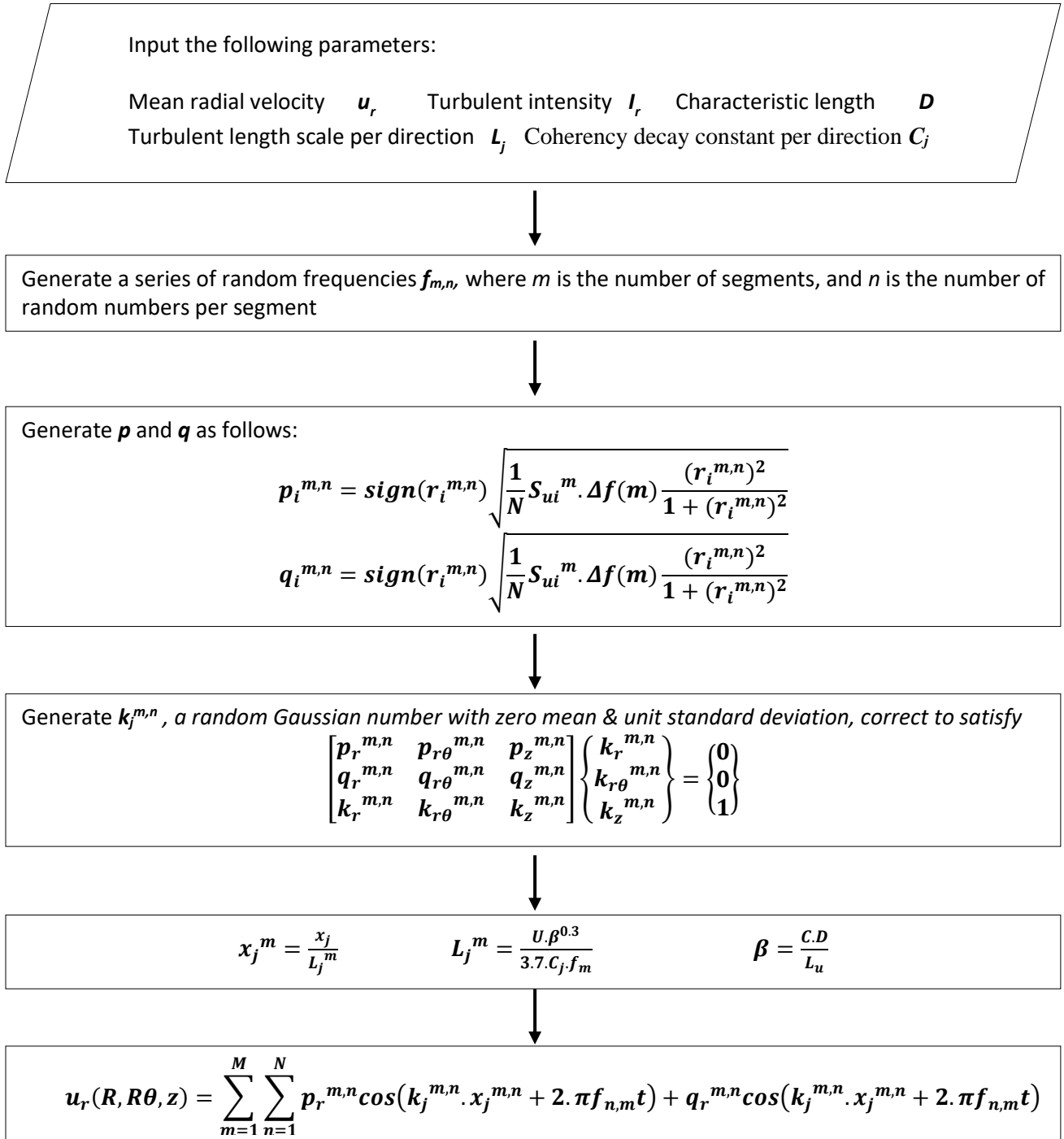
Figure 3- 10 Flow chart of turbulence generation technique

As for the characteristic length D, which is used to calibrate the output to reach a more complying coherency, it was chosen to be ten times the span of the conductor system. This value was intentionally chosen to be relatively large. This is to make sure the coherency of the larger structures of the flow is maintained due to their significant impact on the computed longitudinal reactions. On the other hand, cross-spatial turbulence characteristics (length scales and coherency) are generally less in terms of availability in the literature, specially for field measurements due to the need of a spatially dispersed measuring network to capture such features. This is the case for conventional probes where anemometers were the main source of velocity measurements. Yet, the emergence of modern LIDARs sets hopes high that such characteristics can be detected from field measurements in the soon future. For the current study, these characteristics were deduced from the work done by Aboshosha et al. (2015a), relying on CFD Large Eddy Simulations to find the values of length scales and coherency decay functions for the three coordinate directions, R, $R.\theta$ and Z. The values for length scales were related to the jet diameter, where the ratios between the length scales and the jet diameter were taken to be 0.5,9 and 0.1 for the radial, circumferential and vertical directions respectively. The coherency decay coefficients, C_j, were taken as 10, 0.05 and 10 for the three directions, which, along with the length scale values, imply a much higher correlation in the circumferential direction turbulence than the other two directions.

From that point forward, the algorithm generates a set of random frequencies, for a number of segments m, taken to be 400, with a number of random values n per segment, taken to be 250. As mentioned before, values of segments' mean were discretized using a logarithmic scale to ensure capturing the large flow structures represented by the low

values of frequencies. The values of p and q are then generated following the expression given on the next step. In that expression, S_u represents the spectral distribution for each respective direction i, taken to be the von Karman spectrum. Moreover, r is a normally distributed random number with zero mean and unit standard deviation, and $\varDelta f$ is the bandwidth defining the spectral segment m. In the current study, $\varDelta f$ is now dependant on m as the scale of distribution of the m values is a logarithmic scale. The values of k are then generated and corrected as stated by the next step, before moving to the step where the coherency correction values β, L and x are calculated using the given expressions. It shall also be noted that the bounding limitation of $\beta = 6$ presented by the original study is now removed as it was found to be inapplicable for this scale of application. Finally, the radial turbulence component is generated using the expression presented by the last step. For more details regarding the used technique, the reader is referred to the study done by Aboshosha et al. (2015b). A sample of the generated turbulence for a point is shown in

Figure 3- 11.

$$V_{modulated}(\text{t}) = \frac{V_{mean}(t)}{V_{pr}} \times V_{generated}(t) \qquad\qquad (3\text{-}2)$$
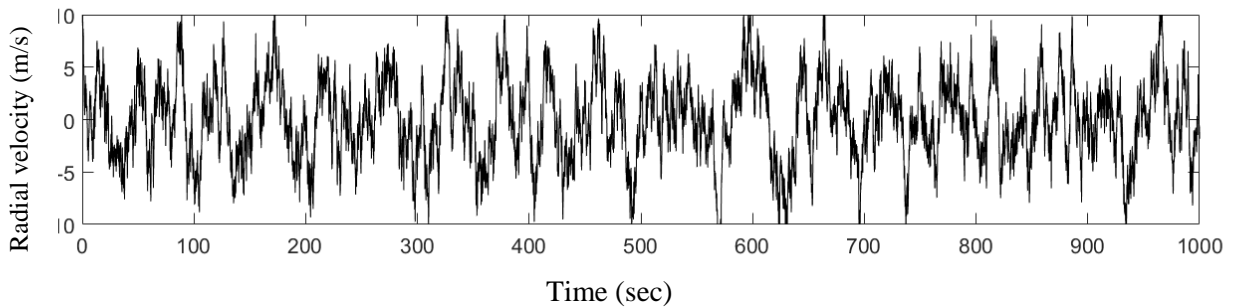

Figure 3- 11 Generated turbulence for a sample point

The coherencies for both the radial and the circumferential directions are compared with the target decay function in Figure 3- 12(a) and Figure 3- 12(b) for separation distances of $D_j/20$ and D_j respectively. It is evident that the agreement in the case of the circumferential direction is much better than that of the radial direction. This is believed to be an effect of the chosen characteristic length D, which was chosen to be large enough to make sure the large flow structures are well represented. It can also be noted that the agreement for both figures seem to be better for the smaller range of frequencies, which again is more desirable in this analysis as it corresponds to larger flow structures.
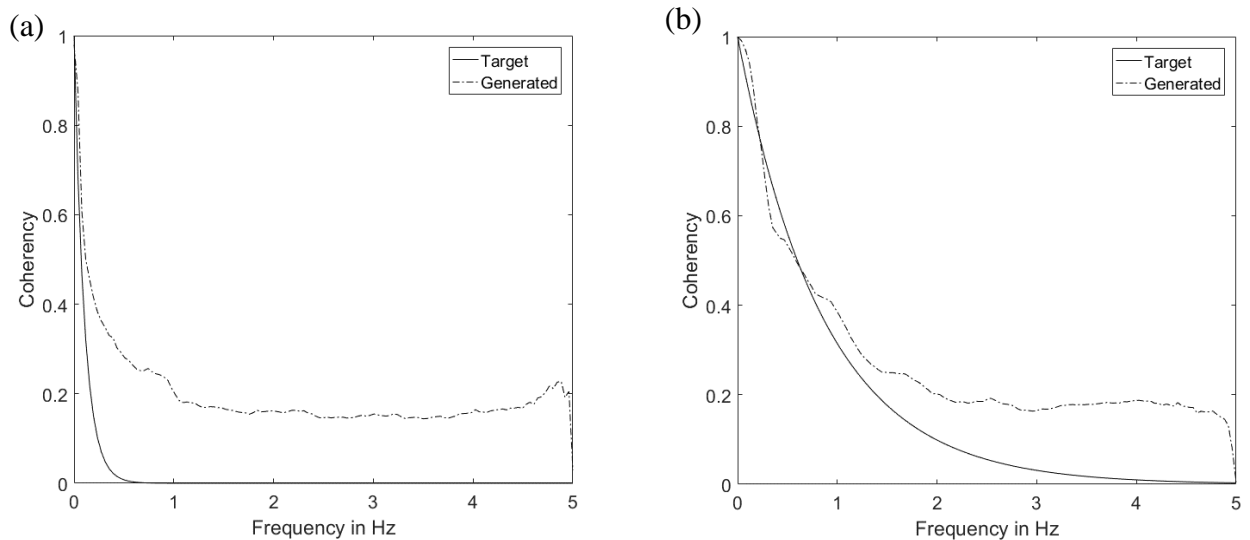
Figure 3- 12 Comparison between target and generated coherencies for (a) radial and (b) circumferential directions

The resulting time histories were then superimposed on the mean values generated from the previous section. Yet, the time histories could not be linearly added for the entire range, as the first part of the mean time history, until the end of the ramp-up, starts from a zero value, and experiences great fluctuations until it reaches the value of V_{pr}. Therefore, the turbulent time history was first calibrated using the modulation function given by equation (3-2), where the generated turbulence velocities were scaled based on the ratio between the

mean velocity of the time instant and V_{pr}. A sample of the resulting time histories is shown in Figure 3- 13.
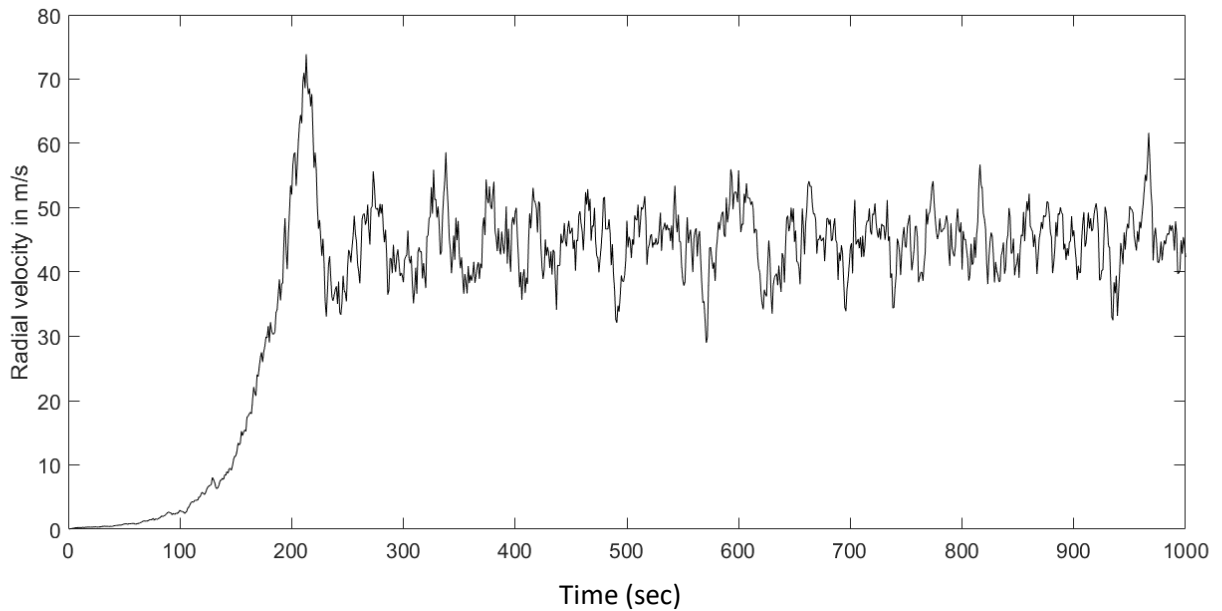
Figure 3- 13 Time history of radial velocity after superimposing generated turbulence

3.3.2   Numerical Model

The next step would be converting the velocity time history of each point into a force time history using equation (3-3), where the force $F(t)$ depends on the air density ρ, the drag coefficient C_D, and finally the velocity $V(t)$. The force time histories are then applied as point loads at the corresponding nodes, similar to the model scale numerical model verified experimentally in the second section of this chapter. A schematic of the modelled structure is shown in Figure 3- 14.
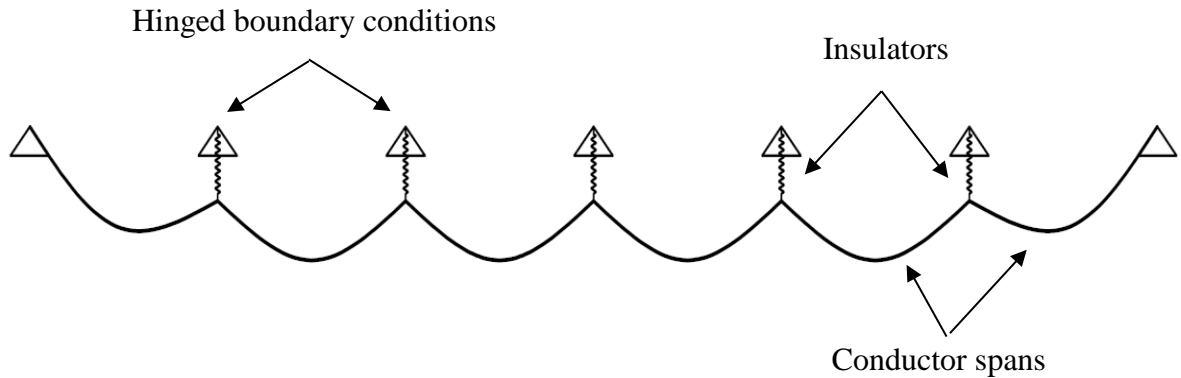
Figure 3- 14 Schematic of analyzed structure system

The considered model is that proposed by Shehata et al. (2005), who suggested that modelling three spans at both sides from the considered tower should suffice to model the effect of consecutive spans on the computed reactions. As illustrated by the schematic, the connection between the conductor system and the supporting tower is modelled as a hinged boundary condition. The connection model is also complimented by insulators at the intermediate connections, which are modelled as frame elements. Finally, the conductor spans are modelled as 2-noded cable elements that are divided into 90 segments per span to enable loading application. Dimensions and properties of the considered conductor system and downburst data are shown in Table 3-1.

$$F(t) = \frac{1}{2}\rho C_D V^2 \tag{3-3}$$

Table 3-1 Properties of the conductor system and the downburst

Property	Conductor Diameter	Conductor weight	Number of spans	Span length	Sag	Insulator length	Downburst jet diameter	Downburst jet velocity
Value	0.04 m	40 N/m	6	500 m	18.5 m	4 m	1000 m	70 m/s

As applied in the model scale analysis, a damping value that is independent of time will be used for the full-scale analysis. The velocity value that will be used to compute damping is the V_{pr} of the node corresponding to the tower of interest. Damping coefficients were then computed, and implemented into the SAP2000 model as discussed in the second section of this chapter.

3.3.3   Results and Discussion

The resulting time history of the longitudinal reaction from the dynamic analysis is shown in Figure 3- 15. It is obvious that the peak response is totally governed by the ramp-up part, which is less sensitive to the dynamic effect as proven in the second section of this chapter. For the sake of comparison, and similar to the what Elawady and El Damatty (2016) used in their analysis, the technique developed by Aboshosha and El Damatty (2015a) has been used to compute the longitudinal reaction quasi-statically using only the mean component
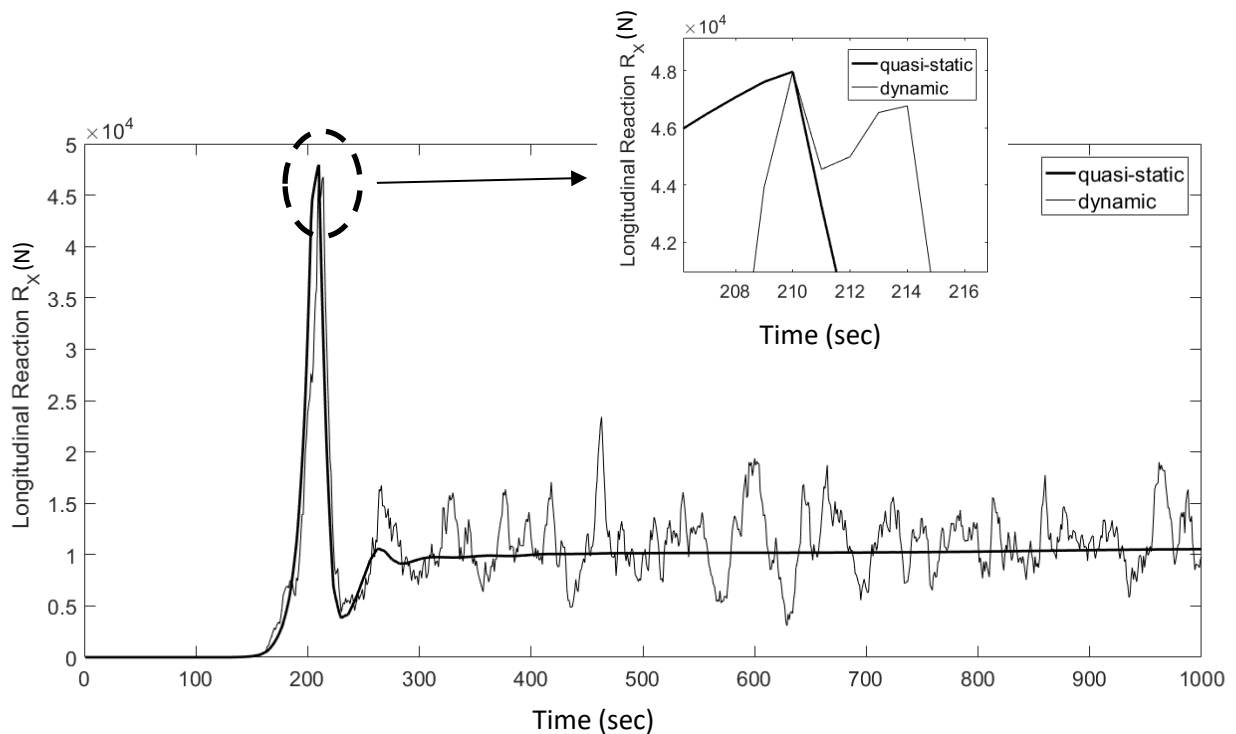
Figure 3- 15 Time history of longitudinal reaction for quasi-static analysis compared to dynamic analysis

of the flow which was scaled up to reach the background values. It should be noted that the background value to which the velocities were scaled up to is the peak value of the ramp-up zone. This is based on the hypothesis that the ramp-up zone does not experience any dynamic amplification, and thus the background value can be considered as the peak value with no reduction. The resulting time history from the quasi-static analysis is also plotted in Figure 3- 15.
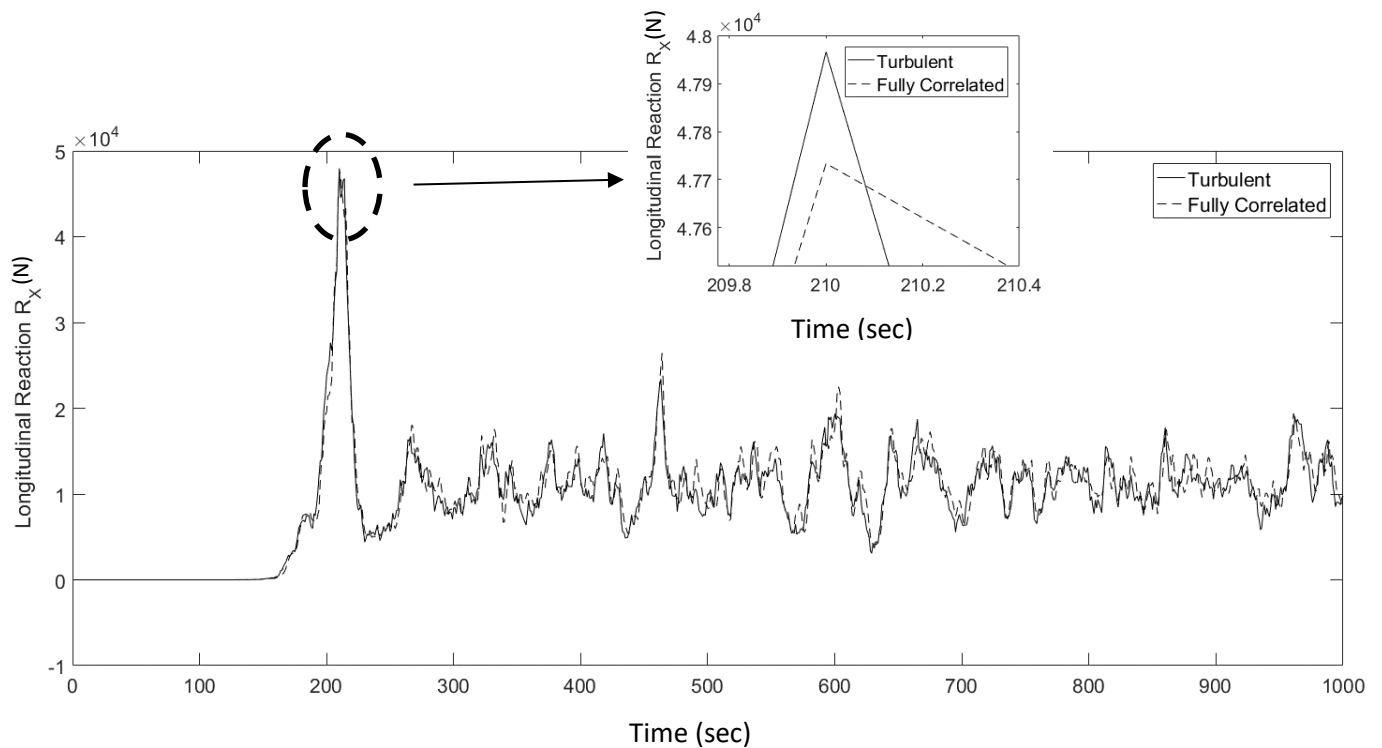
Figure 3- 16 Time history of longitudinal reaction for turbulent wind field compared to fully correlated wind field

Moreover, to be able to quantify the effect of considering the correlation between spatially separated points on the computed reactions, analysis was run using a fully correlated wind field. To achieve the full correlation between the turbulent time histories before superimposing them on mean time histories, a single time history of turbulent component

was used, and was only scaled at each point based on its peak mean velocity. The resulting time history is plotted against that resulting from the turbulent wind field in Figure 3- 16. As shown in the magnified portion of the plot, the increase in the computed reaction due to considering the differential loading arising from accounting for non-correlated turbulence is in the order of 0.5%. This was expected due to the fact that the generated turbulence had significant correlation in the circumferential direction (i.e. C in the $R.\theta$ direction = 0.05).

Accordingly, judging based on the resulting time histories plotted in Figure 3- 15 and Figure 3- 16, the following conclusions can be drawn:

1. The peak value of the reaction is governed by the mean component, as no amplification was found within the ramp-up zone for Figure 3- 15, at which the peak reaction occurs. This clearly means that the dynamic effect on the computed reactions is negligible.

2. Considering that the increase in the computed reaction due to accounting for spatial correlations, shown in Figure 3- 16, reaches no more than 0.5%, advocates for the insignificance of considering the correlation when computing the longitudinal reaction due to downburst loading.

The first point contradicts the findings of Elawady et al. (2017) who studied the effect of downburst loading on an aero-elastic model of transmission line system. One of the responses studied was the cross-arm moment, which is a direct reflection of the longitudinal reaction from the conductors on the tower structures. While the study concluded the dynamic magnification to be in the order of 15 to 30% depending on the tested case and velocity of the downburst, it is believed that this finding is a misleading

output of the judging technique used by the authors. The technique used can be summarized in the following points:

a. Decompose the response to a mean and a fluctuating component using a cut-off frequency as discussed in the previous chapter.

b. Calculate the power spectral density function (PSDF) of the fluctuating component of the entire signal.

c. Calculate the cumulative PSDF of the fluctuating component normalized by the variance of the PSDF.

d. Based on the slope of the cumulative curve, any frequency range with a slope exceeding a threshold value is considered to be dynamically excited.

e. Frequencies from the previous step are filtered out from the response signal to separate the resonant component of the signal, where the ratio between the complete signal, and the complete signal – resonant component at the peak zone is the dynamic amplification factor.

The error in this procedure is in step b, where the entire signal is analyzed to find the PSDF. The procedure assumes the signal has constant statistical properties over its length. This
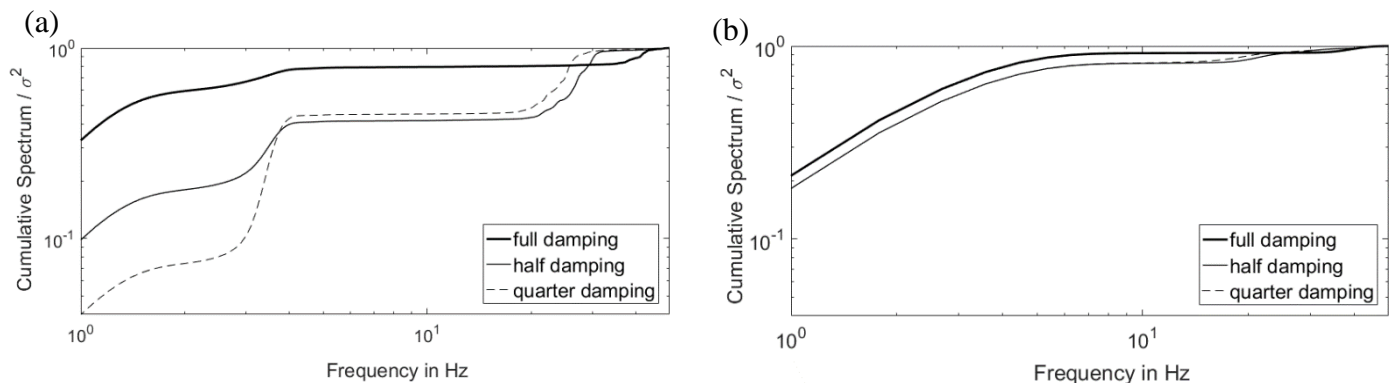

Figure 3- 17 Normalized cumulative PSDF for (a) Full time history (b) peak zone

assumption overlooks the non-stationarity of the downburst phenomenon, which in turn sets doubt in the applicability of step e, where frequencies that might have caused resonance at a relatively distant zone from the peak are filtered out from the peak zone.

To demonstrate the previous point, similar procedures were applied on the signals shown in Figure 3- 7. Results of the analysis shown in Figure 3- 17 were similar to the previously described technique for figure (a), while figure (b) represents the same technique, with a change in step b, where only the peak zone (peak instant $\pm \frac{1}{2 f_{cut}}$) was considered. As shown, the inclusion of the entire time history results in significant increases in the slopes of the normalized cumulative curve compared to the curve representing the peak zone. Accordingly, it is believed that considering only the peak zone in such procedure would result in a dramatic decrease in the computed magnification factors computed by Elawady et al. (2017).

Another observation that has relative significance on the results is that the ratio between V_{pr}, the post ramp-up velocity, and V_p, the peak velocity, where the value considered in the current analysis was about 0.65. This ratio would be squared when considering forces, and thus, as shown from the analysis results, would result in negligible effects of dynamic action, which only exhibits itself through the post ramp-up section of the time history. Therefore, it is essential to know where this ratio stands compared to full scale measurements in the literature, to determine whether this analysis is on the conservative side of computing the longitudinal reaction due to downburst loading or not. Another factor that can be deterministic when calculating the longitudinal reaction due to downburst loading is the period at which the ramp-up occurs T_R shown in Figure 3- 18. This is the

period enclosed by the ramp-up zone between the value of V_{pr} before and after the ramp-up. The fact that the differential loading is the main cause of the longitudinal reaction gives a high significance to the period T_R, since the phenomenon is localized and heavily time dependant. The next section of this study will examine the effect of the ratio between V_{pr} and V_p, as well as the value of T_R, on the computed longitudinal reaction values for different values of jet speed.
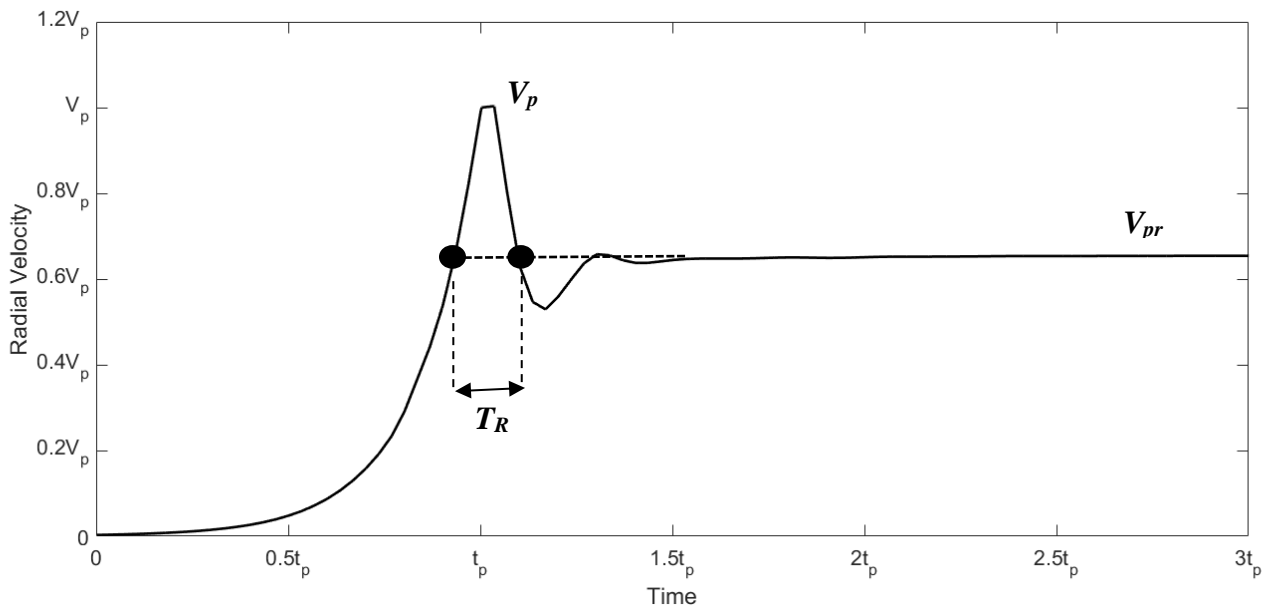
Figure 3- 18 Illustration of the annotations used to characterize the downburst time history

3.4   Further Considerations and Analysis

Due to the locality of the downburst wind field, as well as its time dependency, it is of utmost importance to characterize the wind field, suggested to be through the factors V_{pr}, V_p and T_R as illustrated in Figure 3- 18, to make sure the simulated wind field is representative when compared to field measurements. The current subsection investigates the relevance between the characteristics of the used wind field in comparison to field measured data. A sample of the characteristics of downburst time histories available in the literature is shown in Table 3-2. As shown in the table, the values of V_p vary within a wide

range. It can also be noted that no correlation between the ratio $\frac{V_{pr}}{V_p}$ and the value of V_p can be deduced, especially due to the limited number of data, which limits the deduction of a conclusive relation between the two values. Yet, the ratio $\frac{V_{pr}}{V_p}$ range between 0.1 and 0.3. Comparing these values to the value used in the current analysis, it appears that the dynamic effect of downburst loading will have even less significance if the new values are used, which adds more confidence in using the quasi-static approach. Furthermore, the value of T_R seems to lack any relation to the values of speed, which contradicts the scaling method used in this analysis. As mentioned before, the time scale used in scaling up the wind field is the ratio between the length scale and the velocity scale. This would result in large time scaling ratios for lower jet speeds, and in turn, smaller scaling ratios for higher values of speed, which affects the peak duration, identified by T_R.

Table 3-2 Comparison of downburst characteristics from different studies

Study	Place	V_p m/s	$\frac{V_{pr}}{V_p}$	T_R (seconds)
Zhang et al. (2017)	Livorno, Italy	16	0.25	600
Solari et al. (2017)	Laspezia, Italy	24	0.21	400
Solari et al. (2017)	Laspezia, Italy	32	0.16	600
Holmes et al. (2008)	Lubbock, TX, US	32	0.31	300
Fujita (1985b)	Andrews A.F.B, MD, US	56	0.09	180

Accordingly, time histories were modified, where two modifications were implemented; the first has to do with altering the $\frac{V_{pr}}{V_p}$ ratio varying between values of 0.1 to 0.6, and the second modification was applied on the time histories resulting from the first modification, where the time history was time scaled to reach values of T_R ranging between 100 and 600 seconds. The modifications were done based on velocity scaling ratios and time scaling ratios that were taken as a ratio between the desired values, and the values of the time history corresponding to the node at the tower of interest. The time histories shown in Figure 3- 19 show the original time history, plotted against a modified $\frac{V_{pr}}{V_p}$ ratio of 0.1, and another time history with a modified T_R of 300 seconds.

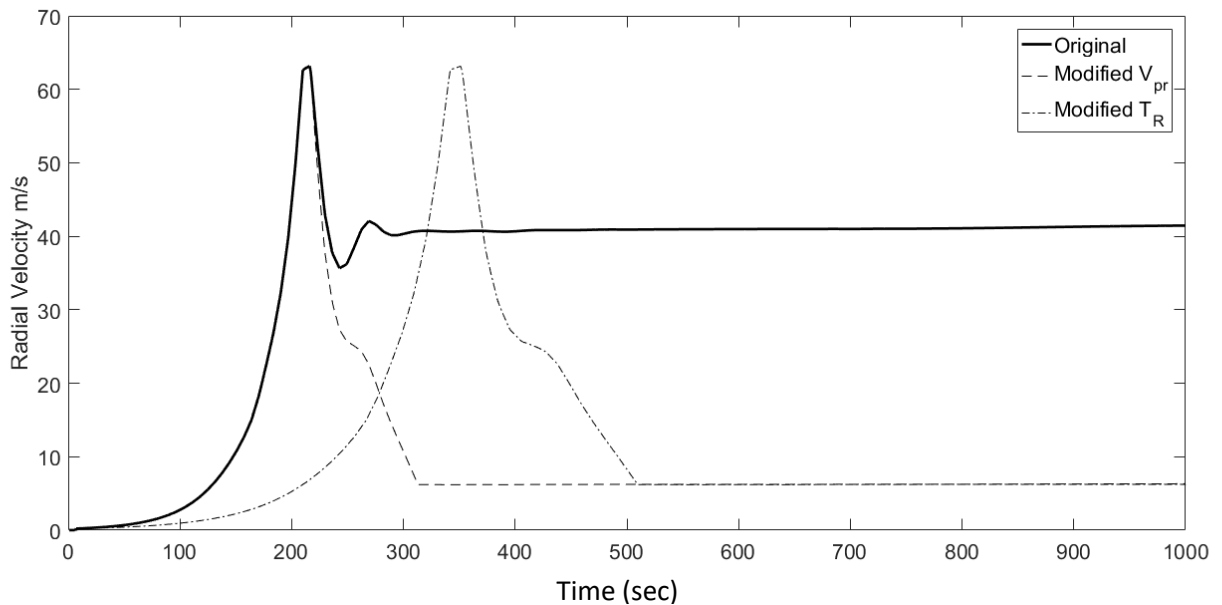**Figure 3- 19 Modified time histories of radial velocity**

Moreover, to judge the applicability of using a quasi-static approach, as well as decide on whether the modification of T_R would alter the previously reached conclusion of excluding the dynamic effect from consideration, the comparison shown in Figure 3- 20 has been conducted. As shown, the shedding frequency, which is considered to be a measure of the

highest energy containing frequency is compared to the first 20 modes of the considered structure. This is plotted on top of the PSDF of the fluctuating component of the resulting longitudinal reactions for (a) the model scale, and (b) the full scale. It is clear that for the case of model scale analysis the mode frequencies are within the same order of the shedding frequency, which implies that the mode frequencies are likely to encounter frequencies that have relative energy, being close to the shedding frequency. This is not the case for the full unmodified full scale analysis shown in figure (b), where the first mode frequency is about two orders of magnitude larger than the shedding frequency, which implies that the frequencies encountered by these modes are expected to have relatively low energy, which
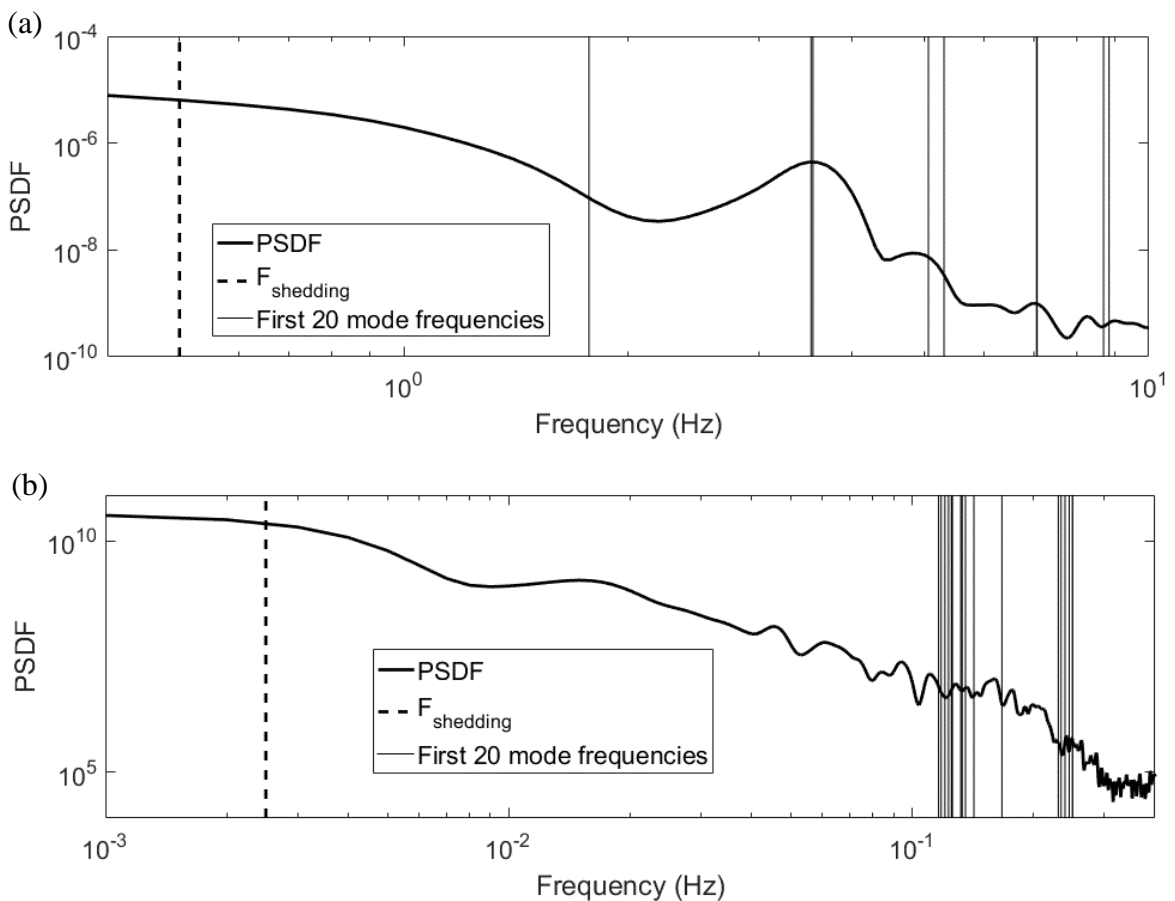
Figure 3- 20 Mode frequencies compared to shedding frequency for (a) model scale and (b) unmodified full scale

is not expected to develop dynamic magnification. Extrapolating from that hypothesis, the effect of increasing T_R is not expected to develop any more dynamic effect than the unmodified case, since the increase in the T_R parameter means less shedding frequency, and thus more distinction between it and the mode frequencies.

Table 3-3 The effect of changing parameters on the computed reaction

Parameter	25 m/s	70 m/s
$\dfrac{V_{pr}}{V_p}$	No change	Linear dependency was observed
T_R	No change	5% decrease

Accordingly, from that point forward, analyses were conducted quasi-statically, using the modified velocity time histories that reflect realistic values of $\dfrac{V_{pr}}{V_p}$ and T_R. This was done using two bounds of jet velocities, 25 and 70 m/s, to examine the effect of time scaling, which is inversely proportional to the velocity scale, and thus depends on the jet velocity. The results shown in Table 3-3 demonstrate no changes in the computed values of longitudinal reactions for different values of T_R. As for the $\dfrac{V_{pr}}{V_p}$ ratio, no change was observed for the lower bound of the jet velocity, and a linear dependency on the $\dfrac{V_{pr}}{V_p}$ ratio was evident for the upper bound of jet velocity as shown in Figure 3- 21. Although affected by the value of $\dfrac{V_{pr}}{V_p}$, the longitudinal reaction only shows a 5% decrease for the least considered value of $\dfrac{V_{pr}}{V_p}$. This indicates that the longitudinal reaction values computed using the original time histories is marginally on the conservative side, yet the difference is arguably acceptable.

Finally, it should be noted that the current study only considered the values of time history characterizing features, $\frac{V_{pr}}{V_p}$ and T_R, are based on the time histories of downburst events available in the literature. A more comprehensive set of field measurements is required to give more confidence in the drawn conclusions.
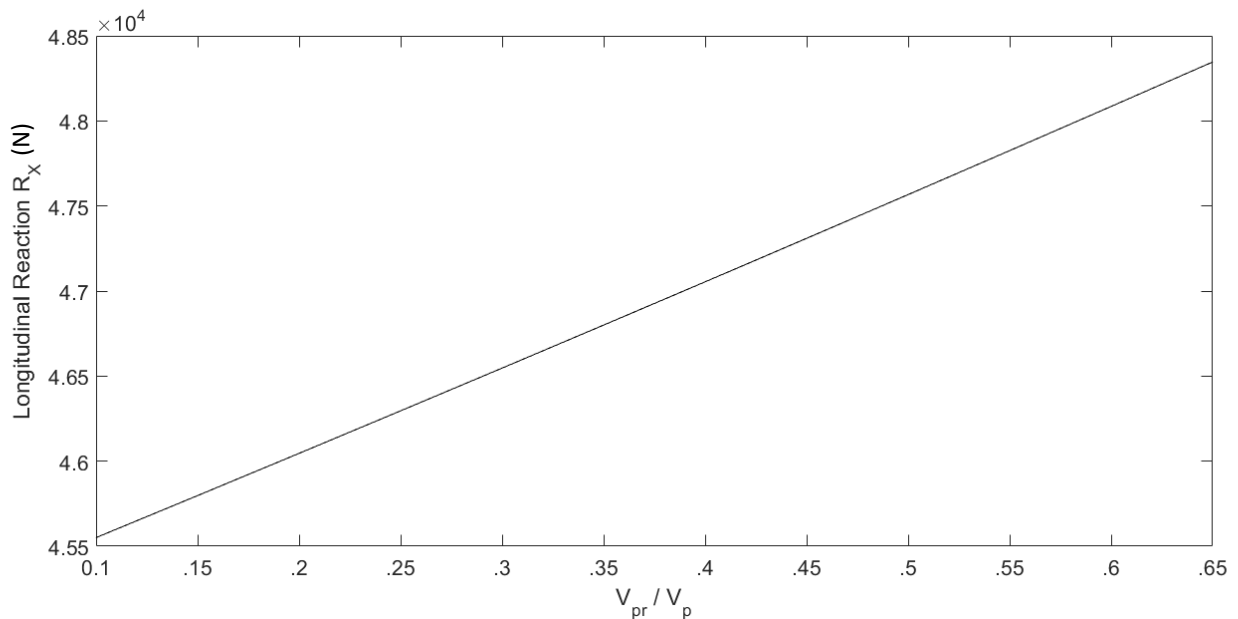
Figure 3- 21 Dependency of R_X on the V_{pr} / V_p ratio

3.5   Conclusions

The current study is focused on the computation of longitudinal reactions on transmission line systems due to the differential loading imposed by downburst wind field. The loading wind field is studied with special interest in the turbulent component that is expected to develop dynamic excitation of the conductor system. In the course of studying this effect, the following points summarize the methodology and findings of this study:

1- The numerical model has been validated using experimental results of a single span conductor provided by a previously conducted experiment. Results of the

comparison between the numerical and the experimental model showed the following:

    a. The ramp-up zone was found to be independent of the used damping values, which suggests it is completely governed by the mean and background components. This facilitated the assumption of using a single value of velocity to compute the aerodynamic damping, which deals with the post ramp-up zone as an ABL flow in a quasi approach.

    b. The quasi approach of estimating the aerodynamic damping value has been verified, where the results of the numerical model were within range of the experimental results, justifying the proposed approach.

2- The wind field of the full-scale model was composed of two parts; a mean component which was taken from a previous CFD study, and a turbulent component that was synthetically generated, and superimposed on the mean component. The resulting time histories were examined to check for the spatial correlations, and a satisfying agreement has been found, specially for the lower range of frequency, which corresponds to larger spatial scales.

3- Results of dynamic analyses showed that the peak reactions were always related to the ramp-up zone, with no evident dynamic effect in the zone of post ramp-up. The comparison of the results with quasi-static models showed the adequacy of using a quasi-static numerical model in resolving for the peak reactions.

4- The downburst wind field used was examined and compared against downburst time histories from the literature, particularly observing two main features, $\frac{V_{pr}}{V_p}$ and T_R. Modifying the time histories to match different values of the two features and

re-conducting the analyses yielded the conclusion of complete independency of the longitudinal reactions on the TR value. This was also the case for different values of $\frac{V_{pr}}{V_p}$ examined at different jet velocities. Yet, the only case that showed a difference was that of higher velocity and least value of $\frac{V_{pr}}{V_p}$, which showed a minor decrease, not more than 5%.

Finally, the results and conclusions drawn from this study are believed to be trustworthy to be used with confidence. Yet, the availability of more structured, and well representative set of metrological data would be useful to draw more firm conclusions, as well as examine more characteristics of the flow, and their effect on the computed values of the longitudinal reactions.

3.6   References

Aboshosha, H., Bitsuamlak, G., El Damatty, A.A., (2015a). Turbulence characterization of downbursts using LES. J. Wind Eng. Ind. Aerodyn. 136, 44–61. doi:10.1016/j.jweia.2014.10.020

Aboshosha, H., El Damatty, A., (2015a). Engineering method for estimating the reactions of transmission line conductors under downburst winds. Eng. Struct. 99, 272–284. doi:10.1016/j.engstruct.2015.04.010

Aboshosha, H., El Damatty, A.A., (2015b). Dynamic response of transmission line conductors under downburst and synoptic winds. Wind Struct. An Int. J. 21, 241–272. doi:10.12989/was.2015.21.2.241

Aboshosha, H., El Damatty, A.A., (2014a). Span Reduction Factor of Transmission Line Conductors Under Downburst Winds Span Reduction Factor of Transmission Line. J. Wind Eng. 11, 13–22. doi:10.3850/978-981-07-8012-8

Aboshosha, H., El Damatty, A.A., (2014b). Effective technique to analyze transmission line conductors under high intensity winds. Wind Struct. An Int. J. 18, 235–252. doi:10.12989/was.2014.18.3.235

Aboshosha, H., El Damatty, A.A., (2013). Downburst induced forces on the conductors of electric transmission lines and the corresponding vulnerability of towers failure. Proc. Can. Soc. Civ. Eng. Conf. (CSCE 2013).

Aboshosha, H., Elshaer, A., Bitsuamlak, G.T., El Damatty, A.A., (2015b). Consistent inflow turbulence generator for LES evaluation of wind-induced responses for tall buildings. J. Wind Eng. Ind. Aerodyn. 142, 198–216. doi:10.1016/j.jweia.2015.04.004

Aboshosha, H., Ibrahim, A., El Damatty, A.A., Hamada, A., (2016). Dynamic Behaviour of Transmission Lines Structures under Synoptic Wind Loads, in: 2016 CIGRE-IEC Colloquium.

ASCE-74, (2010). American Society of Civil Engineers (ASCE). Guidelines for electrical transmission line structural loading. ASCE Manuals and Reports on Engineering Practice, No. 74, New York (NY), USA; 2010.

Darwish, M.M., El Damatty, A.A., (2011). Behavior of self supported transmission line towers under stationary downburst loading. Wind Struct. An Int. J. 14, 481–498. doi:10.12989/was.2011.14.5.481

Darwish, M.M., El Damatty, A.A., Hangan, H., (2010). Dynamic characteristics of transmission line conductors and behaviour under turbulent downburst loading. Wind Struct. An Int. J. 13, 327–346. doi:10.12989/was.2010.13.4.327

Davenport, A.G., (1993). How can we simplify and generalize wind loads?, in: Proceedings of the Third Asia-Pacific Symposium on Wind Engineering. Keynote Lecture, 13–15 December. Hong Kong.

Davenport, A.G., (1962). Buffeting of a suspension bridge by storm winds. J. ASCE Struct. Div. 88, 233–264.

Dua, A., Clobes, M., Höbbel, T., (2015). Dynamic Analysis of Overhead Transmission Line under Turbulent Wind Loading 15, 46–54.

Elawady, A., Aboshosha, H., Damatty, A. El, Bitsuamlak, G., Hangan, H., Elatar, A., (2017). Aero-elastic testing of multi-spanned transmission line subjected to downbursts. J. Wind Eng. Ind. Aerodyn. 169, 194–216. doi:10.1016/j.jweia.2017.07.010

Elawady, A., El Damatty, A.A., (2016). Longitudinal force on transmission towers due to non-symmetric downburst conductor loads. Eng. Struct. 127, 206–226. doi:10.1016/j.engstruct.2016.08.030

Fujita, T.T., (1985a). The downburst: microburst and macroburst. Satellite and Mesometeorology Research Project (SMRP). Res. Pap. 210, Dep. Geophys. Sci. Univ. Chicago.

Fujita, T.T., (1985b). The Downburst. Report of Projects NIMROD and JAWS, University of Chicago.

Holmes, J.D., Hangan, H.M., Schroeder, J.L., Letchford, C.W., Orwig, K.D., (2008). A forensic study of the Lubbock-Reese downdraft of 2002. Wind Struct. An Int. J. 11, 137–152. doi:10.12989/was.2008.11.2.137

Holmes, J.D., Oliver, S.E., (2000). An empirical model of a downburst. Eng. Struct. 22, 1167–1172. doi:10.1016/S0141-0296(99)00058-9

Huang, S.H., Li, Q.S., Wu, J.R., (2010). A general inflow turbulence generator for large eddy simulation. Jnl. Wind Eng. Ind. Aerodyn. 98, 600–617. doi:10.1016/j.jweia.2010.06.002

Ibrahim, I., Aboshosha, H., El Damatty, A.A., (2017). Numerical Simulation of WINDEEE Dome Downburst for Open Terrain Using Physical Roughness Elements, in: Proceedings of the 7th European African Conference on Wind Engineering. Liege, Belgium.

Kanak, J., Benko, M., Simon, A., Sokol, A., (2007). Case study of the 9 May 2003 windstorm in southwestern Slovakia. Atmos. Res. 83, 162–175. doi:10.1016/j.atmosres.2005.09.012

Keyhan, H., Mcclure, G., Habashi, W.G., (2013). Dynamic analysis of an overhead transmission line subject to gusty wind loading predicted by wind – conductor interaction. Comput. Struct. 122, 135–144. doi:10.1016/j.compstruc.2012.12.022

Kim, J., Hangan, H., (2007). Numerical simulations of impinging jets with application to downbursts. J. Wind Eng. Ind. Aerodyn. 95, 279–298. doi:10.1016/j.jweia.2006.07.002

Kim, Y., Castro, I.P., Xie, Z., (2013). Divergence-free turbulence inflow conditions for large-eddy simulations with incompressible flow solvers. Comput. Fluids 84, 56–68. doi:10.1016/j.compfluid.2013.06.001

Klein, M., Sadiki, A., Janicka, J., (2003). A digital filter based generation of inflow data for spatially developing direct numerical or large eddy simulations 186, 652–665. doi:10.1016/S0021-9991(03)00090-1

Kondo, K., Murakami, S., Mochida, A., (1997). Generation of velocity fluctuations for inflow boundary condition of LES. J. Wind Eng. Ind. Aerodyn. 51–64.

Li, C.Q., (2000). A stochastic model of severe thunderstorms for transmission line design. Probabilistic Eng. Mech. 15, 359–364.

Lin, W.E., Savory, E., (2006). Large-scale quasi-steady modelling of a downburst outflow using a slot jet. Wind Struct. An Int. J. 9, 419–440. doi:10.12989/was.2006.9.6.419

Lin, W.E., Savory, E., Mcintyre, R.P., Vandelaar, C.S., King, J.P.C., (2012). The response of an overhead electrical power transmission line to two types of wind forcing. J. Wind Eng. Ind. Aerodyn. 100, 58–69. doi:10.1016/j.jweia.2011.10.005

Mara, T.G., Galsworthy, J.K., Savory, E., (2010). Assessment of vertical wind loads on lattice framework with application to thunderstorm winds. Wind Struct. An Int. J. 13, 413–431.

Mara, T.G., Hong, H.P., (2013). Effect of wind direction on the response and capacity surface of a transmission tower. Eng. Struct. 57, 493–501. doi:10.1016/j.engstruct.2013.10.004

McCarthy, P., Melsness, M., (1996). Severe weather elements associated with September 5, 1996 hydro tower failures near Grosse.

Mcclure, G., Lapointe, M., (2003). Modeling the structural dynamic response of overhead transmission lines 81, 825–834. doi:10.1016/S0045-7949(02)00472-8

Orwig, K.D., Schroeder, J.L., (2007). Near-surface wind characteristics of extreme thunderstorm outflows. J. Wind Eng. Ind. Aerodyn. 95, 565–584. doi:10.1016/j.jweia.2006.12.002

Savory, E., Parke, G.A.R., Zeinoddini, M., Toy, N., Disney, P., (2001). Modelling of tornado and microburst-induced wind loading and failure of a lattice transmission tower. Eng. Struct. 23, 365–375. doi:10.1016/S0141-0296(00)00045-6

Shehata, A.Y., El Damatty, A.A., (2007). Behaviour of guyed transmission line structures under downburst wind loading. Wind Struct. 10, 249–268.

Shehata, A.Y., El Damatty, A.A., Savory, E., (2005). Finite element modeling of transmission line under downburst wind loading. Finite Elem. Anal. Des. 42, 71–89. doi:10.1016/j.finel.2005.05.005

Solari, G., Rainisio, D., De Gaetano, P., (2017). Hybrid simulation of thunderstorm outflows and wind-excited response of structures. Meccanica. doi:10.1007/s11012-017-0718-x

Wang, X., Lou, W., Li, H., Chen, Y., (2009). Wind-induced dynamic response of high-rise transmission tower under downburst wind load. J. Zhejiang Univ. (Engineering Sci. 43, 1520–1525. doi:10.3785/j.issn.1008-973X.2009.08.031

Zhang, S., Solari, G., Gaetano, P. De, Burlando, M., Repetto, M.P., (2017). A refined analysis of thunderstorm outflow characteristics relevant to the wind loading of structures. Probabilistic Eng. Mech. doi:https://doi.org/10.1016/j.probengmech.2017.06.003

Zhang, Y., (2006). Status quo of wind hazard prevention for transmission lines and countermeasures. East China Electr Power 34, 28–31.

Chapter 4

4 Conclusions and future work

4.1 Conclusions

The thesis presents a numerical investigation of the dynamic effect of downburst loading on transmission lines longitudinal reactions. To examine such effect, a series of studies and procedures had to be performed as listed below:

a) Develop a numerical CFD model replicating an experiment simulating downburst at wind tunnel testing scales. The results of this model were compared with those of the experiment to make sure the detailed wind field obtained from the model match with data available from the experiment.

b) Propose and verify a numerical model that is capable of dynamically analyzing conductor systems under downburst loading. Such a model has to account for the conductors' geometric properties, as well as the downburst transient nature. This will directly reflect on the choice of aerodynamic damping expression, which has to be verified.

c) The wind field available from the first step is implemented in the model in the second step to make sure the results match with an aero-elastic model experiment performed at the WindEEE dome.

d) Using the numerical model from the second step, which is now validated at wind tunnel scale, a full-scale model is developed to assess the dynamic effect of downburst loading on transmission lines longitudinal reactions.

e) Since the available full-scale wind field only contains the mean component of the flow, the turbulent component was synthetically generated using a technique that

accounts for the spatial and the temporal relations between time histories of distant points. The resulting time histories had the statistical properties of turbulence assigned based on turbulence characteristics available in the literature.

f) The dynamic effect of downburst loading the longitudinal reactions of transmission lines is then assessed based on the results of the numerical model analysis after implementing the wind field resulting from superimposing the generated turbulent component on the available mean component.

As mentioned in the first chapter of this thesis, these steps were performed within two chapters, the second and the third. The conclusions derived from the second chapter, titled Numerical Simulation of WindEEE Dome Downburst Using Physical Roughness Elements, can be summarized in the following points:

1. The mean component of the flow extracted from the CFD simulation was compared to the experimental results and showed a good agreement.

2. The CFD and the experimental results had the maximum radial speed occur at a radial distance equal to the jet diameter. This is remarkably less than values found in the literature, which is believed to be due to a combination of the inlet flaps cross-section and the roughness elements used.

3. The flaps and the roughness elements were also shown to have an effect on the flow that was shown to be a streaming effect in the case of the flap, and a canopying effect in the case of the roughness blocks. The streaming effect of the flaps mainly affected the descending flow, while the canopying effect of the blocks caused an entrapment of the flow, as well as shedding and channeling effects at the region below the block height.

4. Turbulence characteristics of the flow were also compared with those from the experiment. The spectra showed a reasonable agreement between the model and the experiment. The turbulence intensity was also found to be 16% for the open terrain, and 23% for the suburban terrain at the peak velocity zone.

Adjacently, the third chapter of this thesis represented the implementation of the remaining steps listed in the beginning of this chapter. With the name of The Effect of Downburst Wind Field Characteristics on the Longitudinal Forces on Transmission Towers, the chapter's outcome can be concluded as follows:

1. Comparing the numerical model results to the aero-elastic experimental model results yielded a good agreement that justified the usage of a quasi approach in computing the aerodynamic damping for cable systems. This was found to be due to the insensitivity of the ramp-up zone to any dynamic effects, which implied the possibility of using the post ramp-up velocity to calculate a single value of aerodynamic damping.

2. The synthetically generated turbulent time histories were found to satisfy the spatial correlations for the lower range of frequencies representing larger spatial separation.

3. The analyses showed that the peak reactions were always attributed to the ramp-up zone, and that the post ramp-up zone showed a dynamic effect that failed to override the peak reactions at the peak zone. This justifies the agreement between the quasi-static analyses with dynamic analyses in comparing the values of peak reactions.

4. After examining the mean component of the wind field, and comparing it with field measurements available in the literature, which showed a difference in terms of the

duration of the peak period, as well as the post ramp-up to peak velocity ratio. After rerunning the analyses, it seemed that the discovered differences had no impact on the computed peak values of reactions within the considered range of cases. This was only excepted by the case of high jet velocity that showed a 5% decrease in the computed peak longitudinal reaction values. This implies that no changes in the used wind field are needed to compute peak reactions.

4.2   Future work

The outcome of this thesis can be extended towards exploring any of the following directions:

1. Studying the downburst flow characteristics through a full-scale CFD model utilizing the current model that was experimentally validated.

2. Implementing the suggested replacements of the WindEEE dome's flaps and roughness blocks and exploring the resulting wind field, which is expected to have less dependency on the local features of the geometry.

3. Exploring the most up to date field measurement results that utilized state-of-the-art technologies like LIDARs can be useful to either solidify the drawn conclusions in this study, or suggest further modifications in the wind field used.

4. Although tower structures are more rigid than conductor systems, which makes them less susceptible to wind loading, it might be useful to explore the coupled behavior of a transmission line system where the towers are included in the dynamic analysis due to downburst loading.

Curriculum Vitae

Name: Ibrahim Ibrahim

Post-secondary   Faculty of Engineering, Alexandria University

Education and   Alexandria, Egypt

Degrees: 2007-2012 B.Sc.

The University of Western Ontario

London, Ontario, Canada

2016-2017 M.E.Sc.

Related Work   Teaching Assistant

Experience   The University of Western Ontario

2016-2017

Publications:

Ibrahim, I., Aboshosha, H., El Damatty, A.A., 2017. Numerical Simulation of WINDEEE

Dome Downburst for Open Terrain Using Physical Roughness Elements, in: Proceedings

of the 7th European African Conference on Wind Engineering. Liege, Belgium.